Materials Science & Engineering R 152 (2023) 100712

Contents lists available at ScienceDirect

Materials Science & Engineering R

journal homepage: www.elsevier.com/locate/mser

Antimicrobial micro/nanorobotic materials design: From passive combat to active therapy

Jinhua Li [a], Hao Shen [c], Huaijuan Zhou [b,*], Rui Shi [d], Chengtie Wu [e,*], Paul K. Chu [f,*]

[a] School of Medical Technology, Beijing Institute of Technology, Beijing 100081, China
[b] Advanced Research Institute of Multidisciplinary Sciences, Beijing Institute of Technology, Beijing 100081, China
[c] Department of Orthopaedics, Shanghai Jiao Tong University School of Medicine Affiliated Sixth People's Hospital, Shanghai 200233, China
[d] Beijing Laboratory of Biomedical Material, Beijing Research Institute of Traumatology and Orthopaedics, Beijing Jishuitan Hospital, Beijing 100035, China
[e] State Key Laboratory of High-Performance Ceramics and Superfine Microstructure, Shanghai Institute of Ceramics, Chinese Academy of Sciences, Shanghai 200050, China
[f] Department of Physics, Department of Materials Science and Engineering, and Department of Biomedical Engineering, City University of Hong Kong, Tat Chee Avenue, Kowloon, Hong Kong, China

ARTICLE INFO

Keywords:
Nanorobots
Antibacterial
Infection
Biofilms
Intelligent materials

ABSTRACT

The rise of multidrug-resistant bacteria has emerged as one of the major threats to global public health. Moreover, many pathogenic bacteria can form stubborn biofilms to prevent antibiotic penetration and to protect them from environmental stress. Worse still, it is in dire need of developing novel antibiotics. Such circumstances call urgently for breakthrough strategies beyond traditional antibacterial treatments to fight back against the impending human health disaster. In this connection, micro/nanorobots can perform autonomous or field-driven locomotion, actively deliver therapeutic cargos, precisely implement micromanipulation, exert robust mechanical forces upon movement, and respond to internal (pH, chemical gradients, chemoattractants, etc.) or external (magnetic field, light, ultrasound, etc.) stimuli. These characteristics enable the targeted delivery of antimicrobials to infected sites and boost their deep penetration through bacterial biofilms, making the use of micro/nanorobots an attractive alternative to traditional antimicrobial treatments. In this review, we will comprehensively summarize the recent progress and future outlook for the application-oriented material designs of antimicrobial micro/nanorobots, covering broad topics from traditional antimicrobial nanomaterials to intelligent antimicrobial micro/nanorobots, from passive infection resistance to active antimicrobial therapy, and from eradicating bacteria and biofilms to eliminating bacterial toxins. Our goal is to deliver a comprehensive review that can serve as a useful reference and provide guidance for the rational design and development of novel

Abbreviations: A. actinomycetemcomitans, Actinobacillus actinomycetemcomitans; AC, Alternating current; AMR, Antimicrobial resistance; ATCC, American Type Culture Collection; B. subtilis, Bacillus subtilis; BPs, Black phosphorus nanosheets; BRP, Biological redox potentials; C_{60}, Fullerene; CB, Conduction band; CNT, Carbon nanotubes; CPX, Ciprofloxacin; CTAB, Cetyltrimethylammonium bromide; DC, Direct current; DoF, Degree of freedom; DOX, Doxorubicin; E. coli, Escherichia coli; E. faecalis, Enterococcus faecalis; e^-, Electron; E_{CB}, Conduction band minimum; EET, Extracellular electron transfer; E_F, Fermi level; EPS, Extracellular polymeric substances; F_{420}, Coenzyme F_{420}; $F_{420}H_2$, Reduced coenzyme F_{420}, quinone oxidoreductase; FFP, Field free point; g-C_3N_4, Graphitic carbon nitride; GA, Glutaraldehyde; GO, Graphene oxide; GQDs, Graphene quantum dots; h^+, Hole; HIFU, High intensity focused ultrasound; H_2O_2, Hydrogen peroxide; ICEP, Induced charge electrophoresis; LPS, Lipopolysaccharides; M. tuberculosis, Mycobacterium tuberculosis; MDR, Multidrug resistance; MOF, Metal−organic framework; MPI, Magnetic particle imaging; MPS, Mononuclear phagocyte system; MRI, Magnetic resonance imaging; MRSA, Methicillin-resistant Staphylococcus aureus; mSiO_2, Mesoporous SiO_2; NAD^+, Nicotinamide adenine dinucleotide; NPs, Nanoparticles; $^{\bullet}O_2^-$;, Superoxide radical; $^1O_2$, Singlet oxygen; $^3O_2$, Ground state molecular oxygen; OCT, Optical coherence tomography; $^{\bullet}OH$;, Hydroxyl radical; $OONO^-$, Peroxynitrite; PACT, Photoacoustic computed tomography; PAI, Photoacoustic imaging; P. aeruginosa, Pseudomonas aeruginosa; P. gingivalis, Porphyromonas gingivalis; PABA, Phenylboronic acid; PAH, Poly(allylamine hyhrochloride); PANI, Polyaniline; PCL, Polycaprolactone; PDA, Polydopamine; PDAT, Photodynamic antimicrobial therapy; PDT, Photodynamic therapy; PEDOT, Poly(3,4-ethylenedioxythiophene); PEEK, Polyetheretherketone; PET, Positron emission tomography; PLGA, Poly(lactic-co-glycolic acid); PSs, Photosensitizers; PSS, Poly(styrenesulfonic acid); PTT, Photothermal therapy; PVP, Polyvinylpyrrolidone; RBC, Red blood cell; RGD, Arginine-glycine-aspartic acid; rGO, Reduced graphene oxide; RNOS, Reactive nitrogen oxide species; ROS, Reactive oxygen species; S. aureus, Staphylococcus aureus; S. epidermidis, Staphylococcus epidermidis; S. mutans, Streptococcus mutans; S. oneidensis, Shewanella oneidensis; SPIONs, Superparamagnetic iron oxide nanoparticles; TAPP, 5,10,15,20-tetrakis(4-aminophenyl)porphyrin; β-TCP, β-tricalcium phosphate; TNT, Tuberculosis necrotizing toxin; UV, Ultraviolet; VB, Valence band; X-CT, X-ray computed tomography; ZnL_2, Zinc sulfonate ligand.

* Corresponding authors.
E-mail addresses: huaijuan.zhou@bit.edu.cn (H. Zhou), chengtiewu@mail.sic.ac.cn (C. Wu), paul.chu@cityu.edu.hk (P.K. Chu).

https://doi.org/10.1016/j.mser.2022.100712
Received 24 October 2022; Accepted 10 December 2022
Available online 19 December 2022

antimicrobial micro/nanorobots and bridge the gap between traditional antimicrobial nanomaterials and active antimicrobial micro/nanorobots.

1. Introduction

Since the discovery of mycophenolic acid and due to their subsequent constant development, modern antibiotics have greatly contributed to an increase in human lifespan by means of their lethal and selective effects on pathogenic microorganisms [1]. However, the overuse or abuse of antibiotics has triggered the fast evolution of antimicrobial-resistant bacteria and the emergence of multidrug resistance (MDR) in recent decades, which has been posing a serious challenge to the global health care system [2–4]. According to the 2019 global report by the World Health Organization, antimicrobial resistance (AMR) is responsible for around 700,000 deaths per year. Without taking action, 10 million deaths per year are envisioned by 2050, which is even more than the 8.2 million deaths per year currently caused by cancer and may lead to an estimated cumulative economic loss of over $100 trillion worldwide [5,6]. Despite the wide recognition of the global burden of AMR for decades, the development of new antibiotics is almost at a standstill due to strict regulation rules and low market profits. Worse still, the resistance of bacterial biofilms (i.e., hydrated extracellular polymeric substances (EPS) of polysaccharides and proteins) to antibiotics is 1000 times greater than that of planktonic bacteria [7]. The EPS matrix can reinforce the mechanical strength of biofilms, prevent the penetration of antimicrobials, and protect bacteria from the host immune system (e.g., phagocytes) [8–11]. The formation of bacterial biofilms is apt to hinder the efficient penetration of antibiotics into the core region of an infectious site, thus causing chronic and recurrent infections.

In this context, it is urgently necessary to develop novel and practical strategies to fight refractory bacterial infections, especially those caused by AMR. To address this challenging issue, three aspects should be considered when designing antimicrobial materials: (1) achieving the precise delivery of antimicrobials to the target site of bacterial infections while minimizing potential side effects; (2) developing novel non-antibiotic strategies for treating bacterial infections; and (3) increasing the penetration depth of antimicrobials in the biofilm. Antimicrobial biomaterials, such as metal nanoparticles, semiconductor-based nanomaterials, and polycationic polymers in the forms of powders, scaffolds, surface coatings, etc., and biomaterials-based micro/nanocarriers for the localized delivery of traditional antibiotics or non-antibiotic antimicrobials (e.g., antimicrobial peptides, antimicrobial enzymes, bacteriophages) have enhanced our capability to tackle the issue of AMR and treat recurrent bacterial infections [12–19]. As micro/nanocarriers, biomaterials enable both the targeted delivery and sustained release of multiple antimicrobials at the infectious site to decrease the potential side effects caused by systemic administration.

Micro/nanorobots are miniature mobile machines on the micro- and nanoscale that are designed to move to hard-to-reach sites and implement specific tasks (e.g., various medical tasks) by virtue of autonomous and/or external-powered actuation. With the rapid development of micro/nanomanufacturing technology, the components, structures, and functionalities of micro/nanorobots can be well tailored to achieve on-demand motion control and task execution (e.g., drug delivery) in complex physiological environments [20–27]. Furthermore, surface modification/functionalization and composite strategies can endow micro/nanorobots with versatile capabilities, such as loading and transportation of target cargos [28–30], improvement of biocompatibility [31–34], response to external stimuli [35–37] or microenvironmental cues [38–40], and swarm/collective/cooperative behaviors [41–43]. The micro/nanorobots hold great promise for a variety of applications in biomedical scenarios, encompassing biosensing [44–46], single cell manipulation [47,48] and microsurgery [49,50], minimally invasive microsurgery and intervention [22,51–53], and active therapeutic delivery [54–56]. In particular, the directed locomotion and cargo transportation capacities of micro/nanorobots can be well integrated to enable active, targeted delivery of diverse therapeutic drugs or cells, thereby bridging the gap between micro/nanorobots and nanomedicine.

With the convergence between the rapidly developing medical micro/nanorobots and traditional antimicrobial nanomaterials, antimicrobial micro/nanorobots have emerged as an active direction in the research field of medical micro/nanorobots. In the past decade, researchers have devoted significant efforts to this field, and an increasing number of antimicrobial micro/nanorobots have been designed and produced. Among the very few reviews on the topic of antimicrobial micro/nanorobots [57], we noticed that a comprehensive review is still absent in this field, especially from the perspective of bridging the gap between traditional antimicrobial nanomaterials and active antimicrobial micro/nanorobots. In this review, we will first introduce the design considerations of traditional antimicrobial nanomaterials, including antimicrobial mechanisms, material properties related to antimicrobial activity, and nanovehicles for delivering antimicrobials. Following that, we will summarize a variety of stimuli-responsive antimicrobial nanomaterials encompassing photoresponsive, magnetically responsive, and infection microenvironment-responsive nanomaterials. Thereafter, we will highlight state-of-the-art design strategies for the development of application-oriented micro/nanorobots for tackling issues associated with bacterial infections (such as the recognition, capture, and destruction of bacteria, eradication of bacterial biofilms, and removal of bacterial toxins), demonstrating how antimicrobial micro/nanorobots have been designed and exploited as an efficient strategy to treat bacterial infections. Finally, we will provide an outlook on future directions and challenges in the emerging research field of antimicrobial micro/nanorobots.

2. Traditional antimicrobial nanomaterials

2.1. Interactions between bacteria and nanomaterials

The antimicrobial properties of materials at the nanoscale have attracted enormous interest in recent years. The interactions between nanomaterials and bacteria depend upon their multiple contact forms, including electrostatic attraction, van der Waals forces, hydrophobic interaction, and receptor–ligand interaction [58]. Understanding the interplay mechanism of nanomaterials with bacteria can enable the rational design of novel nano-antimicrobials.

2.1.1. Nanomaterials penetration into bacterial membranes

Bacteria are mainly categorized into Gram-positive and Gram-negative according to the structural characteristics of their cell walls [59]. The cell walls of Gram-positive bacteria have a thick layer of peptidoglycan with polymeric teichoic acids (15–100 nm thickness) underneath which is the cytoplasmic membrane. The phosphates in teichoic acid polymer chains account for the negative charge of bacterial membranes and act as binding sites for divalent/multivalent cations in an aqueous solution [60]. Gram-negative bacteria are enveloped with hydrophobic lipid bilayers comprising lipopolysaccharides (LPSs), underneath which is a thin layer of peptidoglycan (20–50 nm thickness) and the cytoplasmic membrane [61]. This additional lipid bilayer can largely weaken the penetration capability of multiple hydrophobic antimicrobials [62]. The negatively charged membranes of Gram-negative bacteria mainly result from the phosphates and carboxylates present in LPSs. Therefore, the structural features of bacterial cell walls play a

Table 1
The redox potentials of representative ROS-related redox couples (at pH = 7.0) [72,73].

Half-reactions	Redox couples	Redox potentials (E_0/V)
$O_2 + e^- \rightarrow {}^{\bullet}O_2^-$	$O_2/{}^{\bullet}O_2^-$	− 0.16
$O_2 + 2\ H^+ + 2e^- \rightarrow H_2O_2$	O_2/H_2O_2	0.28
$H_2O_2 + H^+ + e^- \rightarrow H_2O + {}^{\bullet}OH$	$H_2O_2/{}^{\bullet}OH$	0.38
${}^{\bullet}O_2^- + 2\ H^+ + e^- \rightarrow H_2O_2$	${}^{\bullet}O_2^-/H_2O_2$	0.89
$H_2O + h^+ \rightarrow H^+ + {}^{\bullet}OH$	$H_2O/{}^{\bullet}OH$	2.32

critical role in determining their interactions with various nanomaterials. Typically, nanomaterials with a positive charge tend to attach to negatively charged bacterial membranes due to their electrostatic interaction, which was demonstrated on positively charged Au nanorods and nanospheres terminated with cetyltrimethylammonium bromide (CTAB) in an early study [63]. After binding to bacterial membranes, disruption of membrane structures or normal functions may occur (e.g., by interacting with sharp edges) and lead to the antimicrobial effect. The physicochemical properties of nanomaterials (such as size, shape, and surface) are key factors that affect their binding and penetrating process upon contact with bacteria, which will be further discussed in **Section 2.2** .

2.1.2. Oxidative damage to bacterial components

The oxidative stress caused by reactive oxygen species (ROS) represents a momentous antimicrobial mechanism of nanomaterials [64,65]. 'ROS' is a general term for molecules and reactive intermediates with strong positive redox potentials. By reducing oxygen molecules (O_2), different kinds of nanomaterials can generate distinct types of ROS. The four types of intrinsic ROS include the hydroxyl radical (${}^{\bullet}OH$), superoxide radical (${}^{\bullet}O_2^-$), singlet oxygen ($^1O_2$), and hydrogen peroxide (H_2O_2), which exhibit varying levels of activity and dynamics [66]. Nanomaterials can form ROS via multiple mechanisms, photocatalysis being considered the main one. When semiconductor nanomaterials (e.g., TiO2 and ZnO) are irradiated by light with energy of no less than the band gap, electrons (e^-) in the valence band (VB) are excited and transition up to the conduction band (CB), which leaves behind a corresponding hole (h^+) in the valence band, thereby leading to the formation of highly reactive reactants (i.e., e^-–h^+ pairs) on their surface and interior. These photogenerated e^-–h^+ pairs then react with diverse molecules or ions to produce different types of ROS. TABLE 1 shows the redox potentials of some representative ROS-related redox couples. Numerous studies have demonstrated that nanomaterials can also generate ROS in the dark and thus achieve the desired antimicrobial effect. A plausible mechanism has been proposed from the viewpoint of extracellular electron transfer (EET). There is an electron transfer system in the respiration chain of the bacterial membrane, inside which there exists a sequence of redox couples with their biological redox potentials (BRPs) listed in Table 2. According to the equation $E^\circ = -4.44 - E$ (where E° is the standard hydrogen electrode potential measured in V and E is the absolute potential level measured in eV) [67], the BRPs of bacteria range from − 4.12 eV to − 4.84 eV. When a nanomaterial has a Fermi level (E_F) or CB minimum (E_{CB}) lower than the BRP, it may cause spontaneous electron leakage and EET interruption [68]. The leaked energetic electrons from bacterial membranes have the potential to generate various ROS in the dark. Ultrasound activation can also induce the production of ROS [69]. Due to excessive ROS formation, the redox balance of bacteria is disrupted, which can cause oxidative stress and damage a variety of individual components of microbial cells [64,70,71].

2.1.3. Inhibition of biofilm formation

Bacteria that adhere to medical implants or damaged tissues can produce biofilms—that is, EPSs consisting of polysaccharides and proteins [10,77]. Antimicrobials have a very poor ability to penetrate biofilms, which thus protect bacteria from environmental antibiotics and provide them with antimicrobial resistance [59]. This phenomenon has inspired the antibacterial tactic of utilizing nanomaterials to destroy biofilm integrity [78]. A previous study demonstrated that nanomaterials can restrain the metabolic activity of bacterial communities [79], since bacterial metabolism plays an important role in the formation of biofilms. Another study showed that after adhering to bacterial biofilms, Mg nanoparticles (NPs) were able to diffuse into the biofilms, disrupt the bacterial membrane potentials, increase lipid peroxidation, and finally reduce the production of bacterial biofilms [80]. According to these results, the inhibitory effect of nanomaterials on biofilm formation is presumably associated with the suppression of bacterial metabolism. Furthermore, nanocatalysts (e.g., Fe_3O_4 and TiO_2) have been reported to facilitate the catalytic/photocatalytic degradation of bacterial biofilms [81,82]. In addition to the aforementioned interactions between bacteria and nanomaterials, other antimicrobial mechanisms also exist: nanomaterial-enabled inhibition of the synthesis of bacterial DNA and proteins, regulation of the expression of bacterial metabolic genes, and enhancement of antibacterial immunity [58,83]. Table 3 summarizes some representative nanomaterials and their toxicity mechanisms toward Gram-positive (+) and Gram-negative (-) bacteria.

2.2. Antimicrobial properties of nanomaterials

2.2.1. Size effect

The size or dimension of nanomaterials plays an important role in determining their interplay with bacteria. Elimelech and co-workers studied how the size of graphene oxide (GO) nanosheets could

Table 2
The redox potentials of redox couples in the electron transfer system of the respiration chain located on bacterial membranes (at pH = 7.0) [74–76].

Half-reactions	Redox couples	Redox potentials (E°/V)
$O_2 + 4\ H^+ + 4e^- \rightarrow 2\ H_2O$	O_2/H_2O	+ 0.816
Cytochrome a_3 ox + $e^- \rightarrow$ Cytochrome a_3 red	Cytochrome a_3 ox/red	+ 0.385
$F_{420} + 2\ H^+ + 2e^- \rightarrow F_{420}H_2$	$F_{420}/F_{420}H_2$	+ 0.357
Cytochrome c_1 ox + $e^- \rightarrow$ Cytochrome c_1 red	Cytochrome c_1 ox/red	+ 0.230
Ubiquinone ox + $e^- \rightarrow$ Ubiquinone red	Ubiquinone ox/red	+ 0.113
Cytochrome b ox + $e^- \rightarrow$ Cytochrome b red	Cytochrome b ox/red	+ 0.035
Rubredoxin ox + $e^- \rightarrow$ Rubredoxin red	Rubredoxin ox/red	− 0.057
Menaquinone ox + $e^- \rightarrow$ Menaquinone red	Menaquinone ox/red	− 0.075
$FMN + 2\ H^+ + 2e^- \rightarrow FMNH_2$	$FMN^{2+}/FMNH_2$	− 0.190
$FAD + 2\ H^+ + 2e^- \rightarrow FADH_2$	$FAD^{2+}/FADH_2$	− 0.220
Cytochrome c_3 ox + $e^- \rightarrow$ Cytochrome c_3 red	Cytochrome c_3 ox/red	− 0.290
$NAD + 2\ H^+ + 2e^- \rightarrow NADH + H^+$	$NAD^+/NADH$	− 0.320
$NADP + 2\ H^+ + 2e^- \rightarrow NADPH + H^+$	$NADP^+/NADPH$	− 0.320
Flavodoxin ox + $e^- \rightarrow$ Flavodoxin red	Flavodoxin ox/red	− 0.371
Ferredoxin ox + $e^- \rightarrow$ Ferredoxin red	Ferredoxin ox/red	− 0.398
$2\ H^+ + 2e^- \rightarrow H_2$	H^+/H_2	− 0.414

Table 3
Summaries on the antimicrobial mechanisms of representative nanomaterials.

Nanomaterials	Bacteria	Antimicrobial mechanisms	Refs
Ag NPs	*Staphylococcus aureus* (*S. aureus*) ATCC 6538 P (+)	Breakdown of the cell walls, the release of cellular contents, reduction in respiratory chain dehydrogenase activity	[84]
	Escherichia coli (*E. coli*) ATCC 8739 (-)	Damage to the bacterial membrane structure, decrease in the activity of several membrane enzymes	[85]
	E. coli (-)	Release of Ag^+ ions	[86]
	Pseudomonas aeruginosa (*P. aeruginosa*) (-)	Elevation of intracellular ROS levels, oxidative damage, the release of dissolved Ag^+ ions	[87]
Au nanoclusters	*S. aureus* ATCC 25923 (+), *Staphylococcus epidermidis* (*S. epidermidis*) NBRC 12993 (+), *E. coli* ATCC 700926 (-), *P. aeruginosa* NRRL-B 3509 (-), *Bacillus subtilis* (*B. subtilis*) NRRL-NRS 762 (+)	Internalization due to ultrasmall size (< 2 nm), induction of metabolic imbalance in bacteria, increase of intracellular ROS levels	[88]
AuAg nanocages	E. coli ATCC 43888 (-), Enterococcus faecalis (E. faecalis) ATCC 19433 (-), S. aureus ATCC BAA-1721 (+), Streptococcus mutans (S. mutans) ATCC 700610 (+)	Destruction of bacterial membranes, increase of ROS production, induction of bacteria apoptosis	[89]
AuPt bimetallic NPs	*E. coli* ATCC 11775 (-)	Rupture in the bacterial inner membrane, the elevation of intracellular adenosine triphosphate (ATP) levels, no involvement of ROS generation	[90]
Cu NPs	Methicillin-resistant Staphylococcus aureus (MRSA) ATCC43300 (+)	Contact killing of bacteria by Cu NPs, the release of Cu^{2+} ions, activation and polarization of macrophages to proinflammatory M1 phenotype, improved phagocytosis of MRSA by macrophages	[91]
Cu^{2+}-loaded bioactive glasses	E. coli DH5α (-)	Release of Cu^{2+} ions	[92,93]
Ta nanofilms	S. aureus ST1792 (+), E. coli ST1 (-)	Enhancement on phagocytosis of bacteria by neutrophils, reduction in neutrophil lysis, enhanced release of proinflammatory cytokines	[83]
Se NPs	S. aureus ATCC 25923 (+)	Strong inhibition on bacterial growth	[94]
V NPs	MRSA ATCC 43300 (+), P. aeruginosa ATCC 27853 (-)	Elevation of intracellular ROS levels	[95]
Graphene	E. coli ATCC 25922 (-), S. aureus ATCC 25923 (+)	Electron transfer mediated antibacterial activity, inhibition on bacterial growth, damage to membrane integrity	[96]
Graphene oxide (GO) nanosheets	E. coli BL21 (DE3) (-)	Electron transfer mediated antibacterial property, ROS mediated oxidative damage to bacteria	[97]
	E. coli (-), B. subtilis (+)	Loss of integrity of bacterial membranes, strong inhibition on bacterial metabolic activity, remarkable loss of bacterial viability	[98,99]
	E. coli DH5α (-)	Destructive extraction of membrane phospholipids from bacteria	[100]
	E. coli ATCC BW26437 (-)	Nanosheet penetration of bacterial membranes, increased edge density of vertically oriented GO, bacterial membrane disruption, direct electron transfer mediated oxidation	[101]
Reduced graphene oxide (rGO) nanosheets	E. coli K12 (-), E. coli ATCC 25922 (-), S. aureus ATCC 25923 (+)	Membrane stress induced by sharp nanosheets upon direct contact, $^{\bullet}O_2^-$ independent oxidation, membrane damage by extremely sharp edges	[102,103]
Carbon nanotubes (CNT)	E. coli K12 ATCC 25404 (-), B. subtilis ATCC 6051 (+), P. aeruginosa ATCC 9027 (-), S. aureus ATCC 6538 (+)	Physical puncture on bacteria by sharp nano darts, destruction of bacterial envelopes, leakage of intracellular contents	[104,105]
Fullerene (C_{60})	E. coli K12 ATCC 25404 (-), B. subtilis 168 ATCC 31578 (+)	ROS-independent oxidative stress	[106]
$Ti_3C_2T_x$ / Nb_2CT_x MXene	E. coli (-), B. subtilis (+)	Damage to bacterial membranes, leakage of cytoplasmic contents	[107]
	S. aureus ATCC 43300 (+), E. coli ATCC 35218 (-)	Downregulation of bacterial energy metabolism pathways, destruction of biofilms, suppression of biofilm formation, photothermal transduction	[108]
TiO_2	S. aureus SF8300 (+), E. coli (-), P. aeruginosa (-), B. subtilis (+), etc	Photocatalytic antibacterial property	[109,110]
ZnO NPs	S. epidermidis ATCC 35984 (+), S. aureus SF8300 (+), E. coli ATCC 35218 (-), P. aeruginosa ATCC 27853 (-)	Inhibition on bacterial adhesion, promoted phagocytosis of bacteria by macrophages and neutrophils, boosted secretion of inflammatory cytokines	[111]
VO_2 NPs/nanofilms	S. aureus ATCC 25923 (+), S. epidermidis ATCC 35984 (+)	Elevation of intracellular ROS levels, oxidative stress to bacteria	[70]
V_2O_5 nanofilms	MRSA ATCC 43300 (+), P. aeruginosa ATCC 27853 (-)	Elevation of intracellular ROS levels	[95]
Amorphous Ta_2O_5 NPs	P. aeruginosa (-)	Interruption of bacterial membrane electron transport chain, elevation of intracellular ROS levels, loss of bacterial viability	[112]
MoS_2 nanosheets	E. coli DH5α (-)	Membrane stress upon contact, oxidative stress, elevation of ROS production, $^{\bullet}O_2^-$ independent oxidation	[113]
g-C_3N_4	E. coli (-), S. aureus (+), MRSA (+), etc	Photocatalytic antibacterial property	[114]
Titanate	E. coli ATCC 25922 (-), S. aureus ATCC 25923 (+)	The joint effect between nanostructure of $Na_2Ti_4O_9$/$SrTi_4O_9$ and local increase of pH	[115]
	E. coli ATCC 25922 (-)	Release of Cu^{2+} ions from $CuTiO_3$	[116]
TiO_2:Co	MRSA ATCC 43300 (+), S. epidermidis ATCC 35984 (+), E. coli ATCC 35218 (-), P. aeruginosa ATCC 27853 (-)	Interruption of bacterial EET, inhibition on biofilm formation, enhanced phagocytosis and killing of bacteria by macrophages and neutrophils due to Co^{2+} ion release	[76]
TiO_2:Zn nanotubes	S. aureus (+)	Release of Zn^{2+} ions	[117]

(*continued on next page*)

Table 3 (*continued*)

Nanomaterials	Bacteria	Antimicrobial mechanisms	Refs
TiO_2:C nanotubes	S. aureus ATCC 29213 (+), E. coli ATCC 25922 (-)	EET between bacteria and capacitive material, deformation of bacterial morphology, elevation of intracellular ROS levels	[118]
TiO_2-Ag	MRSA ST239 (+), E. coli ATCC 25922 (-), S. aureus ATCC 25923 (+)	Contact killing of bacteria, no detectable release of Ag^+ ions, electron storage mediated oxidative damage to bacteria	[119,120]
	S. aureus ATCC 6538 (+), S. epidermidis RP62A (+), MRSA USA 300 (+), Porphyromonas gingivalis (P. gingivalis) ATCC33277 (-), Actinobacillus actinomycetemcomitans (A. actinomycetemcomitans) ATCC29523 (-)	Release of Ag^+ ions, regulation of biofilm-related gene expression levels, inhibition on biofilm formation and bacterial adhesion, synergy effects between Ag NPs and Ag^+ ion release	[121–123]
TiO_2-Ag_2O nanotubes	E. coli ATCC10536 (-), S. aureus ATCC6538 (+)	Controlled release of Ag^+ ions	[124]
TiO_2-Au	S. aureus ATCC 25923 (+), E. coli ATCC 25922 (-),S. aureus ATCC 29213 (+)	Interruption of electron transport in bacterial respiratory chain, loss of membrane electrons, no involvement of ROS production	[125,126]
	E. coli ATCC 25922 (-)	Enhancement on photocatalytic efficiency in bacteria inactivation	[127]
TiO_2-Co_3O_4	MRSA SF8300 (+), S. epidermidis RP62A (+)	Downregulation of bacterial respiratory gene expression levels, oxidative damage to bacterial membranes, loss of bacterial viability	[128]
ZnO-Au	E. coli ATCC 25922 (-)	Electron transfer between bacteria and material, bacteria killing by electron loss	[129]
	E. coli ATCC 25922 (-), S. aureus ATCC 29213 (+)	Photocatalytic antibacterial activity, enhanced generation of ROS and photoinduced charge carriers by Au NPs	[130]
VO_2:W	MRSA ATCC 43300 (+)	Destructive extraction of bacterial membrane electrons, oxidative stress, energy starvation, damage to membrane integrity	[68]
Nb_2O_5-Ag nanobelts	E. coli (-), S. aureus (+)	Presence of Ag NPs	[131]
$Ti_3C_2T_x$ MXene-Bi_2S_3	E. coli ATCC 8099 (-), S. aureus ATCC 25923 (+)	Charge transfer mediated antibacterial property, photocatalytic antibacterial activity, near-infrared (NIR) triggered ROS production and hyperthermia	[132]
$Ti_3C_2T_x$ MXene-Co nanowires	E. coli ATCC 25923 (-), S. aureus ATCC 25922 (+)	NIR triggered ROS production and hyperthermia	[133]
Titanate nanowires-Ag NPs	E. coli (-), S. aureus (+)	Release of Ag^+ ions	[134]
Ag NPs@Ti	S. aureus ATCC 29213 (+), E. coli ATCC 25922 (-),	Electron transfer induced elevation of ROS levels, intracellular oxidation, variation of membrane potential, the release of cellular contents	[135]
MgF_2 nanofilms	Community-acquired MRSA USA300 (+), S. epidermidis RP62A (+)	Potentiated neutrophil phagocytosis and stability, indirect immune enhancement effect	[136]
Quaternary ammonium salts-loaded polycaprolactone (PCL)/ gelatin nanofibres	P. aeruginosa (-), S. aureus (+)	Quaternary ammonium compounds as cationic antimicrobials, contact killing	[137]
Halloysite clay nanotubes loaded with ciprofloxacin (CPX) and polymyxin B sulfate	S. aureus (+), P. aeruginosa (-)	Release of CPX and polymyxin B sulfate	[138]

influence their antibacterial activity against E. coli (Fig. 1A) [139]. GO suspensions with an average nanosheet area of 0.01–0.65 μm^2 were processed into surface coatings. The antibacterial ability of these coatings had a 4-fold increase upon decreasing the GO nanosheet area from 0.65 to 0.01 μm^2, which was due to the oxidative mechanism caused by smaller GO nanosheets having higher defect density. In contrast, the GO suspensions showed enhanced antibacterial properties upon increasing the nanosheet area, which was ascribed to the cell entrapment mechanism of GO nanosheets when interacting with bacteria. The authors also found a diameter-dependent antibacterial effect in carbon nanotubes (CNTs): single-walled CNTs were much more toxic to E. coli than multi-walled CNTs upon direct contact through a bacterial membrane damage mechanism [140].

Ag NPs have been widely used as potent antimicrobials. Previous studies demonstrated that the ROS-generating and antibacterial capacities of Ag NPs were strongly dependent on their dimensions [141,142]. Inspired by the native antimicrobial architectures on insect wings, micro- and nanoscale cone/pillar arrays were prepared on polyetheretherketone (PEEK) via colloidal lithography and plasma etching (Fig. 1B) [143]. The antibacterial effect of microarrays resulted from early mechanical stretching and the subsequent size effect, while the nanoarrays mimicking cicada wings destroyed E. coli solely based on the penetration effect of their sharp tips. In addition, it has been demonstrated that NPs with a size of < 350 nm can diffuse through the pores inside biofilms [144,145]. Collectively, when designing nanomaterial-based antibacterial surface films/coatings, scaffolds, or novel antimicrobials, the size effect should be fully considered to control their antibacterial properties.

2.2.2. Shape effect

The shape factor of nanomaterials is able to further reinforce their contact-killing capabilities, considering that a specific shape may increase the local adhesion forces that cause surface tension changes and integrity damage to bacterial membranes [146]. The sharp edges of graphene nanosheets can perform as nano-blades or nano-knives to physically cut through or puncture the bacterial membranes and cause the leakage of intracellular contents and eventual bacterial death (Fig. 2 A) [147]. A study also demonstrated that single-walled CNTs with sharper nano-darts possessed better antibacterial abilities against *E. coli*, *P. aeruginosa*, *S. aureus*, and *B. subtilis* [104]. Differing from the commonly reported antimicrobial mechanisms of bulk Mg, such as the release of Mg^{2+} ions and an increase of the local pH, hydrothermally formed 2D $Mg(OH)_2$ nanoflakes on Mg were able to impose mechanical tension on bacterial membranes upon direct contact with *S. aureus* or *E. coli*, cause intracellular stress, and finally kill the bacteria through physical interplay, which was consistent with the computational simulations (Fig. 2B) [148]. Song and co-workers fabricated truncated triangular Ag nanoplates, Ag nanospheres, and Ag nanorods to investigate their antimicrobial properties against *E. coli* [149]. The authors observed that the truncated triangular nano-Ag exerted the strongest antibacterial effect compared to the Ag nanospheres and nanorods.

In another study by Epple and co-workers [150], Ag NPs having

different shapes exhibited distinct antibacterial capacities in the following order: Ag nanoplatelets > Ag nanospheres > Ag nanorods > Ag nanocubes. The shape-dependent antimicrobial activity of nano-Ag was mainly correlated with the differences in dissolution rate and specific surface area, modulating the dissolution and release of Ag^+ ions from the surface to affect the antimicrobial ability of nano-Ag in different shapes. From the viewpoint of crystallization, the shape/-morphology of nanocrystals is determined by their crystallographic facet exposures. Wang and co-workers regulated the antibacterial behavior of Au nanocrystals by tailoring their exposed crystallographic facets, thereby demonstrating that nanomaterials could exert facet-dependent antimicrobial activity (Fig. 2C) [151].

2.2.3. Surface chemistry

The appropriate surface chemical functionalization of nanomaterials can be exploited to tailor their antimicrobial activity. The antibacterial pathways of nanomaterials rely intrinsically on their composition, size, shape, and surface chemistry. Chen and co-workers investigated the antimicrobial ability of four kinds of fullerene compounds (i.e., C_{60}, C_{60} −OH, C_{60} −COOH, and C_{60} $-NH_2$) against *E. coli* W3110 and *S. oneidensis* MR-1 [152]. The results showed that positively charged C_{60} $-NH_2$ was able to inhibit bacterial growth at low concentrations, and neutrally charged C_{60} and C_{60} −OH could only exhibit a mild inhibitory effect on *S. oneidensis* MR-1; negatively charged C_{60} −COOH had no effect on bacterial growth. Due to the electrostatic interactions between negatively charged bacterial membranes and positively charged functional groups of amino acids, the surface functionalization of multi-walled CNTs with arginine and lysine enabled significant enhancement of the antibacterial properties against *E. coli*, *S. aureus*, and *S. typhimurium* in the following sequence: multi-walled CNTs-arginine > multi-walled CNTs-lysine > pristine multi-walled CNTs [153].

The surface chemical status of nanomaterials can determine their zeta potential and thus affect their antibacterial activity. In another study, four types of Ag NPs with varied surface charges, from negative to positive, were designed to investigate their toxic effects and mechanisms against *bacillus* species (−37 mV under the test conditions) [154]. Owing to the presence of strong electrostatic attraction, the Ag NPs could be ordered as follows according to their antibacterial activity: branched polyethyleneimine-coated Ag NPs (+40 mV) > polyvinylpyrrolidone-coated Ag NPs (−10 mV) > uncoated H_2-Ag NPs (−22 mV) > citrate-coated Ag NPs (−38 mV), thereby indicating the surface charge-dependent antibacterial capacity of Ag NPs. Nevertheless, highly negatively charged TiO_2 nanopetals and nanorods have been shown to have a favorable bacteriostasis effect on *E. coli* and *S. aureus* [155]. Moreover, element doping and heterojunction creation can be effective ways to control the interactions between nanomaterials and bacteria [68,156,157]. In addition, the surface defects of nano--Ta_2O_5 [112] and nano-ZnO [158] were also shown to affect their ROS-producing ability and antimicrobial activity in the dark. Since the surface chemistry of nanomaterials plays a critical role in governing their interactions with microorganisms, it is expected that their tunable surface chemistry can offer a promising strategy for designing novel nano-antimicrobials for combating bacterial infections. Considering the difficulty in directly introducing antimicrobial metal NPs, such as Ag NPs and Cu NPs, onto the surfaces of bioceramic/bioglass scaffolds due to their complex network structures, suitable surface functionalization of metal NPs or nanocomposite strategies may enable the antimicrobial surface modification of bioceramic/bioglass scaffolds using nanomaterials (i.e., Ag NPs and Cu NPs). For example, Wu and co-workers achieved the surface modification of 3D-printed β-tricalcium phosphate (β-TCP) bioceramic scaffolds using a nanocomposite of Ag NPs and GO nanosheets, both of which possess antimicrobial and osteogenic activities [86].

2.3. Nanocarriers for antimicrobial delivery

The use of nanomaterial-based delivery vehicles can improve the antibacterial efficiency of therapeutic cargos and facilitate their targeted transportation to the site of bacterial infections [59,159]. Such nanocarriers enable the advantages of prolonged drug retention in blood, decreased non-specific distribution, and targeted antimicrobial delivery to an infected site. To this end, the surface chemistry of nanomaterials offers a stealth capacity to render nanomaterials invisible to the host immune defense system. The mononuclear phagocyte system (MPS) can clear the nanocarriers from the bloodstream unless they have been engineered to escape recognition and uptake by phagocytes [160,161]. Another critical biological barrier to nanocarrier-based antimicrobial delivery is the opsonization process. Opsonin proteins in the blood serum can rapidly adhere to non-stealth nanocarriers and allow macrophages of the MPS to recognize, bind, and clear nanocarriers from circulation [162,163]. Numerous methods have been implemented to cloak nanocarriers from the MPS and provide them with phagocytosis resistance by blocking protein adsorption onto their surface and the subsequent complementary interactions. Among these methods, the most promising is the surface camouflage strategy of nanomaterials with a variety of cell membranes [164–166].

Liposomes, dendrimers, polymers, micelles, and mesoporous silica NPs are commonly used as nanocarriers for the loading of antimicrobials, enzymes, or photosensitizers (PSs) to enable direct or stimuli-responsive antimicrobial functions and the targeted delivery of hydrophobic antimicrobials to infected sites that otherwise cannot be reached [167,168]. Hydrophobic antimicrobials (e.g. erythromycin, farnesol, triclosan, and essential oils) can be incorporated into the hydrophobic micelle core as cargo, whereas the hydrophilic liposome core is appropriate for the loading of hydrophilic antimicrobials. Moreover, multi-charged antimicrobials can be packaged into oppositely charged nanocarriers via electrostatic double-layer interactions. In addition to promoting the non-specific delivery of antimicrobial cargos with enhanced antibacterial efficacy, especially against drug-resistant bacteria, nanomaterials-based delivery carriers can be utilized to modulate the release of drug cargos in a controlled and sustained manner. Nitric oxide (NO)-releasing NPs have been developed for antimicrobial applications. As a radical gas, NO imposes its antibacterial actions by producing reactive nitrogen oxide species (RNOSs), which include peroxynitrite ($OONO^-$), NO_2, and N_2O_3 [71,169]. To compensate for the short lifetime of NO and unleash the potential of NO-based gas therapy, researchers have developed versatile NO-releasing NPs or coatings, such as nitrite-containing hydrogel/glass composite nanopowders [170], NO-releasing silica NPs [171], NO-releasing MoS_2 nanovehicles [172], NO-releasing dendritic Fe_3O_4 @polydopamine@polyamidoamine nanocomposites [173], and NO-releasing sol–gel coatings [174], to ensure the sustained formation and release of NO molecules and thus harness their antibacterial capability.

3. Stimuli-responsive antimicrobial nanomaterials

3.1. Photoresponsive antimicrobial nanomaterials

The photoactivated disinfection strategy exploits light irradiation at specific wavelengths, from ultraviolet (UV) to the near infrared (NIR) spectrum, to excite photoresponsive materials; upon irradiation, the designed photoresponsive materials can absorb light energy, generate ROS, or create hyperthermic conditions to efficiently destroy bacteria in a very short time [157,175]. Nowadays, increasing attention is being paid to the design and development of photoresponsive antimicrobial systems, in which two types of antibacterial mechanisms are involved: ROS-based photodynamic therapy (PDT) and hyperthermia-based photothermal therapy (PTT).

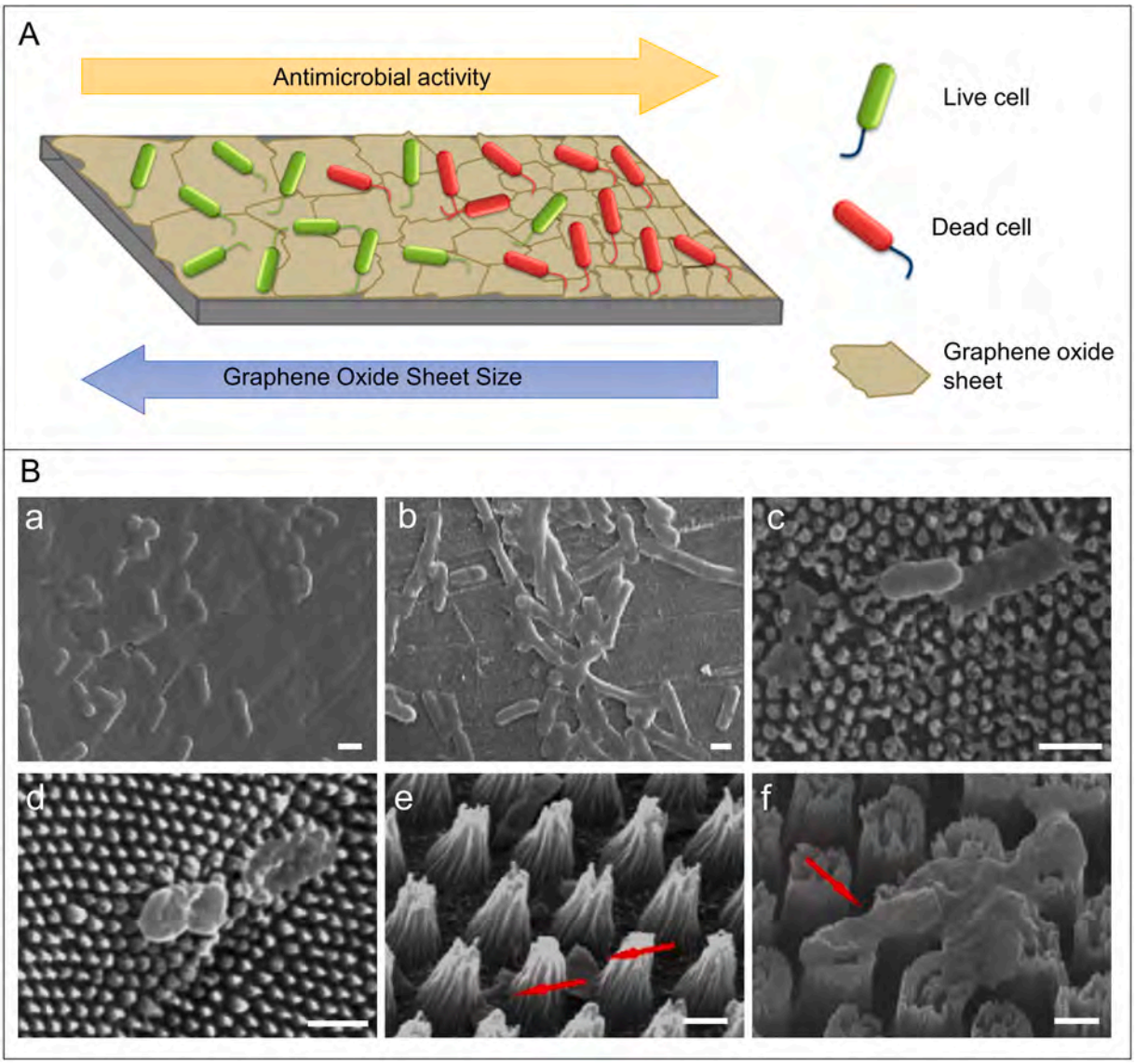

Fig. 1. (A) The dependence of antibacaterial perfomrance on the sheet size of graphene oxide. (B) SEM morphology of E. coli on different PEEK samples: (a) pristine PEEK, (b) PEEK-O (PEEK treated with oxgen plasmas), (c) nanocones, (d) nanopillars, (e) microcones, and (f) micropillars. Scale bar, 1 μm.
(A) Reproduced with permission from ref [139]. Copyright 2015 American Chemical Society. (B) Reproduced with permission from ref [143]. Copyright 2019 Elsevier B.V. All rights reserved.

3.1.1. *Photodynamic antimicrobial nanomaterials*

Photodynamic antimicrobial therapy involves fighting against bacteria through ROS, the main ones being $^{\bullet}O_2^-$, $^{\bullet}OH$, $^1O_2$, and H_2O_2. ROS can cause oxidative stress and integrity damage to bacterial membranes; they can also enter bacteria to trigger oxidative damage to their proteins, lipids, and DNA [176–178]. For photosensitizer-based photodynamic antimicrobial therapy, upon light irradiation, the photosensitizer absorbs a photon and produces ROS via two mechanisms [178,179]: (1) photogenerated electrons are transferred to environmental substrates to form $^{\bullet}O_2^-$ with the capability of dismutation into H_2O_2, which can further generate highly reactive $^{\bullet}OH$ through Fenton-like reactions; (2) energy (but no electrons) is directly transferred to ground state molecular oxygen ($^3O_2$) to produce $^1O_2$. For more details on photosensitizers, readers are referred to these excellent reviews [180–182]. For photocatalyst-based photodynamic antimicrobial therapy, a variety of photocatalytic materials based on semiconductors, doped semiconductors, or their heterojunctions have been widely investigated to fight against bacterial infections [183]. The antimicrobial capacity of photocatalysts originates from the ROS generated during the photoexcitation process. Briefly, the photogenerated electrons reduce O_2 into $^{\bullet}O_2^-$, whereas the photogenerated holes oxidize H_2O to $^{\bullet}OH$; both products are capable of further conversion to other kinds of ROS through varied catalytic reactions [183,184].

A membrane-intercalating conjugated oligoelectrolyte (called 'PTTP') was developed for photodynamic antimicrobial purposes, possessing absorption and emission maxima at 507 nm and 725 nm, respectively (Fig. 3A) [185]. Upon light excitation, PTTP can efficiently produce $^1O_2$ in situ with a quantum efficiency of around 20%. Combining rapid membrane-insertion and photosensitizing capabilities, PTTP has demonstrated highly efficient antimicrobial properties at a low light dose of 0.6 J·cm^{-2} against *E. coli*. Wu and co-workers fabricated a nanocomposite hydrogel containing 2D few-layer black phosphorus nanosheets (BPs) through electrostatic interactions [186]. Because of its strong ability to generate $^1O_2$ under simulated visible light, this nanocomposite hydrogel was able to rapidly destroy 98.90% of *E. coli* and 99.51% of *S. aureus* within 10 min. The same team also developed a photodynamic-ion disinfection strategy based on heterojunction photocatalysts, such as Fe_2O_3-porphyrinic metal−organic framework (MOF)

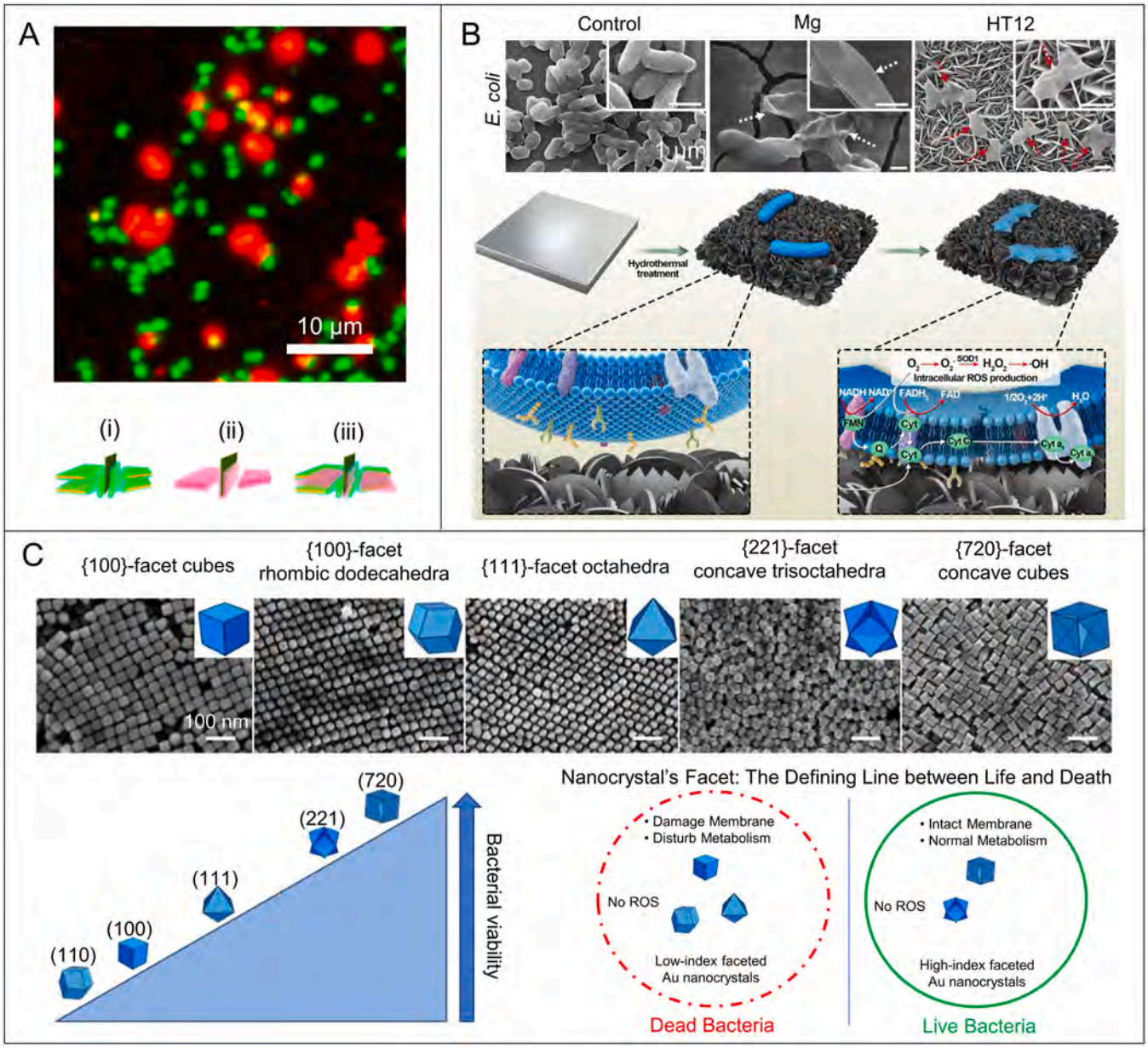

Fig. 2. (A) Confocal microscopy image of S. aureus with and without graphene nanosheet. The insertion of graphene sheet not only leads to increased size of S. aureus cell but also causes the cell death (red color). (b) Simulation of pore formation process via the interaction between graphene sheet and phospholipid membrane, including (i) lipid head and graphene flake, (ii) lipid tail and graphene flake, and (iii) both lipid head and tail with graphene flake. (B) SEM images of *E. coli* cultivated on the surfaces of different samples with the deformed morphology indicated by arrows (top); the proposed antibacterial mechanism (bottom).(C) SEM images of Au nanocrystals (top); facet-dependent antibacterial activity: Au nanocrystals with low-index facets (e.g., cubes, octahedra, and rhombic dodecahedra) exhibit excellent antibacterial activity while those with high-index facets (e.g., trisoctahedra and concave cubes) fail to kill the bacteria (bottom).
(A) Reproduced with permission from ref [147]. Copyright 2015 American Chemical Society. (B) Reproduced with permission from ref [148]. Copyright 2019 The Authors. Published by WILEY-VCH Verlag GmbH & Co. KGaA, Weinheim. (C) Reproduced with permission from ref [151]. Copyright 2020 Published by Elsevier B.V. on behalf of Chinese Chemical Society and Institute of Materia Medica, Chinese Academy of Medical Sciences.

nanosheets (CuTCPP–Fe_2O_3 incorporated into a polyethylene glycol matrix to formulate an ointment) [187] and a Cu_2O–ZnO nanofilm (Fig. 3B) [188], in which the heterojunction photocatalysts promote ROS production with high efficiency and the released ions (i.e., Cu^{2+}, Fe^{3+}, Zn^{2+}) exert a synergistic effect with ROS, thereby leading to an excellent photodynamic antimicrobial efficacy of over 92% against diverse bacteria under respective light irradiation conditions. Nevertheless, it is worth mentioning that photodynamic antimicrobial therapy is more effective on Gram-positive bacteria than on Gram-negative bacteria due to differences in their membrane structures, enabling Gram-positive bacteria to be more sensitive to ROS [189].

3.1.2. *Photothermal antimicrobial nanomaterials*

Nanomaterial-based thermoablation of bacteria has emerged as one of the most promising non-resistant antimicrobial strategies in the post-antibiotic era [108,190]. Wang and co-workers designed a versatile bone implant that has sequential photothermal effects—meaning that it delivers antimicrobial therapy (<50 °C) at an early stage and then boosts bone regeneration (40–42 °C) (Fig. 4A) [191]. This design involved the surface modification of a hydroxylapatite scaffold with zinc sulfonate ligand (ZnL_2)-coordinated BPs, wherein the BPs had a photothermal antibacterial effect and the ZnL_2 caused envelope stress on peri-implant bacteria, thus increasing their thermal sensitivity. In a

recent study by Zhang and co-workers [192], macrophage membrane–coated AuAg nanocages acted as efficient bacteria-targeting photothermal antimicrobial agents under NIR irradiation. Moreover, the nanocages' hollow interior structures and porous walls made them favorable nanocarriers for precisely delivering antibacterial drugs to the infected sites.

The photothermal effect of nanomaterials has often been combined with other types of antimicrobial mechanisms to achieve synergistic, enhanced bacteria-killing outcomes. Chang and co-workers recently developed a bacteria-targeting hot-ion therapy for infected wounds [193]. MCS@PDA@GCS NPs of copper-doped mesoporous silica coated with glycol chitosan and polydopamine possessed multiple functionalities, including NIR photothermal conversion and pH-sensitive bacteria targeting via accumulation on bacteria in response to an acidic infection microenvironment. The local hyperthermia and released Cu^{2+} ions produced a "hot ions effect" that could destroy MRSA, *E. coli*, and biofilms in a rapid, effective, and durable manner. Furthermore, researchers have demonstrated the synergistic enhancement effect of ROS and hyperthermia on the antimicrobial activity of photothermal nanomaterial systems, such as Bi_2S_3-$Ti_3C_2T_x$ MXene (Fig. 4B) [132], polydopamine@Au-hydroxyapatite nanorods [194], and arginine-glycine-aspartic acid (RGD)@polydopamine@TiO_2-MoS_2 nanorod arrays [195]. Additionally, physical puncturing, as well as antimicrobial ions, can further resonate with the photodynamic and/or photothermal bacteria-killing capacity [196,197]. It is worth mentioning that light cannot penetrate nontransparent deep tissues, and the tissue-penetrating depth of NIR light is around 1–2 cm, which is a challenge faced by photoresponsive antimicrobial nanomaterials.

3.2. Magnetically responsive antimicrobial nanomaterials

Magnetic responsivity has been increasingly incorporated into antibacterial nanomaterials. For example, Zheng and co-workers developed a magnetically driven magneto-nanozyme system comprising mesoporous iron oxide nanoparticles (MNPs) that can deliver a synergistic therapy for destroying bacteria and biofilms (Fig. 5A) [198]. The MNPs exhibited three functions: (1) catalytic activity to generate ROS, including $^{\bullet}O_2^-$, $^{\bullet}OH$, and $^1O_2$, in the presence of H_2O_2; (2) magnetic maneuverability for directional locomotion and mechanical destruction under a rotating magnetic field; and (3) magnetic hyperthermia under an alternating magnetic field. Due to their synergy, the MNPs demonstrated excellent capabilities for bacterial destruction and biofilm eradication. Because of the local heating effect, magnetic hyperthermia can also be exploited to trigger the on-demand release of both the antimicrobial peptide melittin and the antibiotic ofloxacin from heterogeneous mesoporous silica NP-based supramolecular assemblies for biofilm eradication and infection treatment with high efficiency (Fig. 5B) [199].

In addition, magnetic iron oxide NPs can be used to produce artificial channels in infectious biofilms, thereby enhancing the penetration depth of gentamicin in biofilms and its bacteria-killing efficiency against *S. aureus* [200]. In a recent study, Wu and co-workers [201], developed a multifunctional microwave-excited antimicrobial nanocapturer system, comprising microwave-responsive mesoporous Fe_3O_4–CNT, gentamicin, and phase-changing 1-tetradecanol (at ~40 °C) to control gentamicin release and treat deep tissue infections (Fig. 5C). The nanocapturer was capable of precise bacteria capturing and magnetic targeting; combined with the synergistic effects exerted by precise microwaveocaloric therapy using Fe_3O_4–CNT and the chemotherapy produced by the localized release of gentamicin in the infected sites, the nanosystem could target and eradicate MRSA-infected rabbit tibia osteomyelitis with high efficiency.

3.3. Ultrasound-responsive antimicrobial nanomaterials

Ultrasound has been employed for a wide range of therapeutic applications, such as ultrasound-triggered drug release [202,203], high intensity focused ultrasound (HIFU) surgery [204,205], and focused ultrasound–induced hyperthermia [206,207], as summarized in Fig. 6. The combination of sonosensitizers and ultrasound can trigger a particular sonochemical reaction to generate ROS, which is termed sonodynamic therapy. It is widely accepted that the cavitation effect of ultrasound can cause sonoluminescence and pyrolysis, which contribute to the formation of ROS from sonosensitizers [208,209]. The energy released from ultrasound-triggered cavitation can dramatically increase the local temperature of the ambient environment, thereby further breaking the sonosensitizers apart to produce ROS. As a non-invasive method, sonodynamic therapy can surmount the depth limits of photoactivation due to the inherently high tissue penetration capacity of ultrasound [210].

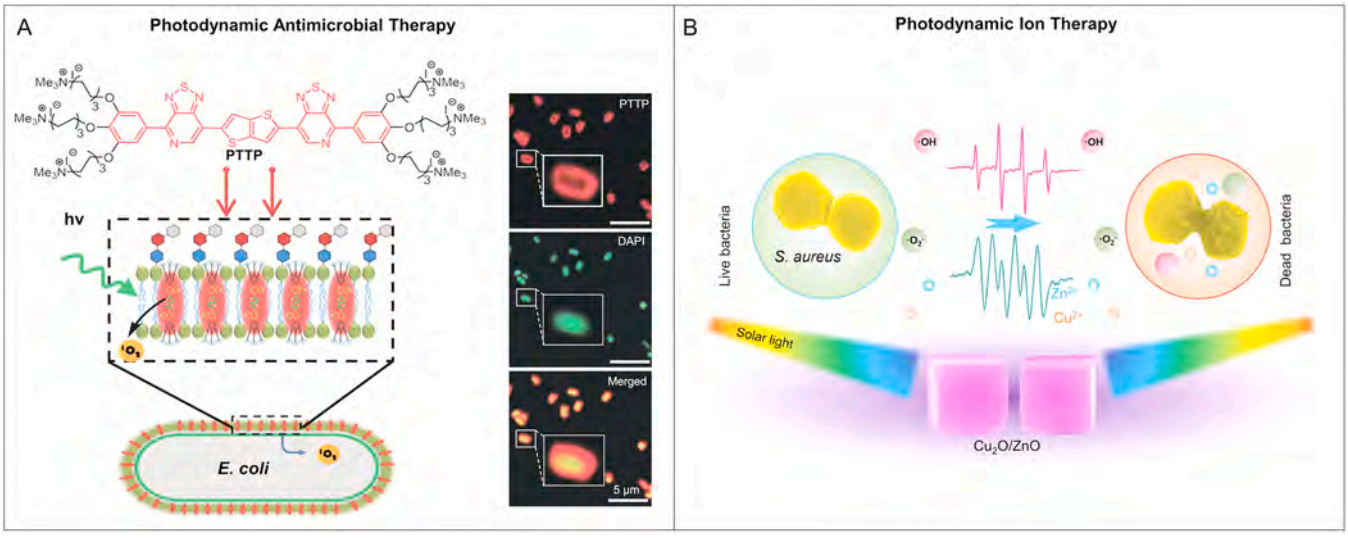

Fig. 3. (A) Schematic image of the insertion of PTTP into a cell membrane and photogeneration of $^1O_2$ through the photodynamic antimicrobial therapy (PDAT) mechanism (left); confocal laser scanning microscopy images of E. coli cells stained with PTTP (right). (B) Scheme of the antibacterial mechanism of photodynamic ion therapy by the synergistic effect of ROS and released Cu and Zn ions.
(A) Reproduced with permission from ref [185]. Copyright 2017 Wiley-VCH Verlag GmbH & Co. KGaA, Weinheim. (B) Reproduced with permission from ref [188]. Copyright 2022 Published by Elsevier Ltd on behalf of The editorial office of Journal of Materials Science & Technology.

Wu and co-workers developed an ultrasound-activated single atom catalyst comprising Au nanorods (NRs)-actuated Pt single atom–doped porphyrin metal−organic framework (HNTM–Pt@Au) and a red blood cell (RBC) membrane, which could effectively treat MRSA-infected osteomyelitis under ultrasound irradiation [211]. The Pt single atoms have strong capabilities of electron trapping and oxygen adsorption, which endows the RBC–HNTM-Pt@Au system with excellent sonocatalytic properties, thereby leading to a remarkable antimicrobial ability with 99.9% efficiency against MRSA after ultrasound irradiation for 15 min. Moreover, the RBC–HNTM-Pt@Au composite can be directionally propelled by ultrasound to dynamically neutralize the toxins secreted by MRSA. As a result, a favorable in vivo anti-infection effect was achieved on the MRSA-infected osteomyelitis model in rat tibias. In addition, ultrasound activation was also shown to induce the formation

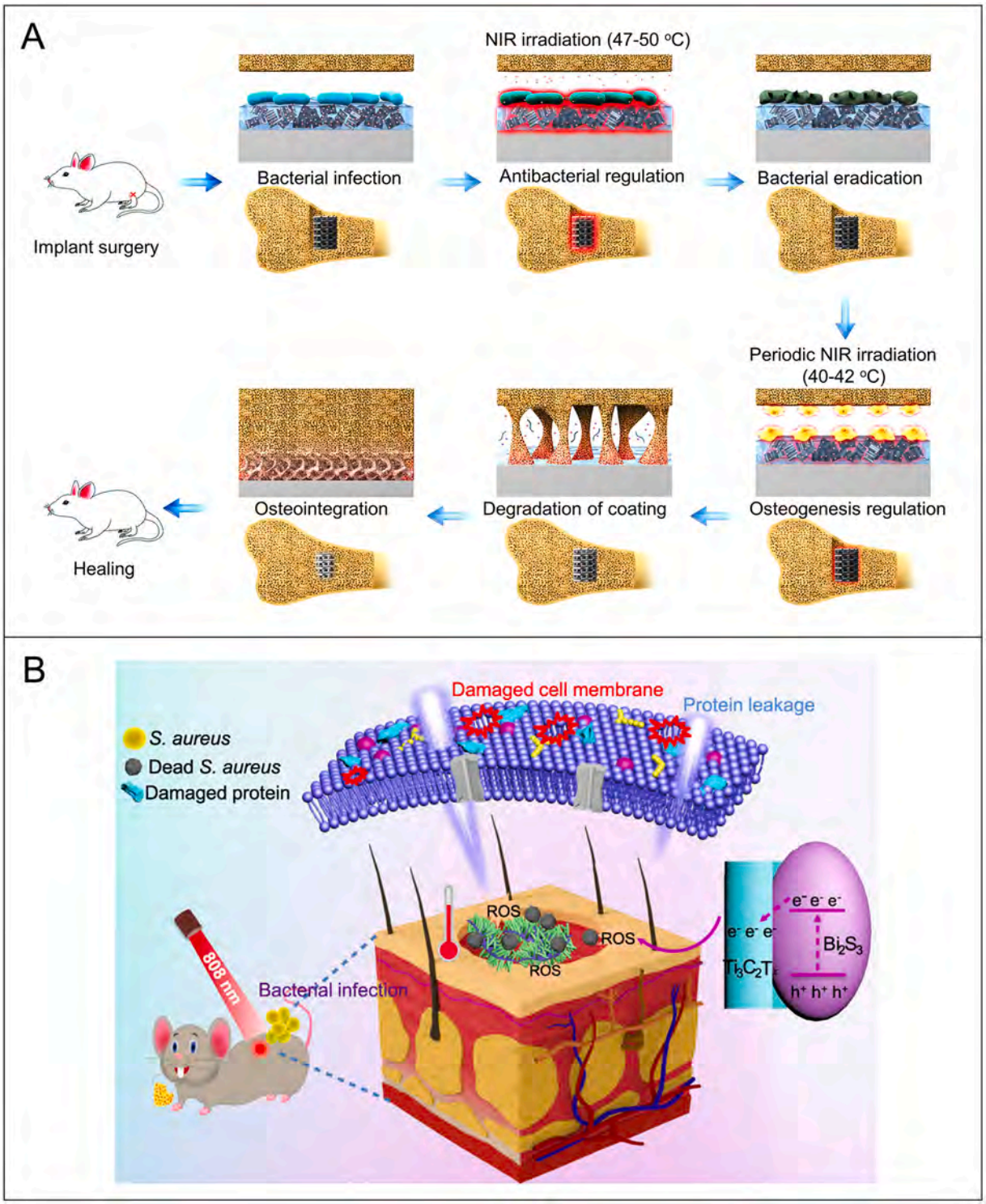

Fig. 4. (A) Schematic illustration of sequential antibacterial and osteogenic regulation by ZnL_2-BPs@HAP integrated bone scaffold upon mild NIR irradiation. (B) Schematic image of Schottky catalyst and photo-excited antibacterial mechanism of $Bi_2S_3/Ti_3C_2T_x$.
(A) Reproduced with permission from ref [191]. Copyright 2021 American Chemical Society. (B) Reproduced with permission from ref [132].Copyright 2021 The Authors.

of ROS from catalysts using rational material designs for ROS-based antimicrobial therapy [212].

3.4. Infection microenvironment–responsive antimicrobial nanomaterials

Considering that pore-forming bacterial toxins are abundant at the sites of infection, these bacterial toxins can serve as effective stimuli for triggering the on-demand release of various antimicrobials from nanovehicles at the infected site. This strategy enables the localized release of antibacterial drugs after targeted arrival at an infected spot to precisely destroy toxin-secreting bacteria while minimizing potential harmful effects on surrounding healthy cells or tissues. Zhang and co-workers reported a strategy based on Au NP-stabilized phospholipid liposomes for the selective delivery of vancomycin to MRSA-infected sites (Fig. 7A) [214]. The surface decoration of liposomes with chitosan-modified Au NPs prevented the fusion of liposomes and undesired release of payload in a non-infectious environment. Once the designed liposomes were in the vicinity of toxin-secreting bacteria, the bacterial toxins were capable of penetrating the liposome membranes and forming pores for the release of the sealed vancomycin. Therefore, this design exerted a precise antimicrobial action localized to the MRSA-infected site.

Due to their high adaptability, bacteria can thrive in a variety of environments in which the low pH is particularly striking, given its correlation with severe infections and its significance for therapy. It is known that certain antibiotics, such as oritavancin, undergo a remarkable loss of killing activity in an acidic environment [215]. In general, bacterial infections are characterized by very low local pH values (~4.5) owing to their hypoxic nature and the inflammation produced at the infectious sites. Researchers have attempted to harness the acidic microenvironment of infectious sites for designing pH-responsive

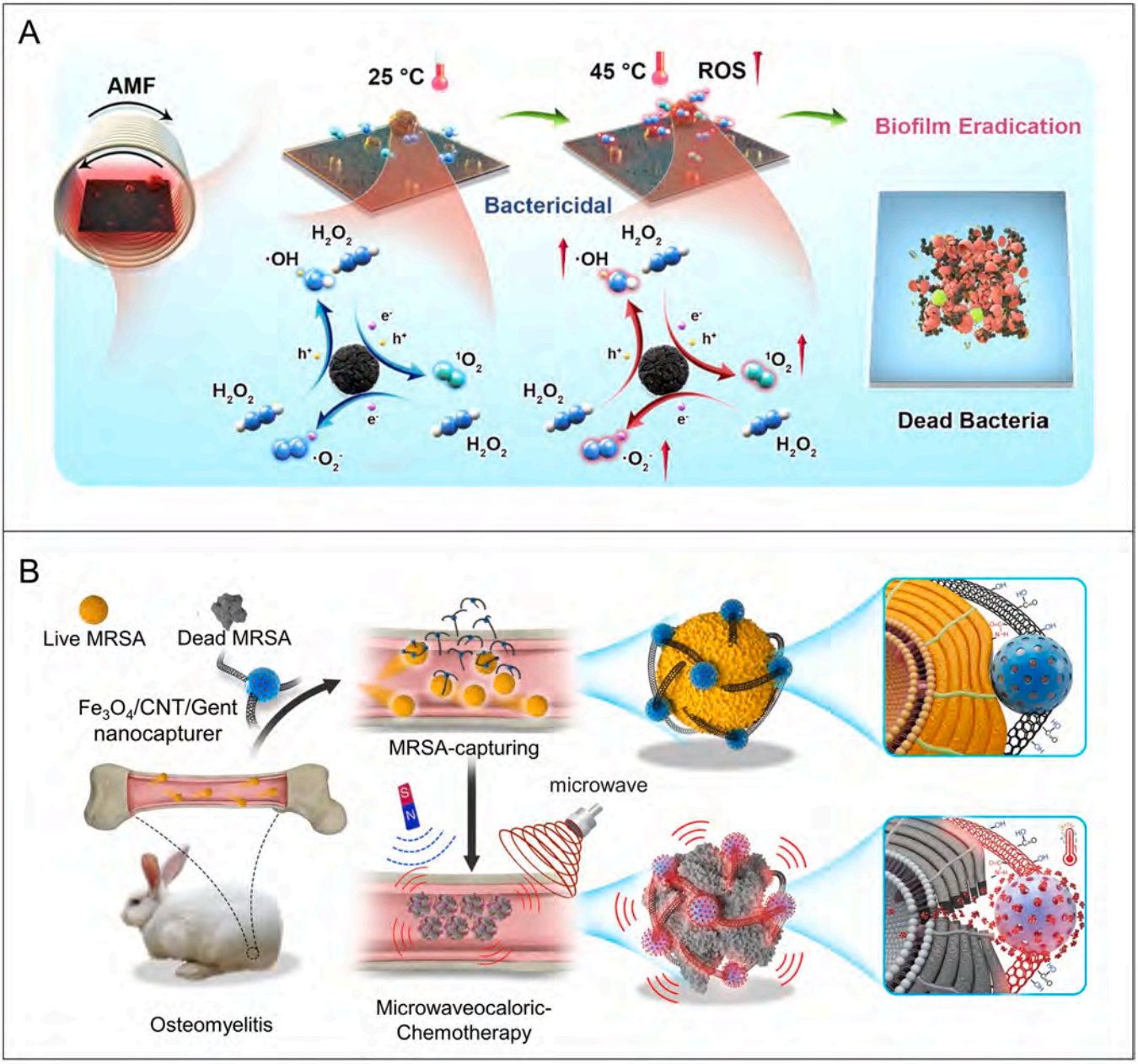

Fig. 5. (A) Biofilm removal by mesoporous iron oxide NPs through electromagnetically actuated magneto-nanozyme mediated synergistic therapy. (B) Microwave-assisted treatment of MRSA-infected osteomyelitisby using Fe_3O_4/CNT/Gent with bacterial capturing, magnetically targeting, and chemotherapy ability. (A) Reproduced with permission from ref [198]. Copyright 2021 The Authors. Published by Elsevier B.V. (B) Reproduced with permission from ref [201]. Copyright 2020 The Authors.

antimicrobial delivery nanosystems. For example, Xu and co-workers designed a type of pH-responsive photodynamic antimicrobial NPs comprising a rose bengal–polydopamine core decorated with polymyxin B and gluconic acid (Fig. 7B) [216]. These NPs were negatively charged at the physiological pH but became positively charged due to pH-sensitive electrostatic interactions in response to an acidic infection environment, which enabled them to adhere efficiently to bacteria. As a result, this design exhibited enhanced photodynamic sterilization efficacy against Gram-negative bacteria and favorable penetration and eradication of bacterial biofilms in an acidic environment and in vivo.

Such pH-responsive and surface charge–switching polymer NPs, such as poly(D,L-lactic-co-glycolic acid)-b-poly(L-histidine)-b-poly(ethylene glycol) [217] and molecularly imprinted polymer nanospheres [218], can also be used to load antibiotics (e.g., vancomycin) for bacteria-targeting precise delivery, mitigating the loss of antibiotic activity in acidic environments and enabling the localized treatment of bacterial infections. Moreover, H_2O_2 is also a local signal at the sites of infection and inflammation [219]. Synthesized metastable $CuFe_5O_8$ nanocubes were also shown to act as intelligent catalysts for Fenton-like reactions and to exhibit pH and H_2O_2 dual responsiveness to an infectious microenvironment for space-selective chemodynamic antimicrobial therapy [220]. In another study, dextran-coated iron oxide nanozymes (peroxidase-like) could respond to the acidic pH of oral biofilms, target the biofilms with high specificity, and activate H_2O_2 for localized bacteria killing and biofilm disruption [221]. Furthermore, the increased expression of enzymes, such as esterase and gelatinase, at the site of bacterial infections [222] can also offer an efficient approach to enzyme-responsive, targeted, and on-demand delivery of various antimicrobials. This has been demonstrated by using core-shell supramolecular gelatin NPs to achieve the controlled release of vancomycin in response to gelatinase at the infectious site [223].

4. Application-oriented designs of active antimicrobial micro/nanorobots

4.1. Propulsion mechanisms for antimicrobial micro/nanorobots

Micro/nanorobots can perform directed locomotion and implement specific on-demand medical tasks via autonomous and/or externally-powered propulsion [224]. They feature a wide range of geometric shapes, motion modes, actuation methods, and functionalities, among which movement is their fundamental ability, especially for executing

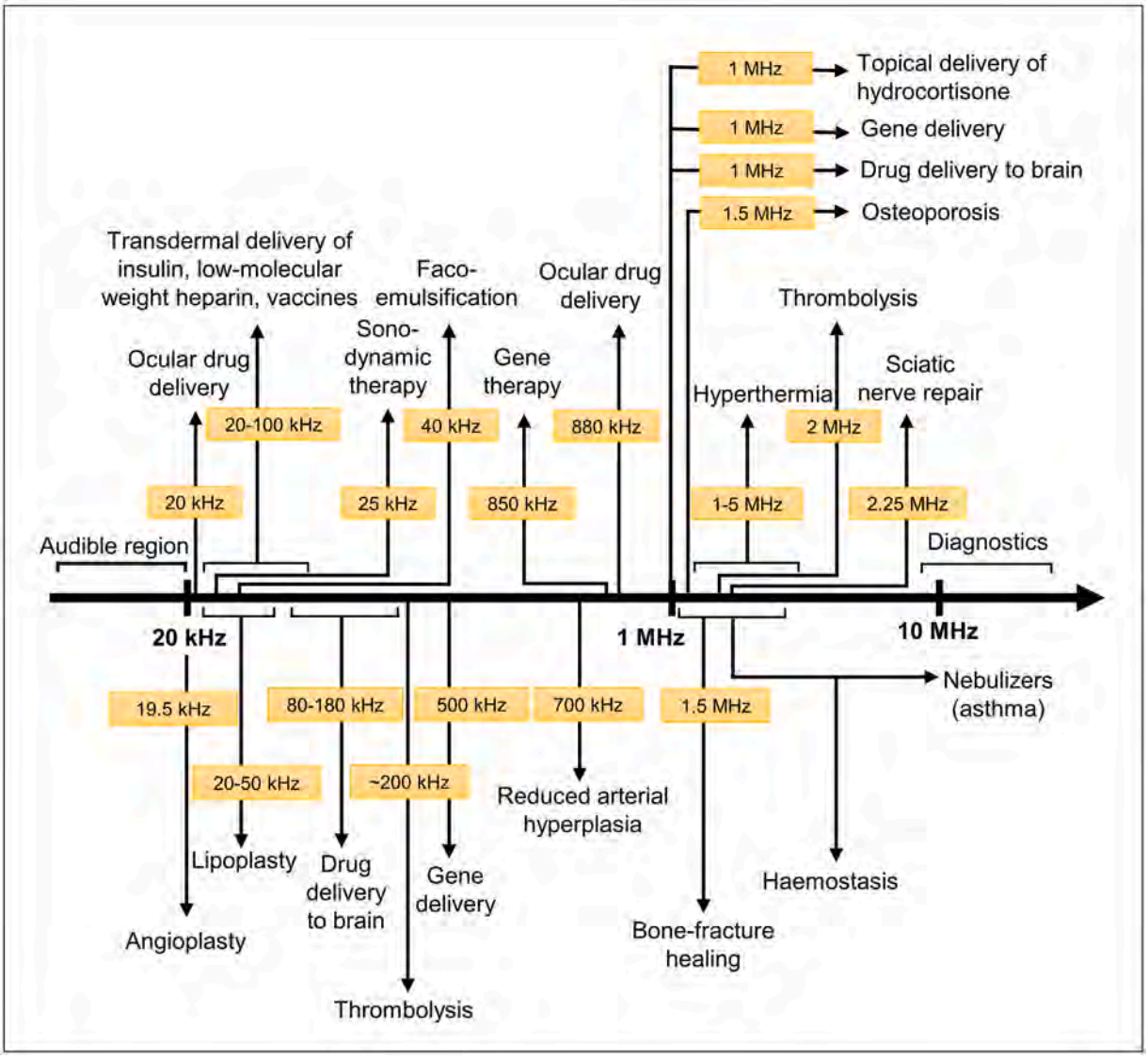

Fig. 6. An illustrative summary of ultrasound frequencies for various medical applications.
Reproduced with permission [213]. Copyright 2005 Nature Publishing Group.

sophisticated medical tasks. In the context of medical applications, the advantages and limitations of conventional actuation methods, including chemical propulsion (self-propulsion), externally powered propulsion (magnetic, ultrasound, light, and electric actuation), biohybrid propulsion, and combined propulsion, are summarized as follows:

(1) Chemical propulsion (self-propulsion) [225]: self-propulsion requires the use of chemical fuels and catalytic engines that convert fuel energy into propulsive forces (e.g., bubbles, chemical gradients, etc.). The chemical fuels include exogenous fuels (e.g., H_2O_2 or $NaBH_4$) and endogenous fuels (e.g., glucose or urea). Most exogenous fuels are cytotoxic, which may limit their medical applications. In contrast, enzyme-catalyzed chemical reactions using endogenous fuels are biocompatible. They do not require external actuation systems and can produce high movement speeds, although a continuous supply of fuel is needed. In addition, self-propelled micro/nanorobots usually exhibit random locomotion and a lack of directionality.

(2) Magnetic propulsion [26]: as a non-invasive method, magnetic actuation holds great promise for driving the locomotion of micro/nanorobots with good controllability and navigation. Magnetic actuation can be produced by rotating, oscillating, or on–off magnetic fields. These can offer high penetration depth in tissue / the body and multiple movement modes for adapting to diverse environments. Remote, precise, and multi–degree of freedom (DoF) motion control can be achieved. Such actuation is safe and biocompatible with the human body. Nevertheless,

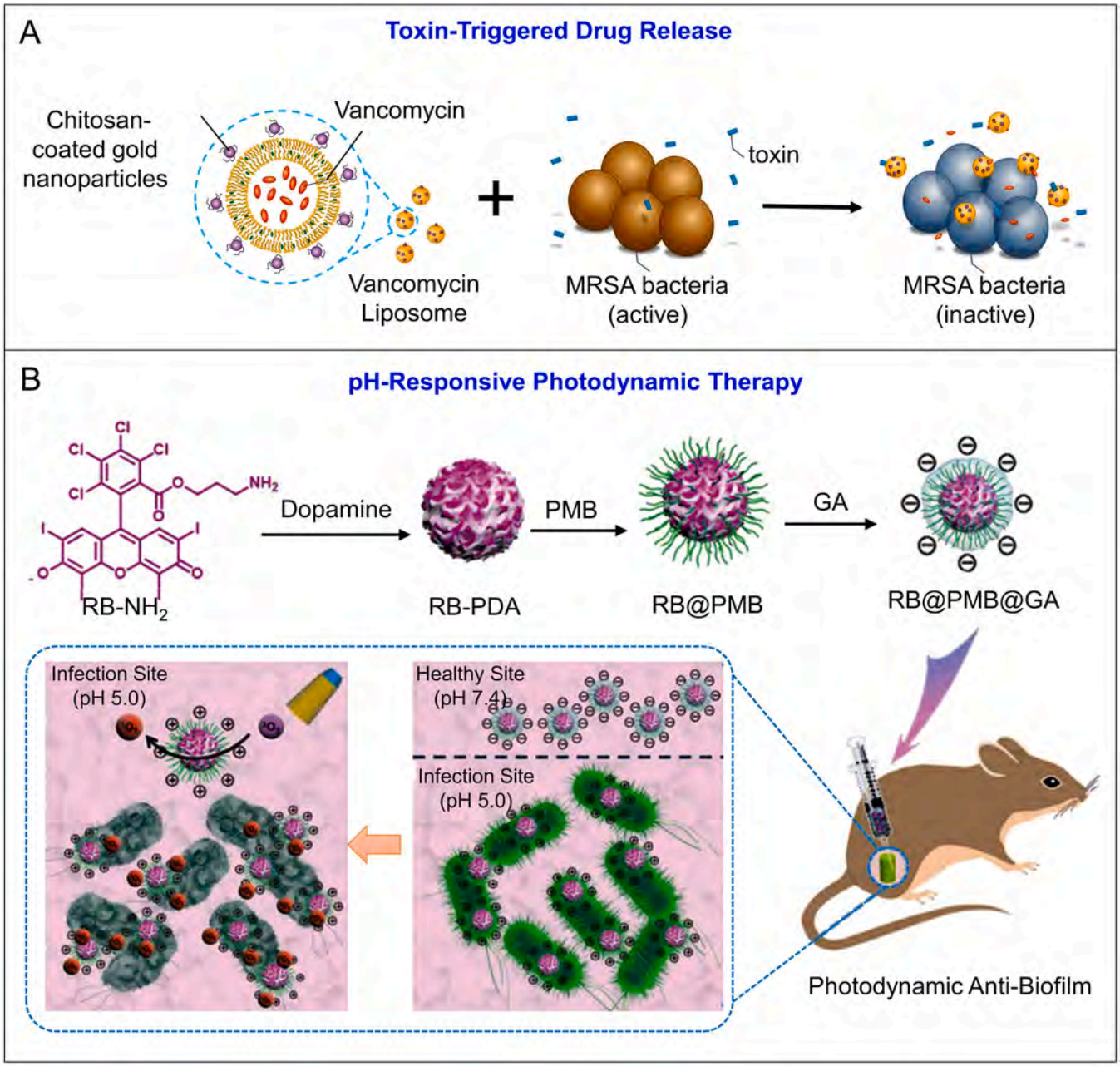

Fig. 7. (A) Scheme of bacterial toxin-induced drug release from gold nanoparticle-stabilized liposomes to kill toxin-secreting bacteria. (B) Fabriction of pH-sensitive photodynamic nanoparticles for enhanced penetration and antibacterial efficiency in biofilms.
(A) Reproduced with permission from ref [214]. Copyright 2011 American Chemical Society. (B) Reproduced with permission from ref [216]. Copyright 2021 Wiley-VCH GmbH.

driving magnetic microrobots at scales of several microns is still a challenge owing to scaling laws.

(3) Ultrasound propulsion [226]: this actuation method can provide a high tissue penetration depth in the body. Both the shape and density of materials can influence the locomotion of ultrasonic micro/nanorobots, thereby offering a wide selection of materials for design and fabrication. This type of propulsion can trigger a localized aggregation effect with fast response. Most importantly, ultrasonic fields with suitable intensities unusually have negligible side effects on organs and tissue.

(4) Light propulsion [227]: the size of the light beam can be tuned to the submicrometer scale. This driving method can provide selective wavelength and multi-beam radiation to produce signals with high spatial and temporal resolution for accomplishing specific motion control. In this way, light propulsion may enable rapid, precise, and multi-DoF locomotion.

(5) Electric propulsion [228]: the electrical actuation method can provide contact-free propulsive forces for micro/nanorobots. Such propulsive forces include electrophoresis (formed by direct current (DC) fields), dielectrophoresis (formed by nonuniform fields), electroosmosis, and induced-charge electrophoresis (formed by alternating current (AC) fields).

(6) Biohybrid propulsion [229,230]: this driving strategy combines various actuation methods with motile viable cells (e.g., sperms, bacteria, microalgae, etc.) for improved control over the directionality and responsiveness to different stimuli.

(7) Combined propulsion [226,231]: this actuation method combines two or more of the above driving strategies to enhance propulsive thrust and execute stimuli-responsive specific tasks. It mainly includes field-driven biohybrid micro/nanorobots and fully synthetic micro/nanorobots.

In this context, Table 4 summarizes several representative propulsion mechanisms for micro/nanorobots. For more details on these different actuation methods for medical micro/nanorobots, the readers are referred to the excellent reviews [26,27,34,228,232,233].

4.2. Antimicrobial micro/nanorobots for actively capturing bacteria

Magnetotactic bacteria, including axial and polar types, are able to swim rapidly along local geomagnetic field lines due to their sensitivity to magnetic fields [301]. The magnetotaxis originates from the organelle magnetosome (comprising Fe_3O_4 or Fe_3S_4) of magnetotactic bacteria [302]. Polar magnetotactic bacteria, such as MC-1 and MO-1, can swim only when directed by the magnetic field. Therefore, they are more suitable for creating bacterial microrobots (bacteriabots) owing to their own driving force and rapid responsiveness to magnetic fields, which enable high-speed motion and external control. For example, a uniform magnetic field slightly stronger than the geomagnetic field can be employed to control their locomotion. Song and co-workers developed pathogen-separating microrobots by binding the magnetotactic bacteria MO-1 with rabbit anti-MO-1 polyclonal antibodies [303]. The MO-1 microrobots could efficiently attach to, transport, and separate *S. aureus* under the actuation and navigation of a rotating and a uniform magnetic field. Bacterial infections can threaten human health because they possess many virulence factors, such as endotoxins, exotoxins, and capsules. Therefore, novel, highly effective tactics are urgently required to capture and detect pathogens for food safety, water quality, medical examinations, and counter-terrorism [304]. To this end, specific pathogen recognition and binding abilities can be integrated with the functional designs of antimicrobial micro/nanorobots. For example, lectins are glycoproteins that can recognize carbohydrate constituents on bacterial surfaces by selectively binding to the mono/oligosaccharide components of cell walls [305]. By functionalizing the outer surface with concanavalin A (a lectin bioreceptor), Wang and co-workers designed self-propelled Au-Ni-polyaniline (PANI)–Pt microtubular engines to isolate *E. coli* (Fig. 8A) [306]. The PANI–Pt bilayer microtube of microengines was fabricated via template-assisted electrodeposition, and their outer Ni–Au layers were deposited via e-beam vapor deposition for surface functionalization and magnetic navigation. Propelled by Pt-catalyzed O_2 bubbles, these microengines can perform on-the-fly selective capture of *E. coli* in the presence of H_2O_2 fuel (7.5% [w/v]) in a direct, label-free optical visualization manner. After that, a triggered release of the captured *E. coli* could be achieved in a low-pH glycine solution capable of dissociating the lectin–bacteria complex.

Although micro/nanorobots can be functionalized with diverse bioreceptors to endow them with the specific recognition capacity of target biomolecules or pathogens, their fate and efficacy are largely dependent on the synthetic nanomaterials they are made of, which are highly susceptible to biofouling or immune phagocytosis in the human body [163], which may impede their circulation and final efficiency. To address these limitations, inspired by nature, the native components of circulating cells (e.g., erythrocytes, leukocytes, platelets, etc.) can be integrated with the material designs of antibacterial micro/nanorobots to inherit desired biological functions from the parental cells, such as immune escape, pathogen interaction, and toxin neutralization [307,308]. Platelets have been widely exploited for developing drug delivery systems [309]. Recently, Wang and co-workers reported the development of platelet-camouflaged nanorobots for the capture and separation of biological threats, such as toxins and pathogens (Fig. 8B) [310]. These functional nanorobots were created by cloaking magnetic Ni–Au@Pd helical nanomotors with human platelet membranes. This design enabled the nanorobots to inherit functional proteins from human platelets, exhibit platelet-like behaviors, and carry out efficient propulsion in whole blood within the rotating magnetic field over a long period of time, avoiding significant biofouling in blood. Collectively, these nanorobots could efficiently bind to and isolate the Shiga toxin and *S. aureus*. RBC membranes also have the capability to target and absorb toxins [307,311], and platelet membranes possess the ability to adhere to pathogens [312]. For the purpose of biodetoxification, the same research group also achieved concurrent removal of bacteria and toxins by designing dual cytomembrane-functionalized nanorobots (Fig. 8C) [313]. Au nanowires were coated with hybrid RBC and platelet (PL) membranes to obtain ultrasound-propelled nanorobots (RBC-PL-robots) with inherited biological properties, such as attaching and binding to pathogens, neutralizing pore-forming toxins, and resisting biofouling in whole blood, thereby leading to the fast and efficient prolonged ultrasonic propulsion of the RBC-PL-robots in blood. As a proof-of-concept study, MRSA USA300 and pore-forming toxins (e.g., the α-toxin, Panton–Valentine leucocidin, and γ-toxin secreted by MRSA USA300) were tested as models to demonstrate that the RBC-PL-robot could simultaneously isolate and remove these biological threats with high efficiency. In addition, visible light–driven star-shaped $BiVO_4$ micromotors were shown to seek and attach to yeast cell walls and exhibited photocatalytic fungicidal activity [270].

4.3. Antimicrobial micro/nanorobots for actively eliminating bacteria

Traditional approaches for the destruction of pathogens involve the use of multiple antimicrobials but may face low efficacy when treating antibiotic-resistant pathogens and biofilm infections. Biomacromolecules or materials with intrinsic antimicrobial activity can be incorporated into micro/nanorobots for bacteria-killing purposes. For example, lysozyme is a glycoside-hydrolase enzyme with a potent antibacterial function that degrades the cell walls of bacteria [314,315]. However, the use of free lysozyme alone to destroy bacteria is often limited by its poor stability and reusability. Therefore, various solid materials (e.g., nanoparticles) have been incorporated to enhance their stability and reusability [316,317]. Nevertheless, such static lysozyme-loaded platforms may suffer from the accumulation of dead bacteria on their surfaces, thereby causing a decrease in their enzymatic activity. To tackle this issue, Wang and co-workers developed

Table 4
Summary of representative propulsion mechanisms for micro/nanorobots.

Propulsion mechanisms		Characteristics	Examples	Refs
Chemical propulsion	Bubble-propelled micro/nanomotors	Catalysts (e.g. Ag, Pt, MnO_2) with asymmetric distribution decompose surrounding chemical fuels (e.g·H_2O_2, N_2H_4, $NaBH_4$) into gas bubbles (e.g. O_2, H_2) to gain kinetic energy.	Cu-Ag segmented tubular micromotors, or Ag-zeolite micromotors	[234,235]
			Fe-Pt rolled-up tubular micromotors, Pt-loaded polymeric stomatocyte-like nanomotors, or Janus Pt-coated mesoporous silica nanomotors	[236–238]
			MnO_2-based micromotors	[239,240]
		Active metals (e.g. Mg, Zn, Fe) or compounds (e.g. $CaCO_3$) react with acids (e.g. HCl) or water to produce gas bubbles (e.g. H_2, CO_2) to obtain propulsive force.	Mg-based micromotors	[241–243]
			Zn-based micromotors	[244–246]
			Fe nanomotors	[247]
			Ti-coated Al-Ga binary alloy Janus micromotors	[248]
			$CaCO_3$-based micromotors	[249,250]
	Enzyme-powered micro/nanomotors	Urea serves as fuel and urease catalyzes the decomposition of urea into CO_2 and NH_3 (urea → CO_2 + NH_3).	Urease-powered non-Janus polystyrene and SiO_2 @polystyrene micromotors, polydopamine microcapsule motors, or mesoporous silica nanomotors	[251–253]
		H_2O_2 serves as fuel and catalase catalyzes the decomposition of H_2O_2 into H_2O and O_2 bubbles (H_2O_2 → H_2O + O_2).	Catalase-powered tubular, Janus, or submarine-like micro/nanomotors	[254–256]
		Triglyceride (e.g. triacetin and tributyrin) act as fuel and lipase catalyzes the reactions: triacetin → acetic acid + glycerol; tributyrin → butyric acid + glycerol.	Lipase-powered mesoporous silica nanomotors	[257,258]
		Proteins/peptides serve as fuels and trypsin cleaves peptide bonds of arginine and lysine to act as complementary motors.	Trypsin-powered Janus microswimmers	[259]
		Acetylcholine acts as fuel and acetylcholinesterase catalyzes the reaction: acetylcholine → acetic acid + choline	Acetylcholinesterase-powered silica microcapsule motors	[260]
		Glucose acts as fuel and glucose oxidase (GO_x) catalyzes the reaction: D-glucose + H_2O + O_2 → D-gluconic acid + H_2O_2.	Glucose oxidase (GO_x)-powered nanoflask motors	[261]
	Reaction heat-driven micro/nanomotors	Au NPs catalyze the reaction: $Fe(CN)_6^{3-} + S_2O_3^{2-} \rightarrow Fe(CN)_6^{4-} + S_4O_6^{2-}$. The reaction heat produces an asymmetric local temperature of solvent surrounding Janus NPs and leads to self-thermophoresis locomotion.	Janus DNA-modified Au plasmonic nanomotors	[262]
External-powered propulsion	Magnetic actuation	(1) Fuel-free, remote spatiotemporal control, programmability, reconfigurability, recyclability; (2) Comprising soft (Fe_3O_4/SPIONs, Ni, Co, etc) and hard (NdFeB, FePt, SmCo, etc) magnetic materials and composites	Helical, flexible, wire-like, or biohybrid magnetic micro/nanorobots	[26,229,232]
	Ultrasound actuation	Acoustic actuation due to ultrasonic forces applying to suspended micro/nanoparticles within an ultrasound field	Ultrasound-propelled tubular, rod/wire/capsule/bullet/cup/shell-shaped, or other asymmetric micro/nanorobots	[226]
	Light driving	NIR tissue penetration depth of about 1–2 cm (with minimal absorption), propulsion due to local self-thermophoresis, reversible on/off motion, ease of localized stimulation	NIR-driven Au@ $(PAH/PSS)_{20}$-Pt microengines, Au-coated Janus mesoporous silica nanomotors, or carbonaceous nanobottle motors	[263–266]
		Propulsion due to local self-thermophoresis	Laser-driven Janus Au-capped polystyrene microswimmers	[267,268]
		Photocatalytic micro/nanomotors, fuel-free, locomotion due to self-electrophoresis of semiconductor micro/nanoparticles or between semiconductor-based heterojunctions	Visible light-driven TiO_2-Au nanocap motors, $BiVO_4$ micromotors, sulfur- and nitrogen-containing porous donor-acceptor polymer micromotors, core-shell $Zn_xCd_{1-x}Se$-Cu_2Se-Pt alloy nanowire motors, BiOI-Au Janus micromotors, or Si-TiO_2 nanotree microswimmers	[269–274]
			UV light-driven AgCl micromotors (self-diffusiophoresis), TiO_2 micromotors and micropumps, isotropic TiO_2-Pt/ZnO/CdS/Ag_3PO_4 micromotors, Janus Pt@Si-TiO_2 nanotree microswimmers, or TiO_2 nanotube microengines	[275–279]
	Electrical actuation	Self-dielectrophoresis, induced charge electrophoresis, electrohydrodynamic flows, asymmetric formation of gas bubbles (e.g. O_2, H_2) in an electric field	Electrically powered microspinners comprising SU-8 body and Au patches, conducting objects (e.g. glassy carbon sphere, stainless steel bead) of sizes from hundreds of micrometers to centimeters, DNA-based nanorobotic arm	[280–282]
Biohybrid propulsion	Bacteria-driven microswimmers	Propulsion due to the swimming bacteria	Magnetic NPs-conjugated E. coli MG1655, DOX/SPIONs co-loaded and E. coli MG1655-binding erythrocyte microswimmers, or nanoliposomes-binding Magnetococcus marinus MC-1 magnetotactic bacteria	[35,283,284]
	Microalgae-driven microswimmers	Propulsion due to the swimming microalgae	$(PAH/PSS)_5$-deposited magnetic polystyrene microbeads-binding green microalgae Chlamydomonas reinhardtii (C. reinhardtii), chitosan-coated iron oxide NPs-binding C. reinhardtii, or Tb^{3+}-incorporated C. reinhardtii	[285–287]
	Sperm-driven microrobots	Propulsion due to the motile sperm	Rolled-up Ti-Fe microtube-trapped sperm, magnetic tubular tetrapod-trapped sperm, streamlined and horned microcap-trapped sperm	[29,288,289]

(*continued on next page*)

Table 4 (*continued*)

Propulsion mechanisms		Characteristics	Examples	Refs
Combined propulsion	Light driving + magnetic control	Multiwavelength responsive from UV to visible (even infrared) light, wavelength steerable, magnetic steering	Visible light-driven magnetic Janus CoO-TiO_2 microswimmers	[290]
	Bubble propulsion + light control	Motion control through light on/off switch	Bubbled-propelled UV-powered Pt@Au@TiO_2 Janus microsphere motors, or bubbled-propelled visible light-controlled Ti-Cr-Pt tubular microengines	[291,292]
	Bubble propulsion + ultrasound irradiation	Motion control by applying ultrasound (e.g. stop/go motion, speed control, and direction switch)	Pt tubular micromotors, or PEDOT-Ni-Pt tubular microengines	[293,294]
	Ultrasound propulsion + magnetic steering	Fuel-free, multi-mode propulsion and switch, magnetic navigation, ease of manipulation at acoustic pressure nodes, reversal of motion direction, digital speed regulation, controlled aggregation and separation	Cup-shaped HfO_2-Ni bubble micro/nanoswimmers, bisegment Au nanorod and Ni-coated Pd nanohelix motors, or superparamagnetic beads	[295–297]
	Light driving + ultrasound actuation	Control over propulsion mode, motion speed and direction, and swarm and collective behavior (e.g. aggregation/separation)	Au@TiO_2 and TiO_2 @Au microbowl motors, or Pd/Ag/Au/polypyrrole nanorod, SiO_2-coated Au nanowire, and SiO_2 microrod motors	[298,299]
	Electric actuation + light driving	Photocatalytic self-electrophoresis, induced charge electrophoresis, synergistic speed enhancement by light and electric field	UV- and AC electric-driven TiO_2-Pt Janus micromotors	[300]

ultrasound-propelled antibacterial nanomotors by combining porous Au nanowires with lysozyme, which can cleave the glycosidic bonds of the peptidoglycans existing in bacterial walls (Fig. 9A) [318]. Ultrasound propulsion can enable the rapid locomotion of these nanomotors, promote lysozyme–pathogen interactions, prevent the aggregation of dead pathogens on the nanomotors' surfaces, and lead to their largely reinforced antimicrobial activity. The nanoporosity endowed these nanomotors with a large specific surface area and offered them a notably higher lysozyme loading ability than that of nonporous Au nanowires, which further enhanced their antimicrobial properties. Using Gram-positive *M. lysodeikticus*, a fast bacteria-killing effect was demonstrated with an efficiency of 69–84% in 1–5 min. This lysozyme modification strategy was also used on self-propelled biohybrid rotifer microcleaners for antimicrobial treatment [319].

Inorganic antimicrobial cations, such as Ag^+ and Cu^{2+}, can be immobilized into ion-exchangeable materials, such as nanoclays and zeolites. Based on this, the same group also developed antimicrobial cubic zeolite-based Janus micromotors by incorporating Ag^+ ions into an aluminosilicate zeolite framework through ion exchange treatment to replace Na^+ ions; next, a Ag layer was deposited to obtain a uniform half-shell coating on the Ag^+-exchanged zeolite cubes [235]. Such a micromotor design can integrate the prominent adsorption ability of zeolites with the excellent catalytic and antibacterial capacities of Ag^+ ions. The presence of Ag catalysts can propel the autonomous locomotion of Ag-zeolite micromotors by catalyzing the decomposition of H_2O_2 fuel into O_2 bubbles. Moreover, the excellent antimicrobial capability of Ag^+ ions were shown to synergize with the fast motion of Ag-zeolite micromotors to facilitate the direct contact of *E. coli* with the micromotors and Ag^+ ions, which resulted in a potent on-the-fly antimicrobial capacity.

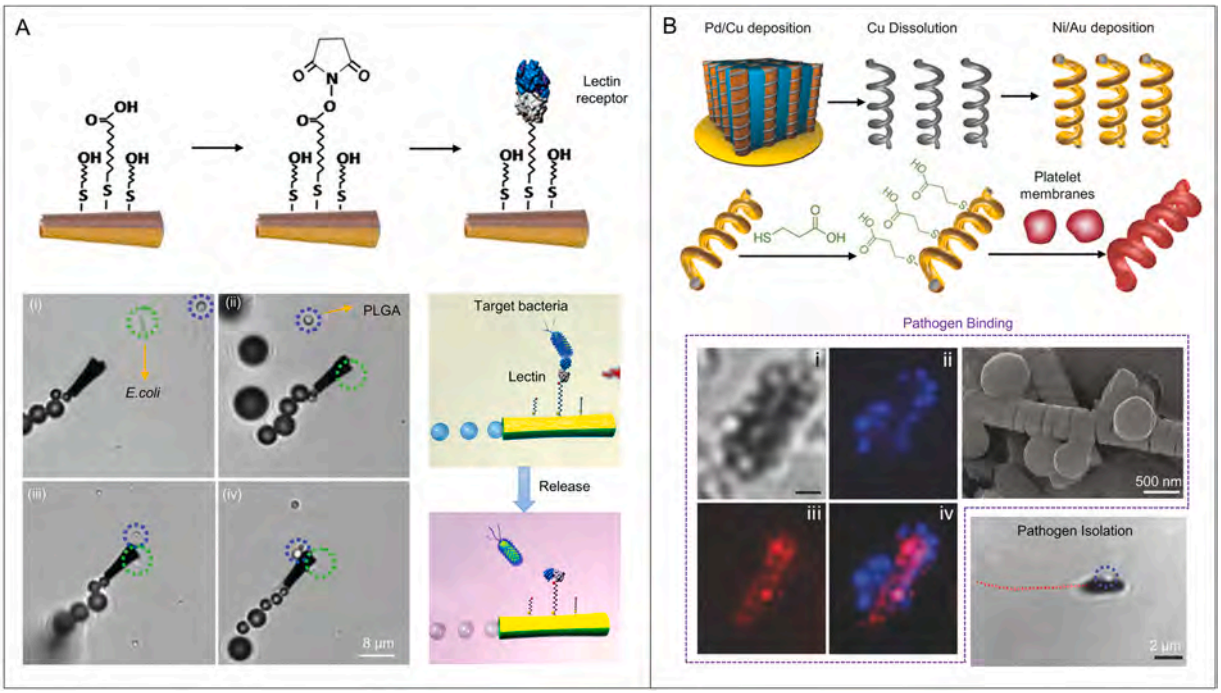

Fig. 8. (A) Schematic image of fabrication procedure of lectin-modified microengines and their applications in selective pick-up, delivery, and release of the target bacteria. (B) Fabrication of platelet-membrane-cloaked helical nanomotors and their applications in pathogen binding and isolation.
(A) Reproduced with permission from ref [306]. Copyright 2012 American Chemical Society. (B) Reproduced with permission from ref [310]. Copyright 2017 WILEY-VCH Verlag GmbH & Co. KGaA, Weinheim.

In addition to metal ions capable of killing bacteria, antimicrobial metal nanomaterials (Ag^0 NPs and Cu^0 NPs in particular) can be also integrated with the structure and composition design of micro/nanorobots. For example, nanosized Ag materials can be obtained by different fabrication methods such as physical vapor deposition (e.g. magnetron sputtering, electron beam evaporation, thermal evaporation), electrochemical deposition (e.g. template electrodeposition), and wet chemical synthesis. To combine the catalytic and antimicrobial activities of Ag NPs, Dong and co-workers reported the fabrication of bimetallic Ag@Mg Janus micromotors via the thermal evaporation of Ag coating on the partial surface of Mg microsphere for bactericidal purpose [320]. Due to the Janus structure design, the movement of Ag@Mg micromotors can be actuated in two opposite directions by O_2 bubbles (from the surface Ag shell, Ag-H_2O_2 reaction) and H_2 bubbles (from the interior Mg core, Mg-H_2O reaction), thereby having two types of engines for bubble-propelled motion control. Owing to the antimicrobial activity of Ag, these self-propelled Ag@Mg Janus micromotors can effectively kill E. coli in solution. Furthermore, such autonomous Ag@Mg Janus micromotors can destroy *E. coli* at a much faster rate (approximately 9 times of that of static counterpart), which demonstrated the superiority of the active antimicrobial Ag@Mg Janus micromotors.

Magnetic micro/nanorobots also possess excellent motion controllability in magnetic fields; when loaded with Ag NPs, micro/nanorobots can be magnetically actuated and navigated to destroy the target bacteria in contact mode. For instance, Pané and co-workers developed an efficient approach to target and kill pathogens using Ag-coated magnetic nanocoils (Fig. 9B) [321]. Pd nanocoils were fabricated by electrodeposition and selective dealloying, followed by the deposition of Ni and Ag layers for magnetic actuation and antimicrobial function, respectively. The synthesized Pd-Ni-Ag nanocoils exhibited high-efficiency antibacterial activity against MDR *E. coli* and MRSA at a low concentration and for a short treatment time. Moreover, it was demonstrated that their bacteria-killing capacity resulted from damage to the bacterial membranes caused by the direct contact between the pathogens and the Pd-Ni-Ag nanocoils. Together with their low cytotoxicity tested on fibroblasts and precise magnetic motility, the Pd-Ni-Ag nanocoils can serve as promising candidates for fighting against MDR bacteria [321].

Recently, Liu and co-workers developed Ag-modified and Fe_3O_4 NPs-containing graphene-based helical micromotors actuated by a rotating magnetic field to achieve excellent antibacterial efficiency against *E. coli* [322]. Liquid metals have also demonstrated great potential in biomedical fields, such as antimicrobial applications [323,324]. For example, Ga^{3+} ions were shown to have strong antimicrobial ability [325]. Nevertheless, their antibacterial efficacy is limited by the passive diffusion of Ga^{3+} ions from the Ga NPs or compounds. To solve this issue, H_2 bubble-propelled Ga@Zn Janus micromotors that release antimicrobial Ga^{3+} ions were developed to kill H. pylori [326]. Graphene-based materials have also been shown to possess excellent antimicrobial property [96,327]. Mei and co-workers developed rolled-up graphene-Ti-Cr-Pt tubular micromotors propelled by the Pt-catalyzed O_2 bubbles in H_2O_2 fuel for antibacterial activity against E. coli and S. aureus [328].

Classical antimicrobials, such as antibiotics and antimicrobial peptides, can also be integrated into the component design of micro/nanorobots to obtain active antibacterial function. Wang and co-workers developed chitosan-clarithromycin@PLGA-TiO_2-Mg Janus micromotors for treating gastric bacterial infections (Fig. 10A) [329]. To fabricate the Janus micromotors, the Mg microparticles (which formed the cores of the micromotors and had an average size ~20 μm) were first asymmetrically coated with a thin layer of TiO_2 via atomic layer deposition, leaving a small aperture for contact with acid fuel. The TiO_2 layer also serves as a shell scaffold to maintain the spherical shape and aperture size of the Mg-based micromotors during bubble propulsion, thereby resulting in consistent and sustained operation. Subsequently, the TiO_2-Mg Janus microparticles were coated with a clarithromycin-loaded PLGA film, followed by the deposition of a thin outer layer of chitosan (thickness ~100 nm) to ensure the effective electrostatic adhesion of the Mg-based micromotors to the mucosal layer of the gastric wall while also protecting the clarithromycin-loaded PLGA layer. Due to the spontaneous Mg-acid reaction to generate H_2 microbubbles, the Mg-based micromotors could be efficiently propelled in the stomach fluid [330]. The small aperture enabled the slow reaction and gradual dissolution of the Mg core, thereby resulting to a prolonged ~6 min lifetime of the Mg-based micromotors. Using an *Helicobacter pylori* (*H. pylori*)-infected mouse stomach model, the propulsion of chitosan-clarithromycin@PLGA-TiO_2-Mg Janus micromotors in gastric fluid was shown to efficiently facilitate clarithromycin delivery and remarkably decrease H. pylori burden in the mouse stomach compared to passive antibiotic carriers and without significant toxicity. With a similar design strategy, onion-like parylene-Ag^+@PVP-L-serine-Mg microtrap vehicles were created for the long-range chemotactic attraction, capture, and killing of motile pathogens, such as *E. coli* [331]. A variety of

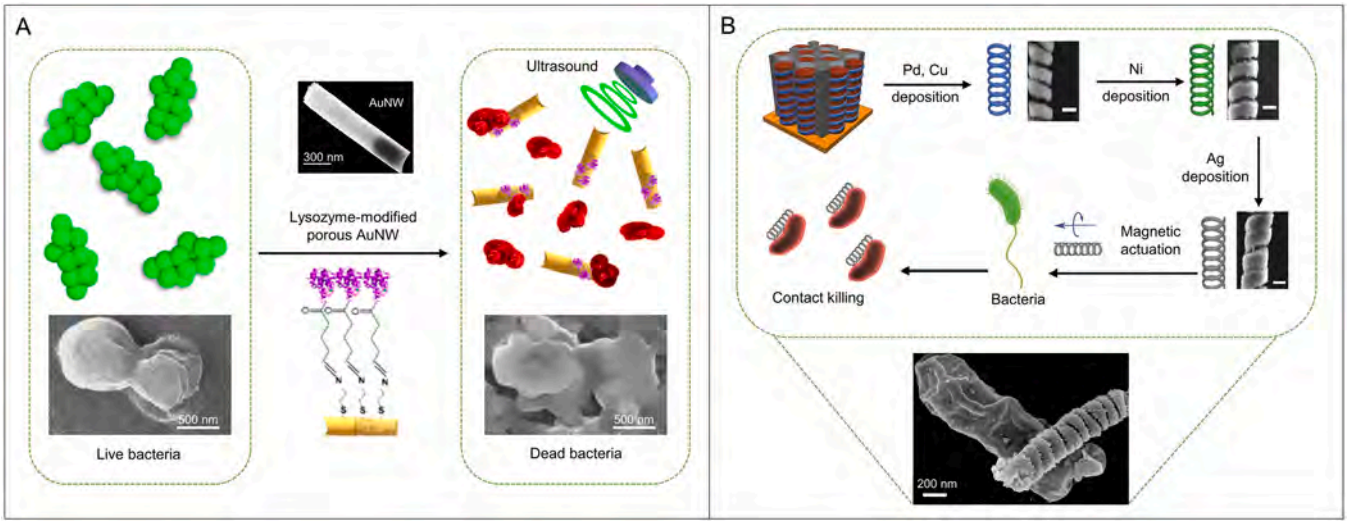

Fig. 9. (A) Ultrasound-driven nanorobots fumctionized with lysozyme to achieve efficient antibacterial activity. Scar bar: 500 nm. (B) Fabrication of Pd/Ni/Ag nanorobot and their antibacterial activity via direct contact killing mechanium with the assistance of magnetic atuation and navigation.
(A) Reproduced with permission from ref [318]. Copyright 2015 American Chemical Society. (B) Reproduced with permission from ref [321]. Copyright 2015 WILEY-VCH Verlag GmbH & Co. KGaA, Weinheim.

microalgae, plant pollen, and fungal spores can be exploited as natural materials or templates to fabricate antibacterial micro/nanorobots. For example, Zhao and co-workers recently developed polydopamine (PDA)-coated, vancomycin-grafted carbonized sunflower pollen grain microrobots for capturing and killing S. aureus with high efficiency [332]. Finally, antimicrobial peptides exhibit broad-spectrum antibacterial activity and can quickly kill target pathogens. Cationic antimicrobial peptides, such as LL-37 and K7-Pol, can also be incorporated into urease-powered hollow silica micro/nanomotors for combating drug-resistant bacterial infections [333].

Stimuli-responsive antimicrobial agents or materials hold great promise for the development of micro/nanorobots with an active on-demand antibacterial capacity. Photosensitizer-based photodynamic antimicrobial therapy employs cytotoxic $^1O_2$ converted from $^3O_2$ upon light excitation to efficiently kill bacteria. Nevertheless, due to the limited amount of available $^3O_2$ around photosensitizers and the extremely short diffusion range of photoactivated $^1O_2$, the effectiveness of photodynamic therapy is often reduced. To overcome this bottleneck, Ma and co-workers developed urease-powered photosensitizer-carrying micromotors as motile photodynamic antibacterial platforms (Fig. 10B) [334]. To obtain these enzymatic micromotors, both hollow mesoporous SiO_2 ($mSiO_2$) microspheres and 5,10,15,20-tetrakis(4-aminophenyl) porphyrin (TAPP) photosensitizer were connected to carboxylated magnetic NPs (Fe_3O_4-COOH) via covalent bonding between the amino group and carboxylic group in one step. Finally, the urease was linked to the external surface of the above microparticles by glutaraldehyde (GA). Owing to the inherent asymmetry of the $mSiO_2$ microspheres, these micromotors could be actuated by ionic diffusiophoresis upon urea decomposition by urease. Such self-propelled micromotors were demonstrated to promote the accessibility of TAPP to $^3O_2$, extend the diffusion range of $^1O_2$, and remarkably enhance the efficacy of photodynamic antimicrobial therapy against *E. coli*, thereby overcoming the perennial problem of photodynamic antimicrobial therapy. The same group also developed urease-powered, PDA-coated, and cefixime trihydrate-loaded liquid metal nanorobots for achieving synergistic photothermal and chemotherapeutic antibacterial effects against *E. coli* [335].

The use of current imaging techniques can be taken into consideration when designing antimicrobial micro/nanorobots so that the interactions between the pathogens and micro/nanorobots can be visualized and tracked in real time. For example, to achieve imaging-guided therapy for bacterial infections, Chen and co-workers developed versatile magnetic microswimmers by coating PDA on magnetized spirulina (MSP) [336]. In addition to the multiple properties of MSP, such as robust magnetic propulsion, tailorable biodegradation, native fluorescence, and selective cytotoxicity [337], the incorporated PDA coating on MSP can intensify its photoacoustic (PA) signal and photothermal effect, which thus endowed the magnetic microswimmers with the capabilities of both PA image tracking and photothermal antimicrobial therapy. In the meantime, the natural fluorescence quenching and varying surface reactivity of PDA enabled the on/off fluorescence diagnosis using a coumarin 7 probe. Based on these designs, PDA-MSP microswimmer swarms were demonstrated in a proof-of-concept study to have real-time PA imaging trackability and desirable theranostic capacities for treating infections caused by MDR Klebsiella pneumoniae (MDR KP). To acquire a dual-mode pathogen-killing function, researchers have also developed other types of antimicrobial micro/-nanorobots, such as magnetic iron oxide@SiO_2 nanorobots conjugated with cell wall-binding domain of endolysin for killing MRSA USA300 through locally generated heat and ROS in response to radiofrequency electromagnetic stimulation [338] and NIR-driven, miconazole nitrate-loaded parachute-like nanomotors for synergetic pharmacological and photothermal antifungal therapy [339].

4.4. Antimicrobial micro/nanorobots for actively eradicating biofilms

Unlike planktonic bacteria, the interactions of microbial communities form EPS matrices [340]. The viscoelastic biofilms and the embedded bacteria on the surface of an object are notoriously difficult to eradicate [341]. The resistant nature of bacterial biofilms to antimicrobials makes them a cause of recalcitrant infections. Owing to their small size and high magnetically actuated mechanical force, magnetically propelled micro/nanorobots can penetrate the EPS matrices, disrupting biofilm formation, and eradicating mature biofilms [26,342]. To

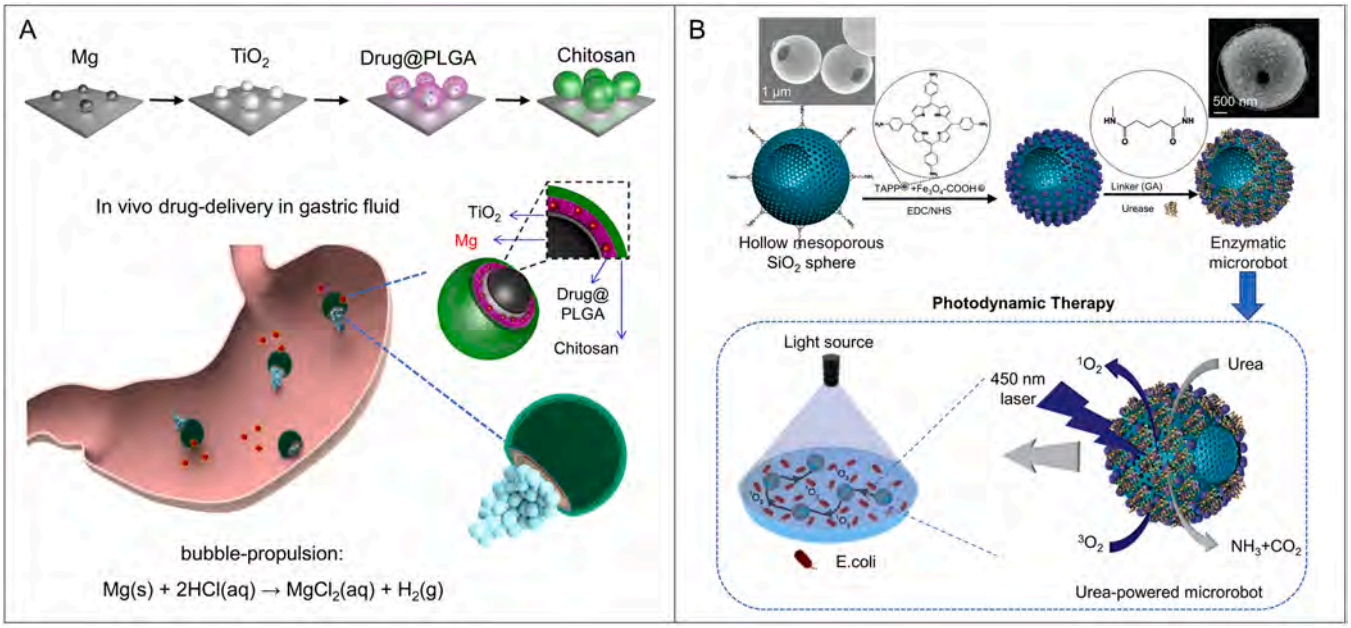

Fig. 10. (A) Mg-based microrobots for drug delivery in a mouse stomach via in vivo bubble-propulsion mechanium. (B) Fabrication of urea-propelled magnetic microrobots and their application in photodynamic therapy against E. coli upon blue light irradiation.
(A) Reproduced with permission from ref [329]. Copyright 2017 The Authors. (B) Reproduced with permission from ref [334]. Copyright 2019 WILEY-VCH Verlag GmbH & Co. KGaA, Weinheim.

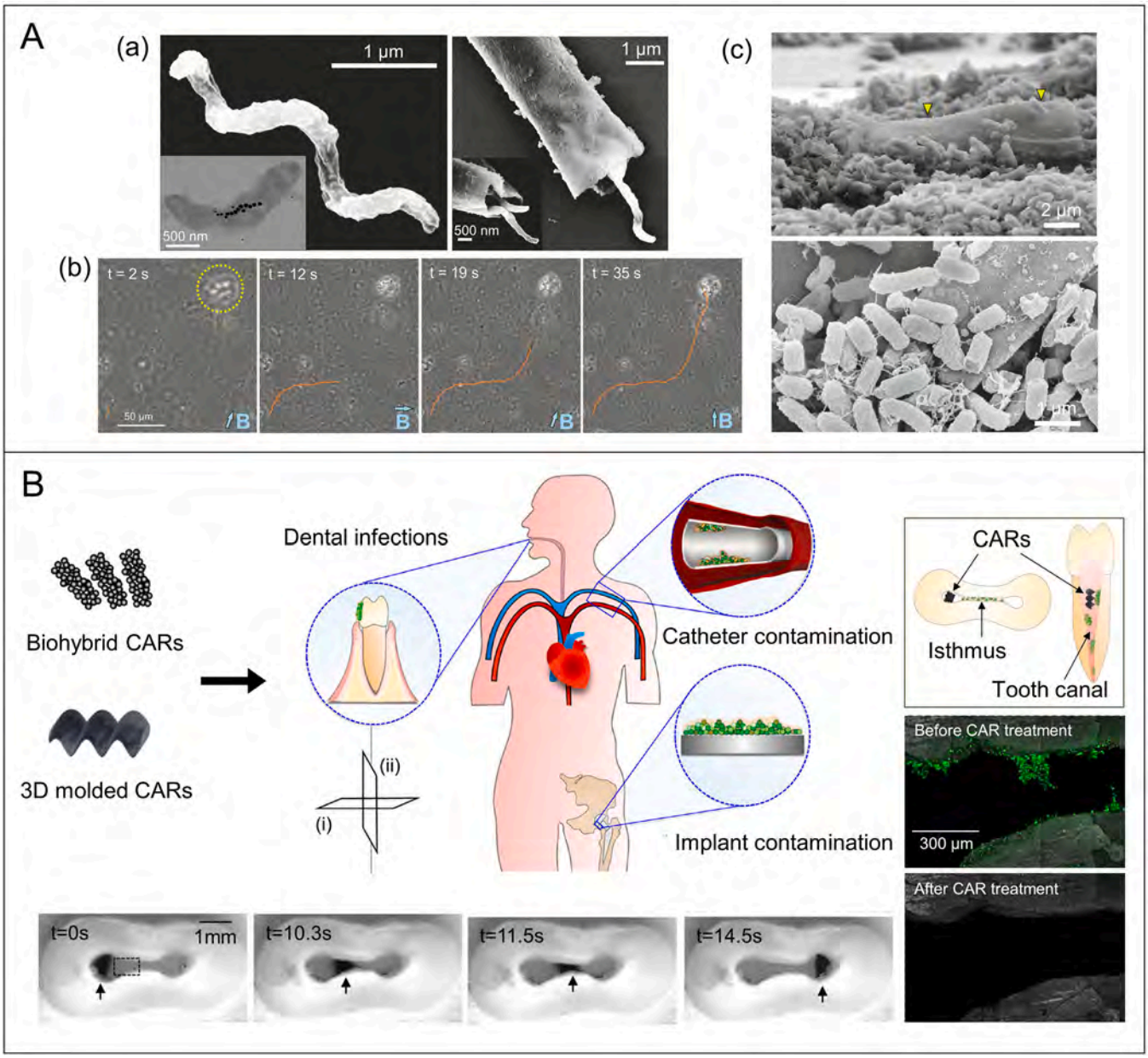

Fig. 11. (A) Antimicrobial microrobots for biofilm eradication. (a) SEM of a magnetotactic bacterium and a biohybrid microbot; (b) Magnetic navigation of biohybrid microbot into an island of E. coli biofilms. (c) SEM images of biohybrid microrobot trapped in an E. coli biofilm. (B) Scheme of potenial applications of catalytic antimicrobial robots (CARs) in the removal of bacterial biofilms under the atuation of external magnetic fields and an experimental example showing the biofilm removal in the tooth.
(A) Reproduced with permission from ref [343]. Copyright 2019 The Authors, some rights reserved; exclusive licensee American Association for the Advancement of Science. (B) Reproduced with permission from ref [345]. Copyright 2019 The Authors, some rights reserved; exclusive licensee American Association for the Advancement of Science.

target the E. coli biofilms, Sánchez and co-workers developed biohybrid magnetic microswimmers by integrating the non-pathogenic magnetotactic bacteria *Magnetosopirrillum gryphiswaldense* (MSR-1) with ciprofloxacin-loaded mesoporous silica microtubes (Fig. 11A) [343]. Under the actuation and guidance of an external magnetic field, the biohybrid microswimmers could be directed to mature E. coli biofilms and forcefully pushed into the EPS matrices. In response to the acidic microenvironment of bacterial biofilms, the release of ciprofloxacin was triggered to fulfill localized, biofilm-targeting antibiotic delivery.

Magnetite Fe_3O_4 NPs exhibit good biocompatibility and intrinsic peroxidase-like activity [344] and have been developed into nanocatalysts for catalyzing H_2O_2 to produce free radicals on site, thereby leading to the degradation of biofilm matrices and the rapid destruction of embedded bacteria to prohibit dental caries [81]. Recently, Koo and co-workers designed magnetically driven catalytic antimicrobial robots (CARs) for the precise, efficient, and controllable killing, degradation, and removal of bacterial biofilms (Fig. 11B) [345]. The CARs employed catalytic and magnetic Fe_3O_4 NPs to produce bactericidal free radicals, break down biofilm EPS matrices, and eradicate fragmented biofilm debris through magnetic field-actuated robotic assemblies. Two different CAR platforms were developed: biohybrid CARs and 3D-molded CARs. The biohybrid CARs were created from Fe_3O_4 NPs and biofilm degradation products. After the catalytic killing of bacteria and disruption of biofilms, the applied magnetic field gradients assembled the Fe_3O_4 NPs and EPS degradation products into plow-like superstructures. The biofilm biomass and debris could thus be completely

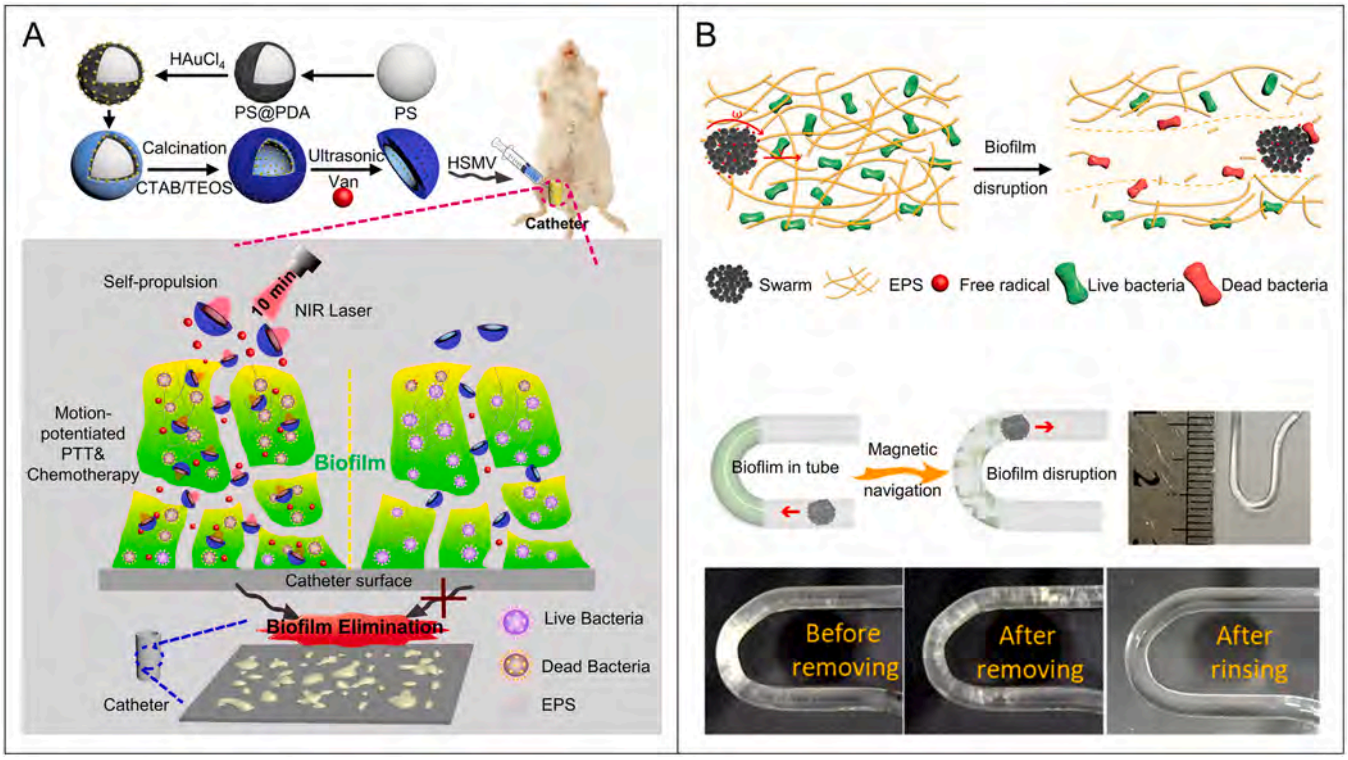

Fig. 12. (A) Synthesis of light-driven nanrobots and their enhanced biofilm elamination via the synergistic effect of photothermal therapy and chemotheropy upon laser illumination. (B) Biofilm disruption demonstrated in a tiny U-shaped tube by a swarm of magnetic nanorobots.
(A) Reproduced with permission from ref [346].Copyright 2020 American Chemical Society. (B) Reproduced with permission from ref [351]. Copyright 2021 American Chemical Society.

removed by the biohybrid CARs to prevent biofilm regrowth under the driving of an external magnetic field in a controlled way, such as sweeping over a wide surface or moving on a well-defined path for localized eradication with microscale precision. The second type of CARs were polymeric soft robots embedded with catalytic and magnetic Fe_3O_4 NPs and created in 3D-printed molds to execute specific removal tasks in enclosed areas [345]. Vane-shaped CARs can remove biofilms from the walls of cylindrical tubes, and helicoid-shaped CARs can drill through biofilm blockages while killing bacteria. Collectively, such "kill-degrade-and-remove" CARs have the potential to actively fight against persistent biofilm infections and the biofouling of medical materials/devices.

The combination of stimuli-responsive therapies (e.g., photothermal/photodynamic therapy, sonodynamic therapy, magnetothermal therapy, etc.) and external field actuation (e.g., light driving, ultrasound propelling, magnetic actuating, etc.) holds great promise for achieving precision treatment of bacterial infections in a controlled way; when further combined with the use of antimicrobial drugs (chemotherapy), a potent synergetic bacteria-killing effect can be achieved. For example, Qu and co-workers designed NIR-driven vancomycin (Van)-loaded $mSiO_2$-SiO_2-Au Janus nanoswimmers (HSMVs) for the deep eradication of bacterial biofilms (Fig. 12A) [346]. To obtain the nanoswimmers, PDA-coated polystyrene (PS) nanospheres served as templates for the on-site growth of Au NPs, followed by the deposition of a SiO_2 layer via the sol-gel method. After calcination to remove the template, a $mSiO_2$ layer was generated on the outer surface, and then moderate ultrasound treatment was performed to produce the asymmetric half-shell nanoswimmers. These NIR-driven HSMVs were shown to efficiently propel and penetrate the bacterial biofilms in 5 min owing to the photothermal conversion of the Au NPs. The localized hyperthermia (~45 °C) and heat-triggered Van release resulted in the synergistic photothermal and chemotherapeutic antibiofilm effect of the HSMVs. The active locomotion of the HSMVs can increase the effective distance of photothermal antibiofilm therapy and enhance the therapeutic efficacy of Van, thereby leading to a superior removal rate of S. aureus biofilms (>90%) in vitro. Prominently, HSMVs can eradicate S. aureus biofilms in vivo upon exposure to 10 min of NIR irradiation without notable damage to the surrounding healthy tissues [346]. This study shows that the active micro/nanorobots can potentiate the penetration of classical antimicrobials into bacterial biofilms and contribute to the deceleration of AMR progression.

To achieve the selective deactivation of Gram-positive bacterial biofilms, Escarpa and co-workers developed catalytic and magnetic Nisin@GO-Pt-Fe_2O_3 Janus micromotors [347]. The Pt NPs enabled bubble-propelled motion in H_2O_2 fuel, and the Fe_2O_3 NPs facilitated the magnetic actuation in a rotating magnetic field. Compared with the free nisin and their static counterparts, the Nisin@GO-Pt-Fe_2O_3 Janus micromotors could bring an approximately 2-fold increase in the capture and killing capacity against S. aureus due to the specific interaction between nisin and S. aureus lipid II unit, enhanced micromotor locomotion, and motion-induced fluid flow. The high stability of nisin and the micromotor pulling force contributed to the efficient operation of micromotors in serum, juice, tap water, and even in (flowing) blood under magnetic actuation [347].

A swarm of micro/nanorobots can also exhibit coordinated behaviors and execute complicated medical tasks with high efficiency [348]. The swarm behavior of micro/nanorobots can be well harnessed to accomplish programmable locomotion and manipulation and to implement complicated medical tasks [41,349,350]. To take advantage of swarming micro/nanorobots for eradicating biofilm obstruction, Zhang and co-workers developed a versatile magnetic microswarm comprising porous Fe_3O_4 mesoparticles (p-Fe_3O_4 MPs) (Fig. 12B) [351]. The p-Fe_3O_4 swarm was created and actuated by a rotating magnetic field, and possessed the capacities of remote driving, high cargo loading, and strong local convection. Furthermore, the p-Fe_3O_4 swarm could efficiently eradicate E. coli biofilms due to the synergetic effects of (1) the

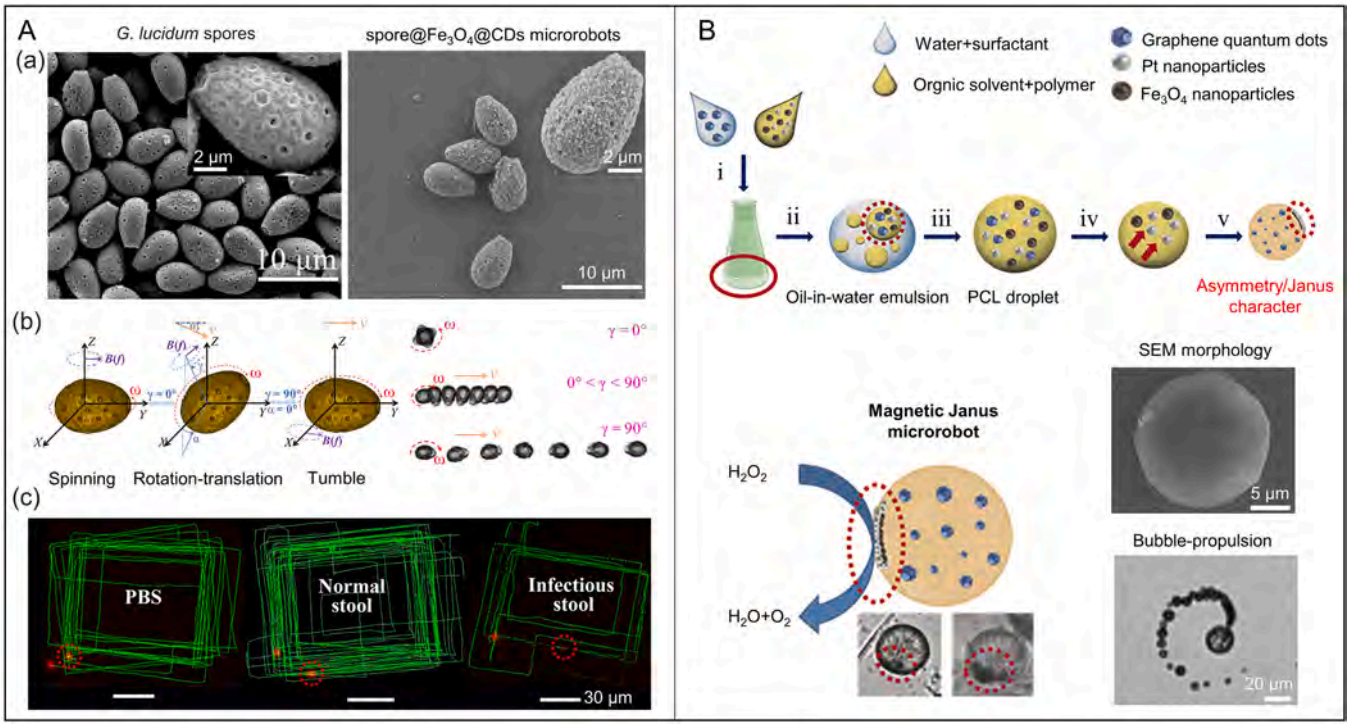

Fig. 13. (A) Spore-based microrobots for toxin detection. (a) SEM images of porous natural spores and spore@Fe_3O_4 @CDs microrobots; (b) Three locomotion modes of microrobots under the actuation of magnetic fields; (c) Autonomous detection of toxins in infectious stool by the mobile microrobots. (B) Fabrication procedure of a magnetic Janus micromotor, which can be driven by chemical fuels and magnetic fields.
(A) Reproduced with permission from ref [354]. Copyright 2019 The Authors, some rights reserved; exclusive licensee American Association for the Advancement of Science. (B) Reproduced with permission from ref [357]. Copyright 2017 Wiley-VCH Verlag GmbH & Co. KGaA, Weinheim.

generation of $^{\bullet}OH$ capable of killing bacteria and degrading biofilms by p-Fe_3O_4 MPs and (2) the physical disruption of biofilms and promoted penetration of $^{\bullet}OH$ deep into the biofilms by p-Fe_3O_4 swarm locomotion. In a proof-of-concept study, the p-Fe_3O_4 swarm demonstrated its capacity for the targeted removal of biofilms along a geometric path on a 2D surface or biofilm blockages within a 3D U-shaped tube when magnetically actuated and navigated, thereby having the potential to clear biofilms in tiny and tortuous spaces. To actively eradicate microbial biofilms, other types of micro/nanorobots have also been designed, such as light-driven ZnO:Ag micromotors [352] and urease-powered photocatalytic TiO_2-CdS microrobots [353].

4.5. *Antimicrobial micro/nanorobots for actively detecting bacterial toxins*

Bacterial toxins can be distinguished into two types: exotoxins, which are secreted outside the bacteria, and endotoxins, which are contained inside the bacteria and released after the bacteria are destroyed. Bacterial toxins cause many diseases, such as food poisoning, acute inflammation (e.g., glomerulonephritis, cholecystitis, or gastroenteritis), and extraintestinal infections (e.g., sepsis, pneumonia, urinary tract infections, etc.). Therefore, the rapid detection of bacterial toxins is crucial for the prevention and treatment of associated diseases. Motion-based detection via tracking the active micro/nanorobots has demonstrated great promise for the fast chemo-/biosensing of bacterial toxins due to the accelerated "analysis on the move". Zhang and coworkers developed fluorescent magnetic spore-based microrobots (FMSMs) to actively detect the toxins secreted by the Clostridium difficile (C. diff) present in the feces of patients (Fig. 13A) [354]. The FMSMs (CDs@Fe_3O_4 @spore) consisted of natural spores, magnetic Fe_3O_4 NPs, and fluorescent carbon dots (CDs). Due to the cooperative effect of these components, FMSMs could accomplish motion-based selective detection of bacterial toxins in C. diff supernatant and clinical fecal samples in tens of minutes, and their analysis time was at least 8 times shorter than that of enzyme-linked immunosorbent assay (ELISA). Considering the ease of degradation and denaturation of C. diff toxins, the advantages of a shorter analysis time, rapid response, and good sensitivity and selectivity make FMSMs promising mobile platforms for the remote active detection of C. diff toxins.

LPSs, a type of bacterial endotoxins, are the main constituents of the outer membranes of Gram-negative bacteria. As toxic inflammatory stimulators, LPSs can trigger the secretion of a broad range of inflammatory cytokines from host immune cells (e.g., monocytes and macrophages), which may eventually cause septic shock and organ failure [355,356]. Escarpa and co-workers designed magnetocatalytic graphene quantum dots (GQDs) Janus micromotors for the ultrafast detection of bacterial endotoxin LPSs (Fig. 13**B**) [357]. To this end, a bottom-up strategy was employed to incorporate a large number of magnetic Fe_3O_4 NPs and catalytic Pt NPs on one side of the micromotor body. In the first step (step i), a certain volume of 10% sodium dodecyl sulfate aqueous solution containing phenylboronic acid (PABA)-modified GQDs was thoroughly mixed with a certain volume of polycaprolactone (PCL) chloroform solution containing Pt NPs (100 nm size) and Fe_3O_4 NPs (20 nm size). After that, emulsion droplets were generated (step ii) and dropped onto a Petri dish to enable chloroform evaporation and PCL solidification (steps iii and iv). The Janus feature was produced in step v-due to the immiscibility of the Pt NPs and Fe_3O_4 NPs with PCL, the NPs tended to separate from the PCL phase and accumulate on the surface of the PCL droplet during chloroform evaporation to decrease the interfacial energy at the water-oil interface. This led to the asymmetric aggregation of the Pt NPs and Fe_3O_4 NPs on one hemisphere of the PCL microparticle for high-efficiency bubble propulsion (in H_2O_2 fuel), magnetic actuation, and controlled directionality. Fluorescence quenching occurred when the GQDs interacted with the LPSs; in this way, the PABA tags could act as recognition receptors of the core polysaccharide region of the LPSs with high specificity.

5. Conclusions and future outlook

This review provides an overview of recent progress in the application-oriented material designs of micro- and nanorobots for antimicrobial purposes. Traditional antimicrobial nanomaterials were introduced and discussed from the perspective of bacteria–nanomaterial interactions, nanomaterial properties, antimicrobial nanocarriers, and stimuli-responsive nano-antimicrobials. Following this, recent advancements in intelligent antimicrobial micro/nanorobots were summarized in detail, with a focus on their application-oriented design strategies. Representative antimicrobial applications were analyzed and discussed to demonstrate how such micro/nanorobots have been exploited for active bacteria elimination, biofilm eradication, and bacterial toxin removal. In the past few years, researchers have made tremendous efforts and impressive progress in the promising research field of antimicrobial micro/nanorobots. Nevertheless, further studies and improvements remain to be done before the practical applications of antimicrobial micro/nanorobots can be realized. To this end, several aspects should be taken into account in the future to design and develop antimicrobial micro/nanorobots for entering real-world application scenarios.

5.1. Design and fabrication of antimicrobial micro/nanorobots

Micro/nanorobots constitute an emerging research field that has attracted ever-increasing interest, especially after the 2016 Nobel Prize in Chemistry was awarded for the design and production of molecular machines. From the initial idea of "swallow the surgeon" [358] to the science fiction film "Fantastic Voyage," medical micro/nanorobots have been envisioned to have huge potential for diverse practical applications, ranging from targeted drug delivery to cell micro/nanosurgery and minimally invasive medicine. In particular, the antimicrobial micro/nanorobots are aimed at developing and deploying a great number of micro/nanoscale machines to perform multiple anti-infection tasks, such as in situ delivery of antimicrobials, localized generation of hyperthermia, targeted interaction with the diseased/infected cells, precise implementation of cellular micro/nanosurgery in complex physiological conditions, and even integrated diagnosis and treatment of infections. Additionally, volant antimicrobial micro/nanorobots can be used to clear pathogenic microorganisms in the air or in space. However, challenges remain in material design, motion control, mass production, and biofunctionality, limitations that need to be overcome to unlock the clinical translational potential of antimicrobial micro/nanorobots.

Micro/nanorobots can be fabricated via multiple methods, including strain engineering [359], physical vapor deposition [360], electron beam evaporation [238], capillary micromolding [361], electroless plating [362], template-assisted electrochemical deposition [363–365], material assembly [366], biohybrid design [229,230], and 3D printing [224,367]. Among these manufacturing techniques, 3D printing has attracted increasing attention due to its remarkable advantage of system integration of structures, compositions, properties, and functionalities into micro/nanorobots created through digital customization and processing for personalized requirements. 3D printing techniques hold great promise for fabricating antimicrobial micro/nanorobots. Nevertheless, two major issues should be noted. (i) To date, most 3D-printable materials do not possess antimicrobial performance and are printed only for the structural and biocompatible parts of the micro/nanorobots. To impart an antimicrobial capacity to the micro/nanorobots, specific antimicrobial agents or nanomaterials must be deposited onto the surfaces of the 3D-printed micro/nanorobots' bodies or incorporated into their matrices after/during the printing. (ii) Functional nanoparticles that can respond to external fields (e.g., magnetic, light, and electric) also need to be coated on the 3D-printed micro/nanorobots or embedded into their bodies after/during the printing. To solve these issues, two possible strategies can be considered: (i) to formulate antimicrobial inks for single-step 3D printing of antimicrobial micro/-nanorobots; (ii) to enable whole 3D printing of antimicrobial micro/nanorobots via a multimaterial 3D printing method. Although 3D printing techniques have not been widely exploited in the area of antimicrobial micro/nanorobots, it is envisioned that the rapid development of 3D printing field, materials science, and chemistry will continually promote the advancement of antimicrobial micro/nanorobots.

5.2. Actuation and imaging of antimicrobial micro/nanorobots

Antimicrobial micro/nanorobots can carry out locomotion through self-propulsive forces or external power sources, which were summarized in **Section 4.1** . To precisely implement diverse antimicrobial tasks (such as biofilm eradication, bacteria elimination, and the removal of bacterial toxins) in a complex physiological environment, antimicrobial micro/nanorobots should be designed for visualized manipulation, navigation, and motion control in 3D on demand. For example, a single antimicrobial micro/nanorobot or a swarm of antimicrobial micro/nanorobots could be visually driven toward a site of bacterial infection with the guidance of clinical imaging equipment and then release the loaded drugs or produce hyperthermia locally to kill the bacteria. For this purpose, conventional clinical imaging methods, such as magnetic resonance imaging (MRI), magnetic particle imaging (MPI), ultrasonography, photoacoustic imaging (PAI), photoacoustic computed tomography (PACT), positron emission tomography (PET), optical coherence tomography (OCT), and X-ray computed tomography (X-CT), have enormous potential for the use of simultaneously actuating and steering antimicrobial micro/nanorobots to the targeted infected sites. Currently, some medical imaging techniques, such as PAI [336,368], PACT [369], and PET [253], have been used only for guiding and tracking (antimicrobial) micro/nanorobots.

Researchers have made great efforts to actuate micro/nanorobots with clinical imaging techniques aimed at a combination of propulsion and visualization. Medical MRI scanners hold great promise for driving magnetic micro/nanorobots and have been employed to provide tetherless actuation [370,371]. By exploiting the gradient between the field free point (FFP) and circumambient magnetic sources, MPI can be utilized to actuate magnetic micro/nanorobots upon repositioning the FFP to generate a lower magnetization area in which magnetic torque actuation can be achieved [372]. Ultrasonography is another real-time, noninvasive clinical imaging method based on the interaction of medical ultrasound waves and soft tissues [373], thereby having the potential to actuate ultrasonic micro/nanorobots. In addition, OCT is expected to provide untethered actuation for light-driven micro/nanorobots along a predefined trajectory in the vasculature (e.g., blood vessels, lymph vessels, etc.). Collectively, medical imaging-actuated antimicrobial micro/nanorobots can accomplish the dual purpose of (i) imaging and tracking for precise localization and (ii) propulsion and motion control for real-time navigation. Nonetheless, when used alone, conventional clinical imaging methods still have some limitations in accomplishing real-time micro/nanorobot tracking, including resolution, definition, latency, and penetration depth [374,375]. Therefore, the combination of multiple imaging techniques may have greater potential for simultaneous imaging and the actuation of antimicrobial micro/nanorobots.

5.3. Targetability and biosecurity of antimicrobial micro/nanorobots

Direct smear dyeing and the microscopic examination of patient specimens are simple and rapid methods for the diagnosis of bacterial infections. To this end, the morphological characteristics and the possible number of bacteria should be considered for the direct examination of specimens collected from certain parts of the human body. However, most bacteria do not possess significant features in morphology and staining, so the culture method (e.g., using agar plates) is further needed to isolate and identify the bacteria. The PCR technique can also efficiently identify pathogens by detecting their DNA or RNA. Nevertheless, these isolation and examination methods are time-consuming and involve sampling and subsequent ex vivo analysis. In this context, the integration of the specific recognition of pathogens into locomotive micro/nanorobots should enable a motion-aided diagnosis approach, thereby leading to fast onboard sensing and the identification of pathogens. Bacteria-binding substances such as lectin and platelet membranes have been adopted to selectively capture and isolate E. coli and S. aureus, respectively, with high efficiency due to locomotion enhancement. Moreover, electrochemical or fluorescence signals can be coupled with motile micro/nanorobots, so that the change in signals can be used to monitor the occurrence and progression of pathogenic infections. One promising diagnostic strategy is to couple aggregation-induced emission (AIE) with mobile micro/nanorobots (AIEbots). AIE has been widely used for bioimaging and biosensing [376]. AIEbots are expected to take full advantage of the swarm/collective behavior of micro/nanorobots to selectively recognize and light up the target bacteria when modified with known specific antibodies or immune serums.

In addition to the specific recognition and capture of target pathogens, selective pathogen killing is of high importance to minimize potential toxicity or damage to normal cells and tissues or probiotics and gut microbiota in the human body, when designing antimicrobial micro/nanorobots for infection treatment. The biocompatibility and biodegradability/retrievability of antimicrobial micro/nanorobots should be fully considered in preclinical studies and prior to clinical applications. Several aspects need to be considered, as follows:

(1) Phagocytes, including neutrophils and mononuclear phagocyte system (monocytes, macrophages, and dendritic cells), are able to phagocytose foreign bodies, such as antimicrobial micro/nanorobots. When carrying out an infection treatment, it is desired that antimicrobial micro/nanorobots finish their target tasks before uptake by phagocytes or to evade phagocytosis through elaborate material designs. For this purpose, two strategies have great potential. One is to camouflage antimicrobial micro/nanorobots with cytomembranes derived from a variety of cell types, such as immune cells, erythrocytes, and leukocytes. The other strategy is to create antimicrobial micro/nanorobots via biohybridization with multiple types of cells, including immunocytes and blood cells [229].
(2) Antimicrobial micro/nanorobots with immunomodulatory functions are also promising. Such micro/nanorobots may be able to regulate inflammatory reactions and promote inflammation resolution during pathogen killing. For example, antimicrobial peptides can selectively modulate innate immune reactions to protect against sepsis [377]. Together with their broad-spectrum bactericidal activity, antimicrobial peptide-loaded micro/-nanorobots are envisioned to have a dual function: pathogen killing and immunoregulation.
(3) When the target cells are innate/adaptive immune cells, antimicrobial micro/nanorobots should not cause undesired immune responses, such as excessive inflammation. Moreover, further efforts should be made to deeply elucidate the interactions between antimicrobial micro/nanorobots and the human immune system so that the material designs of antimicrobial micro/nanorobots can be optimized and predefined to avoid adverse immune reactions or even elicit favorable immune responses.
(4) Antimicrobial micro/nanorobots hold great promise for treating intracellular microbial infections. For example, pulmonary tuberculosis is an acute or chronic infection of the lungs caused by Mycobacterium tuberculosis (M. tuberculosis), which can grow and replicate in the pulmonary macrophages, escape from immune attacks and clearance, and infect more cells in this way [378,379]. The infected pulmonary macrophages deviate from their normal pathway (i.e., the intracellular lysosomal degradation of pathogens), which is caused by NAD^+ depletion due to the M. tuberculosis-secreted tuberculosis necrotizing toxin (TNT) acting as a glycohydrolase. Due to their external field-directed motion, antimicrobial micro/nanorobots can target and enter the infected pulmonary macrophages, release antimicrobials on site, and directly destroy the hidden M. tuberculosis; alternatively, they can deliver therapeutic drugs into the infected macrophages to enhance their cell viability and pathogen-killing capacity. Taken together, antimicrobial micro/nanorobots are expected to inspire a therapy strategy for tackling pulmonary tuberculosis that targets the host immune cells.
(5) Antimicrobial micro/nanorobots should be biodegradable. This means that after finishing their tasks in vivo, they can be degraded by the human body (e.g., via enzymolysis or hydrolysis), and the degradation byproducts are non-toxic to normal cells. Alternatively, non-degradable antimicrobial micro/nanorobots are expected to be retrievable from the human body once they complete their tasks. For example, magnetic antimicrobial micro/nanorobots in the human body can be retrieved by externally applying magnets. Magnetic retrievability can be well integrated into the design of non-degradable antimicrobial micro/nanorobots.
(6) Biodegradable and stimuli-responsive hydrogel materials can be developed into intelligent microrobots that have larger dimensions and serve as “aircraft carriers” to transport and deliver smaller antimicrobial micro/nanorobots to the site of microbial infections. A variety of hydrogel-based stimuli-responsive microrobots can be created to respond to diverse environmental cues, such as fields (magnetic, ultrasound, light, electric, and heat), pH, temperature, chemicals, and ionic strength [380]. For example, hyaluronic acid (HA) hydrogels can be 3D-printed into aircraft carriers and loaded with large numbers of antimicrobial micro/nanorobots. When bacterial infections occur in the human body, the HA hydrogel aircraft carriers can be actuated and navigated to the infected site and then degraded by bacteria-secreted hyaluronidase, thereby leading to the release of the antimicrobial micro/nanorobots to attack and destroy the pathogens. Such hydrogel aircraft carriers may shrink and swell in response to external stimuli (such as light, heat, and ultrasound) or internal stimuli (such as inflammatory factors, local acidic pH, and local temperature increases) that are applied when bacterial infections occur. This shrinking can squeeze out the antimicrobial micro/nanorobots to strike and kill pathogens. Without bacterial infections, the hydrogel aircraft carriers can hide the antimicrobial micro/nanorobots from detection and phagocytosis by immune cells.
(7) Multifunctional antimicrobial micro/nanorobots need to be created to deal with complex infection conditions. For example, to treat infected wounds or bone defects, antimicrobial micro/nanorobots are expected to regenerate the damaged tissues while killing pathogens. After osteosarcoma resection, antimicrobial micro/nanorobots with rational designs may have the functions of killing residual cancer cells, treating surgical site infections, and promoting bone defect repair. Given the limited number of animal studies on antimicrobial micro/nanorobots, more in vivo experiments and clinical tests are required to evaluate and

validate the therapy efficacy and long-term biosafety of antimicrobial micro/nanorobots.

Declaration of Competing Interest

The authors declare the following financial interests/personal relationships which may be considered as potential competing interests: Paul K Chu reports financial support was provided by City University of Hong Kong. Jinhua Li reports financial support was provided by Beijing Institute of Technology. Paul K Chu reports a relationship with City University of Hong Kong that includes: board membership.

Data Availability

Data will be made available on request.

Acknowledgments

This work was supported by the City University of Hong Kong Donation Research Grant (DON-RMG 9229021), City University of Hong Kong Strategic Research Grant (SRG 7005505), City University of Hong Kong Donation Grant (9220061), Hong Kong PDFS - RGC Postdoctoral Fellowship Scheme (PDFS2122–1S08 and CityU 9061014), Hong Kong HMRF (Health and Medical Research Fund) (2120972 and CityU 9211320). Huaijuan Zhou thanks the financial support from the Beijing Institute of Technology Research Fund Program for Young Scholars (1750023022215). Chengtie Wu thanks the support from the National Natural Science Foundation of China (32130062, 32225028), CAS Project for Young Scientists in Basic Research (YSRB073) and Shanghai Pilot Program for Basic Research – Chinese Academy of Sciences, Shanghai Branch (JCYJ-SHFY-2022–003). Hao Shen thanks the support from the Natural Science Foundation of China (82272511) and the experimental animal study support project of Shanghai Science and Technology Commission (21140904800). Rui Shi acknowledges the National Natural Science Foundation of China (82072406) and Beijing Municipal Health Commission (BMHC2019–9, BJRITO-RDP-2023). Jinhua Li gratefully thanks the financial support from the Beijing Institute of Technology Teli Young Fellow Program (3320012222218).

References

[1] K.C. Nicolaou, S. Rigol, A brief history of antibiotics and select advances in their synthesis, J. Antibiot. 71 (2) (2018) 153–184.
[2] R. Laxminarayan, A. Duse, C. Wattal, A.K.M. Zaidi, H.F.L. Wertheim, N. Sumpradit, E. Vlieghe, G.L. Hara, I.M. Gould, H. Goossens, C. Greko, A.D. So, M. Bigdeli, G. Tomson, W. Woodhouse, E. Ombaka, A.Q. Peralta, F.N. Qamar, F. Mir, S. Kariuki, Z.A. Bhutta, A. Coates, R. Bergstrom, G.D. Wright, E.D. Brown, O. Cars, Antibiotic resistance—the need for global solutions, Lancet Infect. Dis. 13 (12) (2013) 1057–1098.
[3] A.H. Holmes, L.S.P. Moore, A. Sundsfjord, M. Steinbakk, S. Regmi, A. Karkey, P. J. Guerin, L.J.V. Piddock, Understanding the mechanisms and drivers of antimicrobial resistance, Lancet 387 (10014) (2016) 176–187.
[4] H. Nikaido, Multidrug resistance in bacteria, Annu. Rev. Biochem. 78 (1) (2009) 119–146.
[5] K.U. Jansen, C. Knirsch, A.S. Anderson, The role of vaccines in preventing bacterial antimicrobial resistance, Nat. Med. 24 (1) (2018) 10–19.
[6] J. O'Neill. Tackling drug-resistant infections globally: final report and recommendations, 2016. https://apo.org.au/node/63983.
[7] T.-F. Mah, B. Pitts, B. Pellock, G.C. Walker, P.S. Stewart, G.A. O'Toole, A genetic basis for Pseudomonas aeruginosa biofilm antibiotic resistance, Nature 426 (6964) (2003) 306–310.
[8] T.-F.C. Mah, G.A. O'Toole, Mechanisms of biofilm resistance to antimicrobial agents, Trends Microbiol. 9 (1) (2001) 34–39.
[9] D. Davies, Understanding biofilm resistance to antibacterial agents, Nat. Rev. Drug Disco 2 (2) (2003) 114–122.
[10] P.S. Stewart, J. William Costerton, Antibiotic resistance of bacteria in biofilms, Lancet 358 (9276) (2001) 135–138.
[11] H.-C. Flemming, J. Wingender, The biofilm matrix, Nat. Rev. Microbiol. 8 (9) (2010) 623–633.
[12] P.P. Kalelkar, M. Riddick, A.J. García, Biomaterial-based antimicrobial therapies for the treatment of bacterial infections, Nat. Rev. Mater. 7 (1) (2022) 39–54.
[13] A. Gupta, S. Mumtaz, C.-H. Li, I. Hussain, V.M. Rotello, Combatting antibiotic-resistant bacteria using nanomaterials, Chem. Soc. Rev. 48 (2) (2019) 415–427.
[14] Y. Liu, L. Shi, L. Su, H.C. van der Mei, P.C. Jutte, Y. Ren, H.J. Busscher, Nanotechnology-based antimicrobials and delivery systems for biofilm-infection control, Chem. Soc. Rev. 48 (2019) 428–446.
[15] M.J. Hajipour, K.M. Fromm, A. Akbar Ashkarran, D. Jimenez de Aberasturi, I. Rd Larramendi, T. Rojo, V. Serpooshan, W.J. Parak, M. Mahmoudi, Antibacterial properties of nanoparticles, Trends Biotechnol. 30 (10) (2012) 499–511.
[16] C. Zhao, W. Liu, M. Zhu, C. Wu, Y. Zhu, Bioceramic-based scaffolds with antibacterial function for bone tissue engineering: A review, Bioact. Mater. 18 (2022) 383–398.
[17] B. Li, Y. Luo, Y. Zheng, X. Liu, L. Tan, S. Wu, Two-dimensional antibacterial materials, Prog. Mater. Sci. 130 (2022), 100976.
[18] M. Cloutier, D. Mantovani, F. Rosei, Antibacterial coatings: challenges, perspectives, and opportunities, Trends Biotechnol. 33 (11) (2015) 637–652.
[19] S. Li, S. Dong, W. Xu, S. Tu, L. Yan, C. Zhao, J. Ding, X. Chen, Antibacterial hydrogels, Adv. Sci. 5 (5) (2018) 1700527.
[20] M. Sitti, Voyage of the microrobots, Nature 458 (7242) (2009) 1121–1122.
[21] C.K. Schmidt, M. Medina-Sánchez, R.J. Edmondson, O.G. Schmidt, Engineering microrobots for targeted cancer therapies from a medical perspective, Nat. Commun. 11 (1) (2020) 5618.
[22] B.J. Nelson, I.K. Kaliakatsos, J.J. Abbott, Microrobots for minimally invasive medicine, Annu. Rev. Biomed. Eng. 12 (1) (2010) 55–85.
[23] S. Palagi, P. Fischer, Bioinspired microrobots, Nat. Rev. Mater. 3 (6) (2018) 113–124.
[24] F. Peng, Y. Tu, D.A. Wilson, Micro/nanomotors towards in vivo application: cell, tissue and biofluid, Chem. Soc. Rev. 46 (17) (2017) 5289–5310.
[25] J. Li, B. Esteban-Fernández de Ávila, W. Gao, L. Zhang, J. Wang, Micro/nanorobots for biomedicine: delivery, surgery, sensing, and detoxification, Sci. Robot. 2 (4) (2017) eaam6431.
[26] H. Zhou, C.C. Mayorga-Martinez, S. Pané, L. Zhang, M. Pumera, Magnetically driven micro and nanorobots, Chem. Rev. 121 (8) (2021) 4999–5041.
[27] B. Wang, K. Kostarelos, B.J. Nelson, L. Zhang, Trends in micro-/nanorobotics: materials development, actuation, localization, and system integration for biomedical applications, Adv. Mater. 33 (4) (2021) 2002047.
[28] H. Ceylan, I.C. Yasa, O. Yasa, A.F. Tabak, J. Giltinan, M. Sitti, 3D-printed biodegradable microswimmer for theranostic cargo delivery and release, ACS Nano 13 (3) (2019) 3353–3362.
[29] H. Xu, M. Medina-Sánchez, M.F. Maitz, C. Werner, O.G. Schmidt, Sperm-micromotors for cargo-delivery through flowing blood, ACS Nano 14 (3) (2020) 2982–2993.
[30] S. Tottori, L. Zhang, F. Qiu, K.K. Krawczyk, A. Franco-Obregón, B.J. Nelson, Magnetic helical micromachines: fabrication, controlled swimming, and cargo transport, Adv. Mater. 24 (6) (2012) 811–816.
[31] H. Ceylan, I.C. Yasa, M. Sitti, 3D chemical patterning of micromaterials for encoded functionality, Adv. Mater. 29 (9) (2017) 1605072.
[32] V.M. Kadiri, C. Bussi, A.W. Holle, K. Son, H. Kwon, G. Schütz, M.G. Gutierrez, P. Fischer, Biocompatible magnetic micro- and nanodevices: fabrication of FePt nanopropellers and cell transfection, Adv. Mater. 32 (25) (2020) 2001114.
[33] S. Keller, S.P. Teora, G.X. Hu, M. Nijemeisland, D.A. Wilson, High-throughput design of biocompatible enzyme-based hydrogel microparticles with autonomous movement, Angew. Chem. Int. Ed. 57 (31) (2018) 9814–9817.
[34] F. Soto, E. Karshalev, F. Zhang, B. Esteban Fernandez de Avila, A. Nourhani, J. Wang, Smart materials for microrobots, Chem. Rev. 122 (5) (2021) 5365–5403.
[35] M.B. Akolpoglu, Y. Alapan, N.O. Dogan, S.F. Baltaci, O. Yasa, G.A. Tural, M. Sitti, Magnetically steerable bacterial microrobots moving in 3D biological matrices for stimuli-responsive cargo delivery, Sci. Adv. 8 (28) (2022) eabo6163.
[36] V. Magdanz, G. Stoychev, L. Ionov, S. Sanchez, O.G. Schmidt, Stimuli-responsive microjets with reconfigurable shape, Angew. Chem. Int. Ed. 53 (10) (2014) 2673–2677.
[37] O.I. Sentürk, O. Schauer, F. Chen, V. Sourjik, S.V. Wegner, Red/far-red light switchable cargo attachment and release in bacteria-driven microswimmers, Adv. Healthc. Mater. 9 (1) (2020) 1900956.
[38] S. Li, Q. Jiang, S. Liu, Y. Zhang, Y. Tian, C. Song, J. Wang, Y. Zou, G.J. Anderson, J.-Y. Han, Y. Chang, Y. Liu, C. Zhang, L. Chen, G. Zhou, G. Nie, H. Yan, B. Ding, Y. Zhao, A DNA nanorobot functions as a cancer therapeutic in response to a molecular trigger in vivo, Nat. Biotechnol. 36 (3) (2018) 258–264.
[39] J. Wang, B.J. Toebes, A.S. Plachokova, Q. Liu, D. Deng, J.A. Jansen, F. Yang, D. A. Wilson, Self-propelled PLGA micromotor with chemotactic response to inflammation, Adv. Healthc. Mater. 9 (7) (2020) 1901710.
[40] A. Llopis-Lorente, A. García-Fernández, E. Lucena-Sánchez, P. Díez, F. Sancenón, R. Villalonga, D.A. Wilson, R. Martínez-Máñez, Stimulus-responsive nanomotors based on gated enzyme-powered Janus Au–mesoporous silica nanoparticles for enhanced cargo delivery, Chem. Commun. 55 (87) (2019) 13164–13167.
[41] H. Xie, M. Sun, X. Fan, Z. Lin, W. Chen, L. Wang, L. Dong, Q. He, Reconfigurable magnetic microrobot swarm: multimode transformation, locomotion, and manipulation, Sci. Robot. 4 (28) (2019) eaav8006.
[42] J. Elgeti, R.G. Winkler, G. Gompper, Physics of microswimmers—single particle motion and collective behavior: a review, Rep. Prog. Phys. 78 (5) (2015), 056601.
[43] M. Sitti, Robotic collectives inspired by biological cells, Nature 567 (2019) 314–315.
[44] J. Wang, Self-propelled affinity biosensors: moving the receptor around the sample, Biosens. Bioelectron. 76 (2016) 234–242.
[45] Y. Zhang, K. Yuan, L. Zhang, Micro/Nanomachines: from Functionalization to Sensing and Removal, Advanced Materials Technologies 4 (4) (2019) 1800636.
[46] B. Esteban-Fernández de Ávila, A. Martín, F. Soto, M.A. Lopez-Ramirez, S. Campuzano, G.M. Vásquez-Machado, W. Gao, L. Zhang, J. Wang, Single cell

real-time miRNAs sensing based on nanomotors, ACS Nano 9 (7) (2015) 6756–6764.
[47] E.W.H. Jager, O. Inganäs, I. Lundström, Microrobots for micrometer-size objects in aqueous media: potential tools for single-cell manipulation, Science 288 (5475) (2000) 2335.
[48] Q. Jin, Y. Yang, J. Jackson, C. Yoon, D.H. Gracias, Untethered grippers for active single cell biopsy, Nano Lett. 20 (7) (2020) 5383–5390.
[49] S.K. Srivastava, M. Medina-Sánchez, B. Koch, O.G. Schmidt, Medibots: dual-action biogenic microdaggers for single-cell surgery and drug release, Adv. Mater. 28 (5) (2016) 832–837.
[50] W. Wang, Z. Wu, X. Lin, T. Si, Q. He, Gold-nanoshell-functionalized polymer nanoswimmer for photomechanical poration of single-cell membrane, J. Am. Chem. Soc. 141 (16) (2019) 6601–6608.
[51] C. Peters, M. Hoop, S. Pané, B.J. Nelson, C. Hierold, Degradable magnetic composites for minimally invasive interventions: device fabrication, targeted drug delivery, and cytotoxicity tests, Adv. Mater. 28 (3) (2016) 533–538.
[52] W. Xi, A.A. Solovev, A.N. Ananth, D.H. Gracias, S. Sanchez, O.G. Schmidt, Rolled-up magnetic microdrillers: towards remotely controlled minimally invasive surgery, Nanoscale 5 (4) (2013) 1294–1297.
[53] B. Wang, K.F. Chan, K. Yuan, Q. Wang, X. Xia, L. Yang, H. Ko, Y.-X.J. Wang, J.J. Y. Sung, P.W.Y. Chiu, L. Zhang, Endoscopy-assisted magnetic navigation of biohybrid soft microrobots with rapid endoluminal delivery and imaging, Sci. Robot. 6 (52) (2021) eabd2813.
[54] P. Erkoc, I.C. Yasa, H. Ceylan, O. Yasa, Y. Alapan, M. Sitti, Mobile microrobots for active therapeutic delivery, Adv. Ther. 2 (1) (2019) 1800064.
[55] H. Zhang, Z. Li, C. Gao, X. Fan, Y. Pang, T. Li, Z. Wu, H. Xie, Q. He, Dual-responsive biohybrid neutrobots for active target delivery, Sci. Robot. 6 (52) (2021) eaaz9519.
[56] X. Wei, M. Beltrán-Gastélum, E. Karshalev, B. Esteban-Fernández de Ávila, J. Zhou, D. Ran, P. Angsantikul, R.H. Fang, J. Wang, L. Zhang, Biomimetic micromotor enables active delivery of antigens for oral vaccination, Nano Lett. 19 (3) (2019) 1914–1921.
[57] Z. Zhang, L. Wang, T.K.F. Chan, Z. Chen, M. Ip, P.K.S. Chan, J.J.Y. Sung, L. Zhang, Micro-/nanorobots in antimicrobial applications: recent progress, challenges, and opportunities, Adv. Healthc. Mater. 11 (6) (2022) 2101991.
[58] L. Wang, C. Hu, L. Shao, The antimicrobial activity of nanoparticles: present situation and prospects for the future, Int J. Nanomed. 12 (2017) 1227–1249.
[59] J.M.V. Makabenta, A. Nabawy, C.-H. Li, S. Schmidt-Malan, R. Patel, V.M. Rotello, Nanomaterial-based therapeutics for antibiotic-resistant bacterial infections, Nat. Rev. Microbiol. 19 (1) (2021) 23–36.
[60] L. Pasquina-Lemonche, J. Burns, R.D. Turner, S. Kumar, R. Tank, N. Mullin, J. S. Wilson, B. Chakrabarti, P.A. Bullough, S.J. Foster, J.K. Hobbs, The architecture of the Gram-positive bacterial cell wall, Nature 582 (7811) (2020) 294–297.
[61] D.A. Dik, J.F. Fisher, S. Mobashery, Cell-wall recycling of the gram-negative bacteria and the nexus to antibiotic resistance, Chem. Rev. 118 (12) (2018) 5952–5984.
[62] A. Gupta, R. Landis, V. Rotello, Nanoparticle-based antimicrobials: surface functionality is critical, F1000Research 5 (2016) 364.
[63] V. Berry, A. Gole, S. Kundu, C.J. Murphy, R.F. Saraf, Deposition of CTAB-terminated nanorods on bacteria to form highly conducting hybrid systems, J. Am. Chem. Soc. 127 (50) (2005) 17600–17601.
[64] Y. Li, W. Zhang, J. Niu, Y. Chen, Mechanism of photogenerated reactive oxygen species and correlation with the antibacterial properties of engineered metal-oxide nanoparticles, ACS Nano 6 (6) (2012) 5164–5173.
[65] F. Vatansever, W.C.M.A. de Melo, P. Avci, D. Vecchio, M. Sadasivam, A. Gupta, R. Chandran, M. Karimi, N.A. Parizotto, R. Yin, G.P. Tegos, M.R. Hamblin, Antimicrobial strategies centered around reactive oxygen species – bactericidal antibiotics, photodynamic therapy, and beyond, FEMS Microbiol. Rev. 37 (6) (2013) 955–989.
[66] Y. Nosaka, A.Y. Nosaka, Generation and detection of reactive oxygen species in photocatalysis, Chem. Rev. 117 (17) (2017) 11302–11336.
[67] Z. Xuming, C. Yu Lim, L. Ru-Shi, T. Din Ping, Plasmonic photocatalysis, Rep. Prog. Phys. 76 (4) (2013), 046401.
[68] J. Li, W. Liu, X. Zhang, P.K. Chu, K.M.C. Cheung, K.W.K. Yeung, Temperature-responsive tungsten doped vanadium dioxide thin film starves bacteria to death, Mater. Today 22 (2019) 35–49.
[69] J.T. Seil, T.J. Webster, Antibacterial effect of zinc oxide nanoparticles combined with ultrasound, Nanotechnology 23 (49) (2012), 495101.
[70] J. Li, H. Zhou, J. Wang, D. Wang, R. Shen, X. Zhang, P. Jin, X. Liu, Oxidative stress-mediated selective antimicrobial ability of nano-VO_2 against Gram-positive bacteria for environmental and biomedical applications, Nanoscale 8 (23) (2016) 11907–11923.
[71] F.C. Fang, Antimicrobial reactive oxygen and nitrogen species: concepts and controversies, Nat. Rev. Microbiol. 2 (10) (2004) 820–832.
[72] P.M. Wood, The potential diagram for oxygen at pH 7, Biochem. J. 253 (1) (1988) 287–289.
[73] J. Li, M. Jiang, H. Zhou, P. Jin, K.M.C. Cheung, P.K. Chu, K.W.K. Yeung, Vanadium dioxide nanocoating induces tumor cell death through mitochondrial electron transport chain interruption, Glob. Chall. 3 (3) (2019) 1800058.
[74] K.A. Weber, L.A. Achenbach, J.D. Coates, Microorganisms pumping iron: anaerobic microbial iron oxidation and reduction, Nat. Rev. Microbiol. 4 (2006) 752.
[75] R.K. Thauer, K. Jungermann, K. Decker, Energy conservation in chemotrophic anaerobic bacteria, Bacteriol. Rev. 41 (1) (1977) 100–180.
[76] J. Li, W. Liu, D. Kilian, X. Zhang, M. Gelinsky, P.K. Chu, Bioinspired interface design modulates pathogen and immunocyte responses in biomaterial-centered infection combination therapy, Mater. Horiz. 6 (2019) 1271–1282.
[77] J.W. Costerton, P.S. Stewart, E.P. Greenberg, Bacterial biofilms: a common cause of persistent infections, Science 284 (5418) (1999) 1318–1322.
[78] C.R. Arciola, D. Campoccia, P. Speziale, L. Montanaro, J.W. Costerton, Biofilm formation in Staphylococcus implant infections. A review of molecular mechanisms and implications for biofilm-resistant materials, Biomaterials 33 (26) (2012) 5967–5982.
[79] F. Pan, A. Xu, D. Xia, Y. Yu, G. Chen, M. Meyer, D. Zhao, C.-H. Huang, Q. Wu, J. Fu, Effects of octahedral molecular sieve on treatment performance, microbial metabolism, and microbial community in expanded granular sludge bed reactor, Water Res. 87 (2015) 127–136.
[80] J. Lellouche, A. Friedman, J.-P. Lellouche, A. Gedanken, E. Banin, Improved antibacterial and antibiofilm activity of magnesium fluoride nanoparticles obtained by water-based ultrasound chemistry, Nanomed.: Nanotechnol., Biol. Med. 8 (5) (2012) 702–711.
[81] L. Gao, Y. Liu, D. Kim, Y. Li, G. Hwang, P.C. Naha, D.P. Cormode, H. Koo, Nanocatalysts promote Streptococcus mutans biofilm matrix degradation and enhance bacterial killing to suppress dental caries in vivo, Biomaterials 101 (2016) 272–284.
[82] M. Hirota, Y. Sugita, M. Ishijima, T. Ikeda, J. Saruta, H. Maeda, T. Ogawa, UV photocatalytic activity of titanium dioxide (TiO_2) surface contaminated with bacterial biofilm: Implications for photo-restoration of osteoconductivity, Mater. Today Adv. 12 (2021), 100182.
[83] C. Yang, J. Li, C. Zhu, Q. Zhang, J. Yu, J. Wang, Q. Wang, J. Tang, H. Zhou, H. Shen, Advanced antibacterial activity of biocompatible tantalum nanofilm via enhanced local innate immunity, Acta Biomater. 89 (2019) 403–418.
[84] W.-R. Li, X.-B. Xie, Q.-S. Shi, S.-S. Duan, Y.-S. Ouyang, Y.-B. Chen, Antibacterial effect of silver nanoparticles on Staphylococcus aureus, BioMetals 24 (1) (2011) 135–141.
[85] W.-R. Li, X.-B. Xie, Q.-S. Shi, H.-Y. Zeng, Y.-S. Ou-Yang, Y.-B. Chen, Antibacterial activity and mechanism of silver nanoparticles on Escherichia coli, Appl. Microbiol. Biotechnol. 85 (4) (2010) 1115–1122.
[86] Z. Yongliang, Z. Dong, X. Mengchi, Y. Qingqiang, Z. Huiying, C. Jiang, W. Chengtie, 3D-printed bioceramic scaffolds with antibacterial and osteogenic activity, Biofabrication 9 (2) (2017), 025037.
[87] X. Yan, B. He, L. Liu, G. Qu, J. Shi, L. Hu, G. Jiang, Antibacterial mechanism of silver nanoparticles in Pseudomonas aeruginosa: proteomics approach†, Metallomics 10 (4) (2018) 557–564.
[88] K. Zheng, M.I. Setyawati, D.T. Leong, J. Xie, Antimicrobial gold nanoclusters, ACS Nano 11 (7) (2017) 6904–6910.
[89] Y. Wang, J. Wan, R.J. Miron, Y. Zhao, Y. Zhang, Antibacterial properties and mechanisms of gold–silver nanocages, Nanoscale 8 (21) (2016) 11143–11152.
[90] Y. Zhao, C. Ye, W. Liu, R. Chen, X. Jiang, Tuning the composition of aupt bimetallic nanoparticles for antibacterial application, Angew. Chem. Int. Ed. 53 (31) (2014) 8127–8131.
[91] W. Liu, J. Li, M. Cheng, Q. Wang, Y. Qian, K.W.K. Yeung, P.K. Chu, X. Zhang, A surface-engineered polyetheretherketone biomaterial implant with direct and immunoregulatory antibacterial activity against methicillin-resistant Staphylococcus aureus, Biomaterials 208 (2019) 8–20.
[92] C. Wu, Y. Zhou, M. Xu, P. Han, L. Chen, J. Chang, Y. Xiao, Copper-containing mesoporous bioactive glass scaffolds with multifunctional properties of angiogenesis capacity, osteostimulation and antibacterial activity, Biomaterials 34 (2) (2013) 422–433.
[93] J. Li, D. Zhai, F. Lv, Q. Yu, H. Ma, J. Yin, Z. Yi, M. Liu, J. Chang, C. Wu, Preparation of copper-containing bioactive glass/eggshell membrane nanocomposites for improving angiogenesis, antibacterial activity and wound healing, Acta Biomater. 36 (2016) 254–266.
[94] P.A. Tran, T.J. Webster, Selenium nanoparticles inhibit Staphylococcus aureus growth, Int. J. Nanomed. 6 (2011) 1553–1558.
[95] J. Wang, H. Zhou, G. Guo, T. Cheng, X. Peng, X. Mao, J. Li, X. Zhang, A functionalized surface modification with vanadium nanoparticles of various valences against implant-associated bloodstream infection, Int. J. Nanomed. 12 (2017) 3121–3136.
[96] J. Li, G. Wang, H. Zhu, M. Zhang, X. Zheng, Z. Di, X. Liu, X. Wang, Antibacterial activity of large-area monolayer graphene film manipulated by charge transfer, Sci. Rep. 4 (2014) 4359.
[97] S. Panda, K. Rout Tapan, D. Prusty Agnish, M. Ajayan Pulickel, S. Nayak, Electron transfer directed antibacterial properties of graphene oxide on metals, Adv. Mater. 30 (7) (2018) 1702149.
[98] J. Zhao, B. Deng, M. Lv, J. Li, Y. Zhang, H. Jiang, C. Peng, J. Li, J. Shi, Q. Huang, C. Fan, Graphene oxide-based antibacterial cotton fabrics, Adv. Healthc. Mater. 2 (9) (2013) 1259–1266.
[99] W. Hu, C. Peng, W. Luo, M. Lv, X. Li, D. Li, Q. Huang, C. Fan, Graphene-based antibacterial paper, ACS Nano 4 (7) (2010) 4317–4323.
[100] Y. Tu, M. Lv, P. Xiu, T. Huynh, M. Zhang, M. Castelli, Z. Liu, Q. Huang, C. Fan, H. Fang, R. Zhou, Destructive extraction of phospholipids from Escherichia coli membranes by graphene nanosheets, Nat. Nanotechnol. 8 (8) (2013) 594–601.
[101] X. Lu, X. Feng, J.R. Werber, C. Chu, I. Zucker, J.-H. Kim, C.O. Osuji, M. Elimelech, Enhanced antibacterial activity through the controlled alignment of graphene oxide nanosheets, Proc. Natl. Acad. Sci. 114 (46) (2017) E9793–E9801.
[102] S. Liu, T.H. Zeng, M. Hofmann, E. Burcombe, J. Wei, R. Jiang, J. Kong, Y. Chen, Antibacterial activity of graphite, graphite oxide, graphene oxide, and reduced graphene oxide: membrane and oxidative stress, ACS Nano 5 (9) (2011) 6971–6980.

[103] O. Akhavan, E. Ghaderi, Toxicity of graphene and graphene oxide nanowalls against bacteria, ACS Nano 4 (10) (2010) 5731–5736.
[104] S. Liu, L. Wei, L. Hao, N. Fang, M.W. Chang, R. Xu, Y. Yang, Y. Chen, Sharper and faster "nano darts" kill more bacteria: a study of antibacterial activity of individually dispersed pristine single-walled carbon nanotube, ACS Nano 3 (12) (2009) 3891–3902.
[105] S. Liu, A.K. Ng, R. Xu, J. Wei, C.M. Tan, Y. Yang, Y. Chen, Antibacterial action of dispersed single-walled carbon nanotubes on Escherichia coli and Bacillus subtilis investigated by atomic force microscopy, Nanoscale 2 (12) (2010) 2744–2750.
[106] D.Y. Lyon, L. Brunet, G.W. Hinkal, M.R. Wiesner, P.J.J. Alvarez, Antibacterial activity of fullerene water suspensions (nC_{60}) is not due to ROS-mediated damage, Nano Lett. 8 (5) (2008) 1539–1543.
[107] K. Rasool, M. Helal, A. Ali, C.E. Ren, Y. Gogotsi, K.A. Mahmoud, Antibacterial activity of $Ti_3C_2T_x$ MXene, ACS Nano 10 (3) (2016) 3674–3684.
[108] C. Yang, Y. Luo, H. Lin, M. Ge, J. Shi, X. Zhang, Niobium carbide MXene augmented medical implant elicits bacterial infection elimination and tissue regeneration, ACS Nano 15 (1) (2021) 1086–1099.
[109] Z. Lin, Y. Zhao, P.K. Chu, L. Wang, H. Pan, Y. Zheng, S. Wu, X. Liu, K.M. C. Cheung, T. Wong, K.W.K. Yeung, A functionalized TiO_2/Mg_2TiO_4 nano-layer on biodegradable magnesium implant enables superior bone-implant integration and bacterial disinfection, Biomaterials 219 (2019), 119372.
[110] H.A. Foster, I.B. Ditta, S. Varghese, A. Steele, Photocatalytic disinfection using titanium dioxide: spectrum and mechanism of antimicrobial activity, Appl. Microbiol. Biotechnol. 90 (6) (2011) 1847–1868.
[111] J. Wang, H. Zhou, G. Guo, J. Tan, Q. Wang, J. Tang, W. Liu, H. Shen, J. Li, X. Zhang, Enhanced anti-infective efficacy of ZnO nano-reservoirs through a combination of intrinsic anti-biofilm activity and reinforced innate defense, ACS Appl. Mater. Interfaces 9 (39) (2017) 33609–33623.
[112] J. Li, G. Guo, J. Wang, H. Zhou, H. Shen, K.W.K. Yeung, Anti-biofouling function of amorphous nano-Ta_2O_5 coating for VO_2-based intelligent windows, Nanotechnology 28 (17) (2017), 175705.
[113] X. Yang, J. Li, T. Liang, C. Ma, Y. Zhang, H. Chen, N. Hanagata, H. Su, M. Xu, Antibacterial activity of two-dimensional MoS_2 sheets, Nanoscale 6 (17) (2014) 10126–10133.
[114] X. Kong, X. Liu, Y. Zheng, P.K. Chu, Y. Zhang, S. Wu, Graphitic carbon nitride-based materials for photocatalytic antibacterial application, Mater. Sci. Eng.: R: Rep. 145 (2021), 100610.
[115] J. Li, G. Wang, D. Wang, Q. Wu, X. Jiang, X. Liu, Alkali-treated titanium selectively regulating biological behaviors of bacteria, cancer cells and mesenchymal stem cells, J. Colloid Interface Sci. 436 (2014) 160–170.
[116] Q. Wu, J. Li, W. Zhang, H. Qian, W. She, H. Pan, J. Wen, X. Zhang, X. Liu, X. Jiang, Antibacterial property, angiogenic and osteogenic activity of Cu-incorporated TiO_2 coating, J. Mater. Chem. B 2 (39) (2014) 6738–6748.
[117] K. Huo, X. Zhang, H. Wang, L. Zhao, X. Liu, P.K. Chu, Osteogenic activity and antibacterial effects on titanium surfaces modified with Zn-incorporated nanotube arrays, Biomaterials 34 (13) (2013) 3467–3478.
[118] G. Wang, H. Feng, L. Hu, W. Jin, Q. Hao, A. Gao, X. Peng, W. Li, K.-Y. Wong, H. Wang, Z. Li, P.K. Chu, An antibacterial platform based on capacitive carbon-doped TiO_2 nanotubes after direct or alternating current charging, Nat. Commun. 9 (1) (2018) 2055.
[119] J. Wang, J. Li, S. Qian, G. Guo, Q. Wang, J. Tang, H. Shen, X. Liu, X. Zhang, P. K. Chu, Antibacterial surface design of titanium-based biomaterials for enhanced bacteria-killing and cell-assisting functions against periprosthetic joint infection, ACS Appl. Mater. Interfaces 8 (17) (2016) 11162–11178.
[120] J. Li, Y. Qiao, H. Zhu, F. Meng, X. Liu, Existence, release, and antibacterial actions of silver nanoparticles on Ag-PIII TiO_2 films with different nanotopographies, Int. J. Nanomed. 9 (2014) 3389–3402.
[121] L. Zhao, H. Wang, K. Huo, L. Cui, W. Zhang, H. Ni, Y. Zhang, Z. Wu, P.K. Chu, Antibacterial nano-structured titania coating incorporated with silver nanoparticles, Biomaterials 32 (24) (2011) 5706–5716.
[122] J. Wang, J. Li, G. Guo, Q. Wang, J. Tang, Y. Zhao, H. Qin, T. Wahafu, H. Shen, X. Liu, X. Zhang, Silver-nanoparticles-modified biomaterial surface resistant to staphylococcus: new insight into the antimicrobial action of silver, Sci. Rep. 6 (2016) 32699.
[123] S. Mei, H. Wang, W. Wang, L. Tong, H. Pan, C. Ruan, Q. Ma, M. Liu, H. Yang, L. Zhang, Y. Cheng, Y. Zhang, L. Zhao, P.K. Chu, Antibacterial effects and biocompatibility of titanium surfaces with graded silver incorporation in titania nanotubes, Biomaterials 35 (14) (2014) 4255–4265.
[124] A. Gao, R. Hang, X. Huang, L. Zhao, X. Zhang, L. Wang, B. Tang, S. Ma, P.K. Chu, The effects of titania nanotubes with embedded silver oxide nanoparticles on bacteria and osteoblasts, Biomaterials 35 (13) (2014) 4223–4235.
[125] J. Li, H. Zhou, S. Qian, Z. Liu, J. Feng, P. Jin, X. Liu, Plasmonic gold nanoparticles modified titania nanotubes for antibacterial application, Appl. Phys. Lett. 104 (26) (2014), 261110.
[126] G. Wang, H. Feng, A. Gao, Q. Hao, W. Jin, X. Peng, W. Li, G. Wu, P.K. Chu, Extracellular electron transfer from aerobic bacteria to Au-loaded TiO_2 semiconductor without light: a new bacteria-killing mechanism other than localized surface plasmon resonance or microbial fuel cells, ACS Appl. Mater. Interfaces 8 (37) (2016) 24509–24516.
[127] Y. Tang, H. Sun, Y. Shang, S. Zeng, Z. Qin, S. Yin, J. Li, S. Liang, G. Lu, Z. Liu, Spiky nanohybrids of titanium dioxide/gold nanoparticles for enhanced photocatalytic degradation and anti-bacterial property, J. Colloid Interface Sci. 535 (2019) 516–523.
[128] J. Li, J. Wang, D. Wang, G. Guo, K.W.K. Yeung, X. Zhang, X. Liu, Band gap engineering of titania film through cobalt regulation for oxidative damage of bacteria respiration and viability, ACS Appl. Mater. Interfaces 9 (33) (2017) 27475–27490.
[129] G. Wang, K. Tang, Z. Meng, P. Liu, S. Mo, B. Mehrjou, H. Wang, X. Liu, Z. Wu, P. K. Chu, A quantitative bacteria monitoring and killing platform based on electron transfer from bacteria to a semiconductor, Adv. Mater. 32 (39) (2020) 2003616.
[130] W. He, H.-K. Kim, W.G. Wamer, D. Melka, J.H. Callahan, J.-J. Yin, Photogenerated charge carriers and reactive oxygen species in ZnO/Au hybrid nanostructures with enhanced photocatalytic and antibacterial activity, J. Am. Chem. Soc. 136 (2) (2013) 750–757.
[131] B. Gao, J. Fu, K. Huo, W. Zhang, Y. Xie, P.K. Chu, Quasi-aligned Ag–Nb_2O_5 nanobelt arrays with enhanced photocatalytic and antibacterial activities, J. Am. Ceram. Soc. 94 (8) (2011) 2330–2338.
[132] J. Li, Z. Li, X. Liu, C. Li, Y. Zheng, K.W.K. Yeung, Z. Cui, Y. Liang, S. Zhu, W. Hu, Y. Qi, T. Zhang, X. Wang, S. Wu, Interfacial engineering of $Bi_2S_3/Ti_3C_2T_x$ MXene based on work function for rapid photo-excited bacteria-killing, Nat. Commun. 12 (1) (2021) 1224.
[133] Y. Liu, Y. Tian, Q. Han, J. Yin, J. Zhang, Y. Yu, W. Yang, Y. Deng, Synergism of 2D/1D MXene/cobalt nanowire heterojunctions for boosted photo-activated antibacterial application, Chem. Eng. J. 410 (2021), 128209.
[134] Z. Xu, M. Li, X. Li, X. Liu, F. Ma, S. Wu, K.W.K. Yeung, Y. Han, P.K. Chu, Antibacterial activity of silver doped titanate nanowires on Ti implants, ACS Appl. Mater. Interfaces 8 (26) (2016) 16584–16594.
[135] G. Wang, W. Jin, A.M. Qasim, A. Gao, X. Peng, W. Li, H. Feng, P.K. Chu, Antibacterial effects of titanium embedded with silver nanoparticles based on electron-transfer-induced reactive oxygen species, Biomaterials 124 (2017) 25–34.
[136] G. Guo, H. Zhou, Q. Wang, J. Wang, J. Tan, J. Li, P. Jin, H. Shen, Nano-layered magnesium fluoride reservoirs on biomaterial surfaces strengthen polymorphonuclear leukocyte resistance to bacterial pathogens, Nanoscale 9 (2017) 875–892.
[137] R. Shi, H. Geng, M. Gong, J. Ye, C. Wu, X. Hu, L. Zhang, Long-acting and broad-spectrum antimicrobial electrospun poly (ε-caprolactone)/gelatin micro/nanofibers for wound dressing, J. Colloid Interface Sci. 509 (2018) 275–284.
[138] R. Shi, Y. Niu, M. Gong, J. Ye, W. Tian, L. Zhang, Antimicrobial gelatin-based elastomer nanocomposite membrane loaded with ciprofloxacin and polymyxin B sulfate in halloysite nanotubes for wound dressing, Mater. Sci. Eng. C 87 (2018) 128–138.
[139] F. Perreault, A.F. de Faria, S. Nejati, M. Elimelech, Antimicrobial properties of graphene oxide nanosheets: why size matters, ACS Nano 9 (7) (2015) 7226–7236.
[140] S. Kang, M. Herzberg, D.F. Rodrigues, M. Elimelech, Antibacterial effects of carbon nanotubes: size does matter!, Langmuir 24 (13) (2008) 6409–6413.
[141] O. Choi, Z. Hu, Size dependent and reactive oxygen species related nanosilver toxicity to nitrifying bacteria, Environ. Sci. Technol. 42 (12) (2008) 4583–4588.
[142] G.A. Martínez-Castañón, N. Niño-Martínez, F. Martínez-Gutierrez, J.R. Martínez-Mendoza, F. Ruiz, Synthesis and antibacterial activity of silver nanoparticles with different sizes, J. Nanopart. Res. 10 (8) (2008) 1343–1348.
[143] S. Mo, B. Mehrjou, K. Tang, H. Wang, K. Huo, A.M. Qasim, G. Wang, P.K. Chu, Dimensional-dependent antibacterial behavior on bioactive micro/nano polyetheretherketone (PEEK) arrays, Chem. Eng. J. 392 (2020), 123736.
[144] T.-O. Peulen, K.J. Wilkinson, Diffusion of nanoparticles in a biofilm, Environ. Sci. Technol. 45 (8) (2011) 3367–3373.
[145] L. Liu, K. Xu, H. Wang, P.K. Jeremy Tan, W. Fan, S.S. Venkatraman, L. Li, Y.-Y. Yang, Self-assembled cationic peptide nanoparticles as an efficient antimicrobial agent, Nat. Nanotechnol. 4 (7) (2009) 457–463.
[146] S. Khalid, A. Gao, G. Wang, P.K. Chu, H. Wang, Tuning surface topographies on biomaterials to control bacterial infection, Biomater. Sci. 8 (24) (2020) 6840–6857.
[147] V.T.H. Pham, V.K. Truong, M.D.J. Quinn, S.M. Notley, Y. Guo, V.A. Baulin, M. Al Kobaisi, R.J. Crawford, E.P. Ivanova, Graphene induces formation of pores that kill spherical and rod-shaped bacteria, ACS Nano 9 (8) (2015) 8458–8467.
[148] G. Wang, W. Jiang, S. Mo, L. Xie, Q. Liao, L. Hu, Q. Ruan, K. Tang, B. Mehrjou, M. Liu, L. Tong, H. Wang, J. Zhuang, G. Wu, P.K. Chu, Nonleaching antibacterial concept demonstrated by in situ construction of 2D nanoflakes on magnesium, Adv. Sci. 7 (1) (2020) 1902089.
[149] S. Pal, Y.K. Tak, J.M. Song, Does the antibacterial activity of silver nanoparticles depend on the shape of the nanoparticle? A study of the gram-negative bacterium Escherichia coli, Appl. Environ. Microbiol. 73 (6) (2007) 1712–1720.
[150] J. Helmlinger, C. Sengstock, C. Groß-Heitfeld, C. Mayer, T.A. Schildhauer, M. Köller, M. Epple, Silver nanoparticles with different size and shape: equal cytotoxicity, but different antibacterial effects, RSC Adv. 6 (22) (2016) 18490–18501.
[151] Y. Zheng, H. Jiang, X. Wang, Facet-dependent antibacterial activity of Au nanocrystals, Chin. Chem. Lett. 31 (12) (2020) 3183–3189.
[152] Y.J. Tang, J.M. Ashcroft, D. Chen, G. Min, C.-H. Kim, B. Murkhejee, C. Larabell, J. D. Keasling, F.F. Chen, Charge-associated effects of fullerene derivatives on microbial structural integrity and central metabolism, Nano Lett. 7 (3) (2007) 754–760.
[153] H.Z. Zardini, A. Amiri, M. Shanbedi, M. Maghrebi, M. Baniadam, Enhanced antibacterial activity of amino acids-functionalized multi walled carbon nanotubes by a simple method, Colloids Surf. B: Biointerfaces 92 (2012) 196–202.
[154] A.M. El Badawy, R.G. Silva, B. Morris, K.G. Scheckel, M.T. Suidan, T.M. Tolaymat, Surface charge-dependent toxicity of silver nanoparticles, Environ. Sci. Technol. 45 (1) (2011) 283–287.
[155] J. Li, X. Liu, Y. Qiao, H. Zhu, J. Li, T. Cui, C. Ding, Enhanced bioactivity and bacteriostasis effect of TiO_2 nanofilms with favorable biomimetic architectures on titanium surface, RSC Adv. 3 (28) (2013) 11214–11225.

[156] R. Wang, M. Shi, F. Xu, Y. Qiu, P. Zhang, K. Shen, Q. Zhao, J. Yu, Y. Zhang, Graphdiyne-modified TiO_2 nanofibers with osteoinductive and enhanced photocatalytic antibacterial activities to prevent implant infection, Nat. Commun. 11 (1) (2020) 4465.
[157] Z. Liu, X. Jiang, Z. Li, Y. Zheng, J.-J. Nie, Z. Cui, Y. Liang, S. Zhu, D. Chen, S. Wu, Recent progress of photo-excited antibacterial materials via chemical vapor deposition, Chem. Eng. J. 437 (2022), 135401.
[158] V. Lakshmi Prasanna, R. Vijayaraghavan, Insight into the mechanism of antibacterial activity of ZnO: surface defects mediated reactive oxygen species even in the dark, Langmuir 31 (33) (2015) 9155–9162.
[159] S. Hussain, J. Joo, J. Kang, B. Kim, G.B. Braun, Z.-G. She, D. Kim, A.P. Mann, T. Mölder, T. Teesalu, S. Carnazza, S. Guglielmino, M.J. Sailor, E. Ruoslahti, Antibiotic-loaded nanoparticles targeted to the site of infection enhance antibacterial efficacy, Nat. Biomed. Eng. 2 (2018) 95–103.
[160] A. Chow, B.D. Brown, M. Merad, Studying the mononuclear phagocyte system in the molecular age, Nat. Rev. Immunol. 11 (11) (2011) 788–798.
[161] G. Storm, S.O. Belliot, T. Daemen, D.D. Lasic, Surface modification of nanoparticles to oppose uptake by the mononuclear phagocyte system, Adv. Drug Deliv. Rev. 17 (1) (1995) 31–48.
[162] V.P. Torchilin, Multifunctional, stimuli-sensitive nanoparticulate systems for drug delivery, Nat. Rev. Drug Discov. 13 (11) (2014) 813–827.
[163] J. Li, X. Jiang, H. Li, M. Gelinsky, Z. Gu, Tailoring materials for modulation of macrophage fate, Adv. Mater. 33 (12) (2021) 2004172.
[164] R.H. Fang, A.V. Kroll, W. Gao, L. Zhang, Cell membrane coating nanotechnology, Adv. Mater. 30 (23) (2018) 1706759.
[165] J. Yan, J. Yu, C. Wang, Z. Gu, Red blood cells for drug delivery, Small Methods 1 (12) (2017) 1700270.
[166] L. Rao, R. Tian, X. Chen, Cell-membrane-mimicking nanodecoys against infectious diseases, ACS Nano 14 (3) (2020) 2569–2574.
[167] M. Elsabahy, K.L. Wooley, Design of polymeric nanoparticles for biomedical delivery applications, Chem. Soc. Rev. 41 (7) (2012) 2545–2561.
[168] W. Chen, C.A. Glackin, M.A. Horwitz, J.I. Zink, Nanomachines and other caps on mesoporous silica nanoparticles for drug delivery, Acc. Chem. Res. 52 (6) (2019) 1531–1542.
[169] D.O. Schairer, J.S. Chouake, J.D. Nosanchuk, A.J. Friedman, The potential of nitric oxide releasing therapies as antimicrobial agents, Virulence 3 (3) (2012) 271–279.
[170] A.J. Friedman, G. Han, M.S. Navati, M. Chacko, L. Gunther, A. Alfieri, J. M. Friedman, Sustained release nitric oxide releasing nanoparticles: characterization of a novel delivery platform based on nitrite containing hydrogel/glass composites, Nitric Oxide 19 (1) (2008) 12–20.
[171] E.M. Hetrick, J.H. Shin, N.A. Stasko, C.B. Johnson, D.A. Wespe, E. Holmuhamedov, M.H. Schoenfisch, Bactericidal efficacy of nitric oxide-releasing silica nanoparticles, ACS Nano 2 (2) (2008) 235–246.
[172] Q. Gao, X. Zhang, W. Yin, D. Ma, C. Xie, L. Zheng, X. Dong, L. Mei, J. Yu, C. Wang, Z. Gu, Y. Zhao, Functionalized MoS_2 nanovehicle with near-infrared laser-mediated nitric oxide release and photothermal activities for advanced bacteria-infected wound therapy, Small 14 (45) (2018) 1802290.
[173] S. Yu, G. Li, R. Liu, D. Ma, W. Xue, Dendritic Fe_3O_4@poly(dopamine)@PAMAM nanocomposite as controllable NO-releasing material: a synergistic photothermal and NO antibacterial study, Adv. Funct. Mater. 28 (20) (2018) 1707440.
[174] B.J. Nablo, A.R. Rothrock, M.H. Schoenfisch, Nitric oxide-releasing sol–gels as antibacterial coatings for orthopedic implants, Biomaterials 26 (8) (2005) 917–924.
[175] Y. Ren, H. Liu, X. Liu, Y. Zheng, Z. Li, C. Li, K.W.K. Yeung, S. Zhu, Y. Liang, Z. Cui, S. Wu, Photoresponsive materials for antibacterial applications, cell reports physical, Science 1 (11) (2020), 100245.
[176] M.R. Hamblin, T. Hasan, Photodynamic therapy: a new antimicrobial approach to infectious disease? Photochem. Photobiol. Sci. 3 (5) (2004) 436–450.
[177] T. Wei, Q. Yu, H. Chen, Responsive and synergistic antibacterial coatings: fighting against bacteria in a smart and effective way, Adv. Healthc. Mater. 8 (3) (2019) 1801381.
[178] F. Cieplik, D. Deng, W. Crielaard, W. Buchalla, E. Hellwig, A. Al-Ahmad, T. Maisch, Antimicrobial photodynamic therapy – what we know and what we don't, Crit. Rev. Microbiol. 44 (5) (2018) 571–589.
[179] Q. Jia, Q. Song, P. Li, W. Huang, Rejuvenated photodynamic therapy for bacterial infections, Adv. Healthcare Mater. 8 (14) (2019) 1900608.
[180] H. Abrahamse, Michael R. Hamblin, New photosensitizers for photodynamic therapy, Biochem. J. 473 (4) (2016) 347–364.
[181] M. Lan, S. Zhao, W. Liu, C.-S. Lee, W. Zhang, P. Wang, Photosensitizers for photodynamic therapy, Adv. Healthcare Mater. 8 (13) (2019) 1900132.
[182] A. Turksoy, D. Yildiz, E.U. Akkaya, Photosensitization and controlled photosensitization with BODIPY dyes, Coord. Chem. Rev. 379 (2019) 47–64.
[183] P. Ganguly, C. Byrne, A. Breen, S.C. Pillai, Antimicrobial activity of photocatalysts: fundamentals, mechanisms, kinetics and recent advances, Appl. Catal. B: Environ. 225 (2018) 51–75.
[184] B. Yang, Y. Chen, J. Shi, Reactive oxygen species (ros)-based nanomedicine, Chem. Rev. 119 (8) (2019) 4881–4985.
[185] B. Wang, M. Wang, A. Mikhailovsky, S. Wang, G.C. Bazan, A. Membrane-Intercalating, Conjugated oligoelectrolyte with high-efficiency photodynamic antimicrobial activity, Angew. Chem. Int. Ed. 56 (18) (2017) 5031–5034.
[186] C. Mao, Y. Xiang, X. Liu, Z. Cui, X. Yang, Z. Li, S. Zhu, Y. Zheng, K.W.K. Yeung, S. Wu, A repeatable photodynamic therapy with triggered signaling pathways of fibroblast cell proliferation and differentiation to promote bacteria-accompanied wound healing, ACS Nano 12 (2) (2018) 1747–1759.
[187] J. Li, S. Song, J. Meng, L. Tan, X. Liu, Y. Zheng, Z. Li, K.W.K. Yeung, Z. Cui, Y. Liang, S. Zhu, X. Zhang, S. Wu, 2D MOF periodontitis photodynamic ion therapy, J. Am. Chem. Soc. 143 (37) (2021) 15427–15439.
[188] Z. Liu, X. Liu, Z. Cui, Y. Zheng, Z. Li, Y. Liang, X. Yuan, S. Zhu, S. Wu, Surface photodynamic ion sterilization of ITO-Cu_2O/ZnO preventing touch infection, J. Mater. Sci. Technol. 122 (2022) 10–19.
[189] Y.-D. Sun, Y.-X. Zhu, X. Zhang, H.-R. Jia, Y. Xia, F.-G. Wu, Role of cholesterol conjugation in the antibacterial photodynamic therapy of branched polyethylenimine-containing nanoagents, Langmuir 35 (44) (2019) 14324–14331.
[190] Y. Zhao, Q. Guo, X. Dai, X. Wei, Y. Yu, X. Chen, C. Li, Z. Cao, X. Zhang, A. Biomimetic, Non-antibiotic approach to eradicate drug-resistant infections, Adv. Mater. 31 (7) (2019) 1806024.
[191] Y. Wu, Q. Liao, L. Wu, Y. Luo, W. Zhang, M. Guan, H. Pan, L. Tong, P.K. Chu, H. Wang, ZnL_2-BPs integrated bone scaffold under sequential photothermal mediation: a win–win strategy delivering antibacterial therapy and fostering osteogenesis thereafter, ACS Nano 15 (11) (2021) 17854–17869.
[192] C. Wang, Y. Wang, L. Zhang, R.J. Miron, J. Liang, M. Shi, W. Mo, S. Zheng, Y. Zhao, Y. Zhang, Pretreated macrophage-membrane-coated gold nanocages for precise drug delivery for treatment of bacterial infections, Adv. Mater. 30 (46) (2018) 1804023.
[193] Q. Xu, F. Jiang, G. Guo, E. Wang, M.R. Younis, Z. Zhang, F. Zhang, Z. Huan, C. Fan, C. Yang, H. Shen, J. Chang, Targeted hot ion therapy of infected wound by glycol chitosan and polydopamine grafted Cu-SiO_2 nanoparticles, Nano Today 41 (2021), 101330.
[194] X. Xu, X. Liu, L. Tan, Z. Cui, X. Yang, S. Zhu, Z. Li, X. Yuan, Y. Zheng, K.W. K. Yeung, P.K. Chu, S. Wu, Controlled-temperature photothermal and oxidative bacteria killing and acceleration of wound healing by polydopamine-assisted Au-hydroxyapatite nanorods, Acta Biomater. 77 (2018) 352–364.
[195] G. Zhang, X. Zhang, Y. Yang, R. Chi, J. Shi, R. Hang, X. Huang, X. Yao, P.K. Chu, X. Zhang, Dual light-induced in situ antibacterial activities of biocompatibleTiO_2/MoS_2/PDA/RGD nanorod arrays on titanium, Biomater. Sci. 8 (1) (2020) 391–404.
[196] X. Zhang, G. Zhang, M. Chai, X. Yao, W. Chen, P.K. Chu, Synergistic antibacterial activity of physical-chemical multi-mechanism by TiO_2 nanorod arrays for safe biofilm eradication on implant, Bioact. Mater. 6 (1) (2021) 12–25.
[197] M. Li, X. Liu, L. Tan, Z. Cui, X. Yang, Z. Li, Y. Zheng, K.W.K. Yeung, P.K. Chu, S. Wu, Noninvasive rapid bacteria-killing and acceleration of wound healing through photothermal/photodynamic/copper ion synergistic action of a hybrid hydrogel, Biomater. Sci. 6 (8) (2018) 2110–2121.
[198] X. Ma, L. Wang, P. Wang, Z. Liu, J. Hao, J. Wu, G. Chu, M. Huang, L.O. Mair, C. Huang, T. Xu, T. Ying, X. Tang, Y. Chen, X. Cai, Y. Zheng, An electromagnetically actuated magneto-nanozyme mediated synergistic therapy for destruction and eradication of biofilm, Chem. Eng. J. 431 (2022), 133971.
[199] Q. Yu, T. Deng, F.-C. Lin, B. Zhang, J.I. Zink, Supramolecular assemblies of heterogeneous mesoporous silica nanoparticles to Co-deliver antimicrobial peptides and antibiotics for synergistic eradication of pathogenic biofilms, ACS Nano 14 (5) (2020) 5926–5937.
[200] K. Quan, Z. Zhang, H. Chen, X. Ren, Y. Ren, B.W. Peterson, H.C. van der Mei, H. J. Busscher, Artificial channels in an infectious biofilm created by magnetic nanoparticles enhanced bacterial killing by antibiotics, Small 15 (39) (2019) 1902313.
[201] Y. Qiao, X. Liu, B. Li, Y. Han, Y. Zheng, K.W.K. Yeung, C. Li, Z. Cui, Y. Liang, Z. Li, S. Zhu, X. Wang, S. Wu, Treatment of MRSA-infected osteomyelitis using bacterial capturing, magnetically targeted composites with microwave-assisted bacterial killing, Nat. Commun. 11 (1) (2020) 4446.
[202] S. Hernot, A.L. Klibanov, Microbubbles in ultrasound-triggered drug and gene delivery, Adv. Drug Deliv. Rev. 60 (10) (2008) 1153–1166.
[203] V. Frenkel, Ultrasound mediated delivery of drugs and genes to solid tumors, Adv. Drug Deliv. Rev. 60 (10) (2008) 1193–1208.
[204] J.E. Kennedy, G.R. ter Haar, D. Cranston, High intensity focused ultrasound: surgery of the future? Br. J. Radiol. 76 (909) (2003) 590–599.
[205] J.E. Kennedy, High-intensity focused ultrasound in the treatment of solid tumours, Nat. Rev. Cancer 5 (4) (2005) 321–327.
[206] R.O. Illing, J.E. Kennedy, F. Wu, G.R. ter Haar, A.S. Protheroe, P.J. Friend, F. V. Gleeson, D.W. Cranston, R.R. Phillips, M.R. Middleton, The safety and feasibility of extracorporeal high-intensity focused ultrasound (HIFU) for the treatment of liver and kidney tumours in a Western population, Br. J. Cancer 93 (8) (2005) 890–895.
[207] H. Ter, G.T. Gail, C. Coussios, High intensity focused ultrasound: physical principles and devices, Int. J. Hyperth. 23 (2) (2007) 89–104.
[208] H. Chen, X. Zhou, Y. Gao, B. Zheng, F. Tang, J. Huang, Recent progress in development of new sonosensitizers for sonodynamic cancer therapy, Drug Discov. Today 19 (4) (2014) 502–509.
[209] D. Costley, C. Mc Ewan, C. Fowley, A.P. McHale, J. Atchison, N. Nomikou, J. F. Callan, Treating cancer with sonodynamic therapy: a review, Int. J. Hyperth. 31 (2) (2015) 107–117.
[210] X. Qian, Y. Zheng, Y. Chen, Micro/nanoparticle-augmented sonodynamic therapy (SDT): breaking the depth shallow of photoactivation, Adv. Mater. 28 (37) (2016) 8097–8129.
[211] Y. Yu, L. Tan, Z. Li, X. Liu, Y. Zheng, X. Feng, Y. Liang, Z. Cui, S. Zhu, S. Wu, Single-atom catalysis for efficient sonodynamic therapy of methicillin-resistant staphylococcus aureus-infected osteomyelitis, ACS Nano 15 (6) (2021) 10628–10639.

[212] J. Lei, C. Wang, X. Feng, L. Ma, X. Liu, Y. Luo, L. Tan, S. Wu, C. Yang, Sulfur-regulated defect engineering for enhanced ultrasonic piezocatalytic therapy of bacteria-infected bone defects, Chem. Eng. J. 435 (2022), 134624.
[213] S. Mitragotri, Healing sound: the use of ultrasound in drug delivery and other therapeutic applications, Nat. Rev. Drug Discov. 4 (3) (2005) 255–260.
[214] D. Pornpattananangkul, L. Zhang, S. Olson, S. Aryal, M. Obonyo, K. Vecchio, C.-M. Huang, L. Zhang, Bacterial toxin-triggered drug release from gold nanoparticle-stabilized liposomes for the treatment of bacterial infection, J. Am. Chem. Soc. 133 (11) (2011) 4132–4139.
[215] R.-C. Mercier, C. Stumpo, M.J. Rybak, Effect of growth phase and pH on the in vitro activity of a new glycopeptide, oritavancin (LY333328), against Staphylococcus aureus and Enterococcus faecium, J. Antimicrob. Chemother. 50 (1) (2002) 19–24.
[216] S. Wu, C. Xu, Y. Zhu, L. Zheng, L. Zhang, Y. Hu, B. Yu, Y. Wang, F.-J. Xu, Biofilm-sensitive photodynamic nanoparticles for enhanced penetration and antibacterial efficiency, Adv. Funct. Mater. 31 (33) (2021) 2103591.
[217] A.F. Radovic-Moreno, T.K. Lu, V.A. Puscasu, C.J. Yoon, R. Langer, O. C. Farokhzad, Surface charge-switching polymeric nanoparticles for bacterial cell wall-targeted delivery of antibiotics, ACS Nano 6 (5) (2012) 4279–4287.
[218] C. Mao, X. Xie, X. Liu, Z. Cui, X. Yang, K.W.K. Yeung, H. Pan, P.K. Chu, S. Wu, The controlled drug release by pH-sensitive molecularly imprinted nanospheres for enhanced antibacterial activity, Mater. Sci. Eng. C 77 (2017) 84–91.
[219] A. van der Vliet, Y.M.W. Janssen-Heininger, Hydrogen peroxide as a damage signal in tissue injury and inflammation: murderer, mediator, or messenger? J. Cell. Biochem. 115 (3) (2014) 427–435.
[220] G. Guo, H. Zhang, H. Shen, C. Zhu, R. He, J. Tang, Y. Wang, X. Jiang, J. Wang, W. Bu, X. Zhang, Space-selective chemodynamic therapy of $CuFe_5O_8$ nanocubes for implant-related infections, ACS Nano 14 (10) (2020) 13391–13405.
[221] P.C. Naha, Y. Liu, G. Hwang, Y. Huang, S. Gubara, V. Jonnakuti, A. Simon-Soro, D. Kim, L. Gao, H. Koo, D.P. Cormode, Dextran-coated iron oxide nanoparticles as biomimetic catalysts for localized and pH-activated biofilm disruption, ACS Nano 13 (5) (2019) 4960–4971.
[222] P.A. Forsyth, H. Wong, T.D. Laing, N.B. Rewcastle, D.G. Morris, H. Muzik, K. J. Leco, R.N. Johnston, P.M.A. Brasher, G. Sutherland, D.R. Edwards, Gelatinase-A (MMP-2), gelatinase-B (MMP-9) and membrane type matrix metalloproteinase-1 (MT1-MMP) are involved in different aspects of the pathophysiology of malignant gliomas, Br. J. Cancer 79 (11) (1999) 1828–1835.
[223] L.-L. Li, J.-H. Xu, G.-B. Qi, X. Zhao, F. Yu, H. Wang, Core–shell supramolecular gelatin nanoparticles for adaptive and "on-demand" antibiotic delivery, ACS Nano 8 (5) (2014) 4975–4983.
[224] J. Li, M. Pumera, 3D printing of functional microrobots, Chem. Soc. Rev. 50 (4) (2021) 2794–2838.
[225] S. Sánchez, L. Soler, J. Katuri, Chemically powered micro- and nanomotors, Angew. Chem. Int. Ed. 54 (5) (2015) 1414–1444.
[226] J. Li, C.C. Mayorga-Martinez, C.-D. Ohl, M. Pumera, Ultrasonically propelled micro- and nanorobots, Adv. Funct. Mater. 32 (5) (2022) 2102265.
[227] L. Xu, F. Mou, H. Gong, M. Luo, J. Guan, Light-driven micro/nanomotors: from fundamentals to applications, Chem. Soc. Rev. 46 (22) (2017) 6905–6926.
[228] X.-Z. Chen, B. Jang, D. Ahmed, C. Hu, C. De Marco, M. Hoop, F. Mushtaq, B. J. Nelson, S. Pané, Small-scale machines driven by external power sources, Adv. Mater. 30 (15) (2018) 1705061.
[229] J. Li, L. Dekanovsky, B. Khezri, B. Wu, H. Zhou, Z. Sofer, Biohybrid micro- and nanorobots for intelligent drug delivery, Cyborg Bionic Syst. 2022 (2022) 9824057.
[230] Y. Alapan, O. Yasa, B. Yigit, I.C. Yasa, P. Erkoc, M. Sitti, Microrobotics and microorganisms: biohybrid autonomous cellular robots, Annu. Rev. Control, Robot., Auton. Syst. 2 (2018) 205–230.
[231] S. Zhao, D. Sun, J. Zhang, H. Lu, Y. Wang, R. Xiong, K.T.V. Grattan, Actuation and biomedical development of micro-/nanorobots – a review, Mater. Today Nano 18 (2022), 100223.
[232] M. Sitti, D.S. Wiersma, Pros and cons: magnetic versus optical microrobots, Adv. Mater. 32 (20) (2020) 1906766.
[233] W. Wang, W. Duan, S. Ahmed, T.E. Mallouk, A. Sen, Small power: autonomous nano- and micromotors propelled by self-generated gradients, Nano Today 8 (5) (2013) 531–554.
[234] W.Z. Teo, H. Wang, M. Pumera, Beyond platinum: silver-catalyst based bubble-propelled tubular micromotors, Chem. Commun. 52 (23) (2016) 4333–4336.
[235] V.V. Singh, B. Jurado-Sánchez, S. Sattayasamitsathit, J. Orozco, J. Li, M. Galarnyk, Y. Fedorak, J. Wang, Multifunctional silver-exchanged zeolite micromotors for catalytic detoxification of chemical and biological threats, Adv. Funct. Mater. 25 (14) (2015) 2147–2155.
[236] L. Soler, V. Magdanz, V.M. Fomin, S. Sanchez, O.G. Schmidt, Self-propelled micromotors for cleaning polluted water, ACS Nano 7 (11) (2013) 9611–9620.
[237] D.A. Wilson, R.J.M. Nolte, J.C.M. van Hest, Autonomous movement of platinum-loaded stomatocytes, Nat. Chem. 4 (2012) 268.
[238] X. Ma, K. Hahn, S. Sanchez, Catalytic mesoporous janus nanomotors for active cargo delivery, J. Am. Chem. Soc. 137 (15) (2015) 4976–4979.
[239] H. Wang, G. Zhao, M. Pumera, Beyond platinum: bubble-propelled micromotors based on Ag and MnO_2 catalysts, J. Am. Chem. Soc. 136 (7) (2014) 2719–2722.
[240] W. Liu, H. Ge, X. Ding, X. Lu, Y. Zhang, Z. Gu, Cubic nano-silver-decorated manganese dioxide micromotors: enhanced propulsion and antibacterial performance, Nanoscale 12 (38) (2020) 19655–19664.
[241] J. Li, V.V. Singh, S. Sattayasamitsathit, J. Orozco, K. Kaufmann, R. Dong, W. Gao, B. Jurado-Sanchez, Y. Fedorak, J. Wang, Water-driven micromotors for rapid photocatalytic degradation of biological and chemical warfare agents, ACS Nano 8 (11) (2014) 11118–11125.
[242] C. Chen, E. Karshalev, J. Guan, J. Wang, Magnesium-based micromotors: water-powered propulsion, multifunctionality, and biomedical and environmental applications, Small 14 (23) (2018) 1704252.
[243] C. Xu, S. Wang, H. Wang, K. Liu, S. Zhang, B. Chen, H. Liu, F. Tong, F. Peng, Y. Tu, Y. Li, Magnesium-based micromotors as hydrogen generators for precise rheumatoid arthritis therapy, Nano Lett. 21 (5) (2021) 1982–1991.
[244] W. Gao, R. Dong, S. Thamphiwatana, J. Li, W. Gao, L. Zhang, J. Wang, Artificial micromotors in the mouse's stomach: a step toward in vivo use of synthetic motors, ACS Nano 9 (1) (2015) 117–123.
[245] W. Gao, A. Uygun, J. Wang, Hydrogen-bubble-propelled zinc-based microrockets in strongly acidic media, J. Am. Chem. Soc. 134 (2) (2012) 897–900.
[246] B. Esteban-Fernández de Ávila, M.A. Lopez-Ramirez, R. Mundaca-Uribe, X. Wei, D.E. Ramírez-Herrera, E. Karshalev, B. Nguyen, R.H. Fang, L. Zhang, J. Wang, Multicompartment tubular micromotors toward enhanced localized active delivery, Adv. Mater. 32 (25) (2020) 2000091.
[247] W.Z. Teo, R. Zboril, I. Medrik, M. Pumera, Fe^0 nanomotors in ton quantities (10^{20} Units) for environmental remediation, Chem. – A Eur. J. 22 (14) (2016) 4789–4793.
[248] W. Gao, A. Pei, J. Wang, Water-driven micromotors, ACS Nano 6 (9) (2012) 8432–8438.
[249] M. Guix, A.K. Meyer, B. Koch, O.G. Schmidt, Carbonate-based Janus micromotors moving in ultra-light acidic environment generated by HeLa cells in situ, Sci. Rep. 6 (2016) 21701.
[250] J.R. Baylis, J.H. Yeon, M.H. Thomson, A. Kazerooni, X. Wang, A.E. John St., E. B. Lim, D. Chien, A. Lee, J.Q. Zhang, J.M. Piret, L.S. Machan, T.F. Burke, N. J. White, C.J. Kastrup, Self-propelled particles that transport cargo through flowing blood and halt hemorrhage, Sci. Adv. 1 (9) (2015), e1500379.
[251] T. Patiño, N. Feiner-Gracia, X. Arqué, A. Miguel-López, A. Jannasch, T. Stumpp, E. Schäffer, L. Albertazzi, S. Sánchez, Influence of enzyme quantity and distribution on the self-propulsion of non-janus urease-powered micromotors, J. Am. Chem. Soc. 140 (25) (2018) 7896–7903.
[252] H. Choi, S.H. Jeong, T.Y. Kim, J. Yi, S.K. Hahn, Bioinspired urease-powered micromotor as an active oral drug delivery carrier in stomach, Bioact. Mater. 9 (2022) 54–62.
[253] A.C. Hortelao, C. Simó, M. Guix, S. Guallar-Garrido, E. Julián, D. Vilela, L. Rejc, P. Ramos-Cabrer, U. Cossío, V. Gómez-Vallejo, T. Patiño, J. Llop, S. Sánchez, Swarming behavior and in vivo monitoring of enzymatic nanomotors within the bladder, Sci. Robot. 6 (52) (2021) eabd2823.
[254] S. Sanchez, A.A. Solovev, Y. Mei, O.G. Schmidt, Dynamics of biocatalytic microengines mediated by variable friction control, J. Am. Chem. Soc. 132 (38) (2010) 13144–13145.
[255] X. Ma, A. Jannasch, U.-R. Albrecht, K. Hahn, A. Miguel-López, E. Schäffer, S. Sánchez, Enzyme-powered hollow mesoporous janus nanomotors, Nano Lett. 15 (10) (2015) 7043–7050.
[256] Z. Guo, T. Wang, A. Rawal, J. Hou, Z. Cao, H. Zhang, J. Xu, Z. Gu, V. Chen, K. Liang, Biocatalytic self-propelled submarine-like metal-organic framework microparticles with pH-triggered buoyancy control for directional vertical motion, Mater. Today 28 (2019) 10–16.
[257] L. Wang, A.C. Hortelão, X. Huang, S. Sánchez, Lipase-powered mesoporous silica nanomotors for triglyceride degradation, Angew. Chem. Int. Ed. 58 (24) (2019) 7992–7996.
[258] L. Wang, M. Marciello, M. Estévez-Gay, P.E.D.S. Rodriguez, Y.L. Morato, J. Iglesias-Fernández, X. Huang, S. Osuna, M. Filice, S. Sanchez, Enzyme conformation influences the performance of lipase-powered nanomotors, Angew. Chem. Int. Ed. 59 (47) (2020) 21080–21087.
[259] P.S. Schattling, M.A. Ramos-Docampo, V. Salgueiriño, B. Städler, Double-fueled janus swimmers with magnetotactic behavior, ACS Nano 11 (4) (2017) 3973–3983.
[260] X. Arqué, A. Romero-Rivera, F. Feixas, T. Patiño, S. Osuna, S. Sánchez, Intrinsic enzymatic properties modulate the self-propulsion of micromotors, Nat. Commun. 10 (1) (2019) 2826.
[261] C. Gao, C. Zhou, Z. Lin, M. Yang, Q. He, Surface wettability-directed propulsion of glucose-powered nanoflask motors, ACS Nano 13 (11) (2019) 12758–12766.
[262] W. Qin, T. Peng, Y. Gao, F. Wang, X. Hu, K. Wang, J. Shi, D. Li, J. Ren, C. Fan, Catalysis-driven self-thermophoresis of janus plasmonic nanomotors, Angew. Chem. Int. Ed. 56 (2) (2017) 515–518.
[263] Z. Wu, X. Lin, Y. Wu, T. Si, J. Sun, Q. He, Near-infrared light-triggered "on/off" motion of polymer multilayer rockets, ACS Nano 8 (6) (2014) 6097–6105.
[264] M. Xuan, Z. Wu, J. Shao, L. Dai, T. Si, Q. He, Near infrared light-powered janus mesoporous silica nanoparticle motors, J. Am. Chem. Soc. 138 (20) (2016) 6492–6497.
[265] M. Xuan, J. Shao, C. Gao, W. Wang, L. Dai, Q. He, Self-propelled nanomotors for thermomechanically percolating cell membranes, Angew. Chem. Int. Ed. 130 (38) (2018) 12643–12647.
[266] M. Xuan, R. Mestre, C. Gao, C. Zhou, Q. He, S. Sánchez, Noncontinuous super-diffusive dynamics of a light-activated nanobottle motor, Angew. Chem. Int. Ed. 57 (23) (2018) 6838–6842.
[267] A.P. Bregulla, H. Yang, F. Cichos, Stochastic localization of microswimmers by photon nudging, ACS Nano 8 (7) (2014) 6542–6550.
[268] B. Qian, D. Montiel, A. Bregulla, F. Cichos, H. Yang, Harnessing thermal fluctuations for purposeful activities: the manipulation of single micro-swimmers by adaptive photon nudging, Chem. Sci. 4 (4) (2013) 1420–1429.
[269] X. Wang, V. Sridhar, S. Guo, N. Talebi, A. Miguel-López, K. Hahn, P.A. van Aken, S. Sánchez, Fuel-free nanocap-like motors actuated under visible light, Adv. Funct. Mater. 28 (25) (2018) 1705862.

[270] K. Villa, F. Novotný, J. Zelenka, M.P. Browne, T. Ruml, M. Pumera, Visible-light-driven single-component $BiVO_4$ micromotors with the autonomous ability for capturing microorganisms, ACS Nano 13 (7) (2019) 8135–8145.
[271] Y.S. Kochergin, K. Villa, F. Novotný, J. Plutnar, M.J. Bojdys, M. Pumera, Multifunctional visible-light powered micromotors based on semiconducting sulfur- and nitrogen-containing donor–acceptor polymer, Adv. Funct. Mater. 30 (38) (2020) 2002701.
[272] J. Zheng, J. Wang, Z. Xiong, Z. Wan, X. Zhan, S. Yang, J. Chen, J. Dai, J. Tang, Full spectrum tunable visible-light-driven alloy nanomotor, Adv. Funct. Mater. 29 (27) (2019) 1901768.
[273] R. Dong, Y. Hu, Y. Wu, W. Gao, B. Ren, Q. Wang, Y. Cai, Visible-light-driven BiOI-based janus micromotor in pure water, J. Am. Chem. Soc. 139 (5) (2017) 1722–1725.
[274] J. Zheng, B. Dai, J. Wang, Z. Xiong, Y. Yang, J. Liu, X. Zhan, Z. Wan, J. Tang, Orthogonal navigation of multiple visible-light-driven artificial microswimmers, Nat. Commun. 8 (1) (2017) 1438.
[275] M. Ibele, T.E. Mallouk, A. Sen, Schooling behavior of light-powered autonomous micromotors in water, Angew. Chem. Int. Ed. 48 (18) (2009) 3308–3312.
[276] Y. Hong, M. Diaz, U.M. Córdova-Figueroa, A. Sen, Light-driven titanium-dioxide-based reversible microfireworks and micromotor/micropump systems, Adv. Funct. Mater. 20 (10) (2010) 1568–1576.
[277] C. Chen, F. Mou, L. Xu, S. Wang, J. Guan, Z. Feng, Q. Wang, L. Kong, W. Li, J. Wang, Q. Zhang, Light-steered isotropic semiconductor micromotors, Adv. Mater. 29 (3) (2017) 1603374.
[278] B. Dai, J. Wang, Z. Xiong, X. Zhan, W. Dai, C.-C. Li, S.-P. Feng, J. Tang, Programmable artificial phototactic microswimmer, Nat. Nanotechnol. 11 (2016) 1087.
[279] M. Enachi, M. Guix, V. Postolache, V. Ciobanu, V.M. Fomin, O.G. Schmidt, I. Tiginyanu, Light-induced motion of microengines based on microarrays of TiO_2 nanotubes, Small 12 (39) (2016) 5497–5505.
[280] G. Loget, A. Kuhn, Electric field-induced chemical locomotion of conducting objects, Nat. Commun. 2 (1) (2011) 535.
[281] C.W. Shields IV, K. Han, F. Ma, T. Miloh, G. Yossifon, O.D. Velev, Supercolloidal spinners: complex active particles for electrically powered and switchable rotation, Adv. Funct. Mater. 28 (35) (2018) 1803465.
[282] E. Kopperger, J. List, S. Madhira, F. Rothfischer, D.C. Lamb, F.C. Simmel, A self-assembled nanoscale robotic arm controlled by electric fields, Science 359 (6373) (2018) 296.
[283] Y. Alapan, O. Yasa, O. Schauer, J. Giltinan, A.F. Tabak, V. Sourjik, M. Sitti, Soft erythrocyte-based bacterial microswimmers for cargo delivery, Sci. Robot. 3 (17) (2018) eaar4423.
[284] S. Taherkhani, M. Mohammadi, J. Daoud, S. Martel, M. Tabrizian, Covalent binding of nanoliposomes to the surface of magnetotactic bacteria for the synthesis of self-propelled therapeutic agents, ACS Nano 8 (5) (2014) 5049–5060.
[285] O. Yasa, P. Erkoc, Y. Alapan, M. Sitti, Microalga-powered microswimmers toward active cargo delivery, Adv. Mater. 30 (45) (2018) 1804130.
[286] M.B. Akolpoglu, N.O. Dogan, U. Bozuyuk, H. Ceylan, S. Kizilel, M. Sitti, High-yield production of biohybrid microalgae for on-demand cargo delivery, Adv. Sci. 7 (16) (2020) 2001256.
[287] G. Santomauro, A.V. Singh, B.-W. Park, M. Mohammadrahimi, P. Erkoc, E. Goering, G. Schütz, M. Sitti, J. Bill, Incorporation of terbium into a microalga leads to magnetotactic swimmers, Adv. Biosyst. 2 (12) (2018) 1800039.
[288] V. Magdanz, S. Sanchez, O.G. Schmidt, Development of a sperm-flagella driven micro-bio-robot, Adv. Mater. 25 (45) (2013) 6581–6588.
[289] H. Xu, M. Medina-Sánchez, V. Magdanz, L. Schwarz, F. Hebenstreit, O.G. Schmidt, Sperm-hybrid micromotor for targeted drug delivery, ACS Nano 12 (1) (2018) 327–337.
[290] V. Sridhar, B.-W. Park, S. Guo, P.A. van Aken, M. Sitti, Multi-wavelength steerable visible light-driven magnetic CoO-TiO_2 microswimmers, ACS Appl. Mater. Interfaces 12 (21) (2020) 24149–24155.
[291] C. Chen, S. Tang, H. Teymourian, E. Karshalev, F. Zhang, J. Li, F. Mou, Y. Liang, J. Guan, J. Wang, Chemical/light-powered hybrid micromotors with "on-the-fly" optical brakes, Angew. Chem. 130 (27) (2018) 8242–8246.
[292] A.A. Solovev, E.J. Smith, C.C. Bof 'Bufon, S. Sanchez, O.G. Schmidt, Light-controlled propulsion of catalytic microengines, Angew. Chem. Int. Ed. 50 (46) (2011) 10875–10878.
[293] J.G.S. Moo, C.C. Mayorga-Martinez, H. Wang, W.Z. Teo, B.H. Tan, T.D. Luong, S. R. Gonzalez-Avila, C.-D. Ohl, M. Pumera, Bjerknes forces in motion: long-range translational motion and chiral directionality switching in bubble-propelled micromotors via an ultrasonic pathway, Adv. Funct. Mater. 28 (25) (2018) 1702618.
[294] T. Xu, F. Soto, W. Gao, V. Garcia-Gradilla, J. Li, X. Zhang, J. Wang, Ultrasound-modulated bubble propulsion of chemically powered microengines, J. Am. Chem. Soc. 136 (24) (2014) 8552–8555.
[295] J.M. McNeill, N. Nama, J.M. Braxton, T.E. Mallouk, Wafer-scale fabrication of micro- to nanoscale bubble swimmers and their fast autonomous propulsion by ultrasound, ACS Nano 14 (6) (2020) 7520–7528.
[296] J. Li, T. Li, T. Xu, M. Kiristi, W. Liu, Z. Wu, J. Wang, Magneto–acoustic hybrid nanomotor, Nano Lett. 15 (7) (2015) 4814–4821.
[297] D. Ahmed, T. Baasch, N. Blondel, N. Läubli, J. Dual, B.J. Nelson, Neutrophil-inspired propulsion in a combined acoustic and magnetic field, Nat. Commun. 8 (1) (2017) 770.
[298] S. Tang, F. Zhang, J. Zhao, W. Talaat, F. Soto, E. Karshalev, C. Chen, Z. Hu, X. Lu, J. Li, Z. Lin, H. Dong, X. Zhang, A. Nourhani, J. Wang, Structure-dependent optical modulation of propulsion and collective behavior of acoustic/light-driven hybrid microbowls, Adv. Funct. Mater. 29 (23) (2019) 1809003.
[299] D. Zhou, Y. Gao, J. Yang, Y.C. Li, G. Shao, G. Zhang, T. Li, L. Li, Light-ultrasound driven collective "firework" behavior of nanomotors, Adv. Sci. 5 (7) (2018) 1800122.
[300] Z. Xiao, S. Duan, P. Xu, J. Cui, H. Zhang, W. Wang, Synergistic speed enhancement of an electric-photochemical hybrid micromotor by tilt rectification, ACS Nano 14 (7) (2020) 8658–8667.
[301] R. Blakemore, Magnetotactic bacteria, Science 190 (4212) (1975) 377.
[302] D.A. Bazylinski, R.B. Frankel, Magnetosome formation in prokaryotes, Nat. Rev. Microbiol. 2 (2004) 217.
[303] C.-Y. Chen, C.-F. Chen, Y. Yi, L.-J. Chen, L.-F. Wu, T. Song, Construction of a microrobot system using magnetotactic bacteria for the separation of Staphylococcus aureus, Biomed. Micro 16 (5) (2014) 761–770.
[304] R.A. Greenfield, D.A. Drevets, L.J. Machado, G.W. Voskuhl, P. Cornea, M. S. Bronze, Bacterial pathogens as biological weapons and agents of bioterrorism, Am. J. Med. Sci. 323 (6) (2002) 299–315.
[305] P.J. Vikesland, K.R. Wigginton, Nanomaterial enabled biosensors for pathogen monitoring - a review, Environ. Sci. Technol. 44 (10) (2010) 3656–3669.
[306] S. Campuzano, J. Orozco, D. Kagan, M. Guix, W. Gao, S. Sattayasamitsathit, J. C. Claussen, A. Merkoçi, J. Wang, Bacterial isolation by lectin-modified microengines, Nano Lett. 12 (1) (2012) 396–401.
[307] F. Wang, W. Gao, S. Thamphiwatana, B.T. Luk, P. Angsantikul, Q. Zhang, C.-M. J. Hu, R.H. Fang, J.A. Copp, D. Pornpattananangkul, W. Lu, L. Zhang, Hydrogel retaining toxin-absorbing nanosponges for local treatment of methicillin-resistant staphylococcus aureus infection, Adv. Mater. 27 (22) (2015) 3437–3443.
[308] S. Thamphiwatana, P. Angsantikul, T. Escajadillo, Q. Zhang, J. Olson, B.T. Luk, S. Zhang, R.H. Fang, W. Gao, V. Nizet, L. Zhang, Macrophage-like nanoparticles concurrently absorbing endotoxins and proinflammatory cytokines for sepsis management, Proc. Natl. Acad. Sci. 114 (43) (2017) 11488–11493.
[309] Y. Lu, Q. Hu, C. Jiang, Z. Gu, Platelet for drug delivery, Curr. Opin. Biotechnol. 58 (2019) 81–91.
[310] J. Li, P. Angsantikul, W. Liu, B. Esteban-Fernández de Ávila, X. Chang, E. Sandraz, Y. Liang, S. Zhu, Y. Zhang, C. Chen, W. Gao, L. Zhang, J. Wang, Biomimetic platelet-camouflaged nanorobots for binding and isolation of biological threats, Adv. Mater. 30 (2) (2018) 1704800.
[311] C.-M.J. Hu, R.H. Fang, J. Copp, B.T. Luk, L. Zhang, A biomimetic nanosponge that absorbs pore-forming toxins, Nat. Nanotechnol. 8 (5) (2013) 336–340.
[312] C.-M.J. Hu, R.H. Fang, K.-C. Wang, B.T. Luk, S. Thamphiwatana, D. Dehaini, P. Nguyen, P. Angsantikul, C.H. Wen, A.V. Kroll, C. Carpenter, M. Ramesh, V. Qu, S.H. Patel, J. Zhu, W. Shi, F.M. Hofman, T.C. Chen, W. Gao, K. Zhang, S. Chien, L. Zhang, Nanoparticle biointerfacing by platelet membrane cloaking, Nature 526 (7571) (2015) 118–121.
[313] B. Esteban-Fernández de Ávila, P. Angsantikul, D.E. Ramírez-Herrera, F. Soto, H. Teymourian, D. Dehaini, Y. Chen, L. Zhang, J. Wang, Hybrid biomembrane–functionalized nanorobots for concurrent removal of pathogenic bacteria and toxins, Sci. Robot. 3 (18) (2018) eaat0485.
[314] I. Banerjee, R.C. Pangule, R.S. Kane, Antifouling coatings: recent developments in the design of surfaces that prevent fouling by proteins, bacteria, and marine organisms, Adv. Mater. 23 (6) (2011) 690–718.
[315] S.A. Ragland, A.K. Criss, From bacterial killing to immune modulation: recent insights into the functions of lysozyme, PLoS Pathog. 13 (9) (2017), e1006512.
[316] N. Tripathy, R. Ahmad, S.H. Bang, J. Min, Y.-B. Hahn, Tailored lysozyme–ZnO nanoparticle conjugates as nanoantibiotics, Chem. Commun. 50 (66) (2014) 9298–9301.
[317] T. Wu, C. Wu, S. Fu, L. Wang, C. Yuan, S. Chen, Y. Hu, Integration of lysozyme into chitosan nanoparticles for improving antibacterial activity, Carbohydr. Polym. 155 (2017) 192–200.
[318] M. Kiristi, V.V. Singh, B. Esteban-Fernández de Ávila, M. Uygun, F. Soto, D. Aktaş Uygun, J. Wang, Lysozyme-based antibacterial nanomotors, ACS Nano 9 (9) (2015) 9252–9259.
[319] F. Soto, M.A. Lopez-Ramirez, I. Jeerapan, B. Esteban-Fernandez de Avila, R. K. Mishra, X. Lu, I. Chai, C. Chen, D. Kupor, A. Nourhani, J. Wang, Rotibot: use of rotifers as self-propelling biohybrid microcleaners, Adv. Funct. Mater. 29 (22) (2019) 1900658.
[320] Y. Ge, M. Liu, L. Liu, Y. Sun, H. Zhang, B. Dong, Dual-fuel-driven bactericidal micromotor, Nano Micro Lett. 8 (2) (2016) 157–164.
[321] M. Hoop, Y. Shen, X.-Z. Chen, F. Mushtaq, L.M. Iuliano, M.S. Sakar, A. Petruska, M.J. Loessner, B.J. Nelson, S. Pané, Magnetically driven silver-coated nanocoils for efficient bacterial contact killing, Adv. Funct. Mater. 26 (7) (2016) 1063–1069.
[322] Y. Dong, L. Wang, J. Wang, S. Wang, Y. Wang, D. Jin, P. Chen, W. Du, L. Zhang, B.-F. Liu, Graphene-based helical micromotors constructed by "microscale liquid rope-coil effect" with microfluidics, ACS Nano 14 (12) (2020) 16600–16613.

[323] J. Yan, Y. Lu, G. Chen, M. Yang, Z. Gu, Advances in liquid metals for biomedical applications, Chem. Soc. Rev. 47 (2018) 2518–2533.
[324] A. Elbourne, S. Cheeseman, P. Atkin, N.P. Truong, N. Syed, A. Zavabeti, M. Mohiuddin, D. Esrafilzadeh, D. Cozzolino, C.F. McConville, M.D. Dickey, R. J. Crawford, K. Kalantar-Zadeh, J. Chapman, T. Daeneke, V.K. Truong, Antibacterial liquid metals: biofilm treatment via magnetic activation, ACS Nano 14 (1) (2020) 802–817.
[325] A. Rangel-Vega, L.R. Bernstein, E.A. Mandujano-Tinoco, S.J. García-Contreras, R. García-Contreras, Drug repurposing as an alternative for the treatment of recalcitrant bacterial infections, Front Microbiol 6 (2015) 282.
[326] Z. Lin, C. Gao, D. Wang, Q. He, Bubble-propelled janus gallium/zinc micromotors for the active treatment of bacterial infections, Angew. Chem. Int. Ed. 60 (16) (2021) 8750–8754.
[327] X. Zou, L. Zhang, Z. Wang, Y. Luo, Mechanisms of the antimicrobial activities of graphene materials, J. Am. Chem. Soc. 138 (7) (2016) 2064–2077.
[328] B. Zhang, G. Huang, L. Wang, T. Wang, L. Liu, Z. Di, X. Liu, Y. Mei, Rolled-up monolayer graphene tubular micromotors: enhanced performance and antibacterial property, Chem. Asian J. 14 (14) (2019) 2479–2484.
[329] B.E.-F. de Ávila, P. Angsantikul, J. Li, M. Angel Lopez-Ramirez, D.E. Ramírez-Herrera, S. Thamphiwatana, C. Chen, J. Delezuk, R. Samakapiruk, V. Ramez, M. Obonyo, L. Zhang, J. Wang, Micromotor-enabled active drug delivery for in vivo treatment of stomach infection, Nat. Commun. 8 (1) (2017) 272.
[330] J. Li, P. Angsantikul, W. Liu, B. Esteban-FernándezdeÁvila, S. Thamphiwatana, M. Xu, E. Sandraz, X. Wang, J. Delezuk, W. Gao, L. Zhang, J. Wang, Micromotors spontaneously neutralize gastric acid for pH-responsive payload release, Angew. Chem. Int. Ed. 56 (8) (2017) 2156–2161.
[331] F. Soto, D. Kupor, M.A. Lopez-Ramirez, F. Wei, E. Karshalev, S. Tang, F. Tehrani, J. Wang, Onion-like multifunctional microtrap vehicles for attraction–trapping–destruction of biological threats, Angew. Chem. Int. Ed. 59 (9) (2020) 3480–3485.
[332] L. Song, S. Zhang, Q. Wang, W. Chen, B. Liu, Y.-D. Zhao, Light-controlled microbots gathering as a sterilization platform for highly efficient capturing, concentrating and killing targeted bacteria, Chem. Eng. J. 435 (2022), 135067.
[333] X. Arqué, M.D.T. Torres, T. Patiño, A. Boaro, S. Sánchez, C. de la Fuente-Nunez, Autonomous treatment of bacterial infections in vivo using antimicrobial micro- and nanomotors, ACS Nano 16 (5) (2022) 7547–7558.
[334] D. Xu, C. Zhou, C. Zhan, Y. Wang, Y. You, X. Pan, J. Jiao, R. Zhang, Z. Dong, W. Wang, X. Ma, Enzymatic micromotors as a mobile photosensitizer platform for highly efficient on-chip targeted antibacteria photodynamic therapy, Adv. Funct. Mater. 29 (17) (2019) 1807727.
[335] D. Xu, J. Hu, X. Pan, S. Sánchez, X. Yan, X. Ma, Enzyme-powered liquid metal nanobots endowed with multiple biomedical functions, ACS Nano 15 (7) (2021) 11543–11554.
[336] L. Xie, X. Pang, X. Yan, Q. Dai, H. Lin, J. Ye, Y. Cheng, Q. Zhao, X. Ma, X. Zhang, G. Liu, X. Chen, Photoacoustic imaging-trackable magnetic microswimmers for pathogenic bacterial infection treatment, ACS Nano 14 (3) (2020) 2880–2893.
[337] X. Yan, Q. Zhou, M. Vincent, Y. Deng, J. Yu, J. Xu, T. Xu, T. Tang, L. Bian, Y.-X. J. Wang, K. Kostarelos, L. Zhang, Multifunctional biohybrid magnetite microrobots for imaging-guided therapy, Sci. Robot. 2 (12) (2017) eaaq1155.
[338] N. Batool, S. Yoon, S. Imdad, M. Kong, H. Kim, S. Ryu, J.H. Lee, A.K. Chaurasia, K. K. Kim, An antibacterial nanorobotic approach for the specific targeting and removal of multiple drug-resistant staphylococcus aureus, Small 17 (20) (2021) 2100257.
[339] X. Ji, H. Yang, W. Liu, Y. Ma, J. Wu, X. Zong, P. Yuan, X. Chen, C. Yang, X. Li, H. Lin, W. Xue, J. Dai, Multifunctional parachute-like nanomotors for enhanced skin penetration and synergistic antifungal therapy, ACS Nano 15 (9) (2021) 14218–14228.
[340] H.-C. Flemming, J. Wingender, U. Szewzyk, P. Steinberg, S.A. Rice, S. Kjelleberg, Biofilms: an emergent form of bacterial life, Nat. Rev. Microbiol. 14 (9) (2016) 563–575.
[341] K. Lewis, Riddle of biofilm resistance, Antimicrob. Agents Chemother. 45 (4) (2001) 999–1007.
[342] Y. Dong, L. Wang, Z. Zhang, F. Ji, T.K.F. Chan, H. Yang, C.P.L. Chan, Z. Yang, Z. Chen, W.T. Chang, J.Y.K. Chan, J.J.Y. Sung, L. Zhang, Endoscope-assisted magnetic helical micromachine delivery for biofilm eradication in tympanostomy tube, Sci. Adv. 8 (40) (2022) eabq8573.
[343] M.M. Stanton, B.-W. Park, D. Vilela, K. Bente, D. Faivre, M. Sitti, S. Sánchez, Magnetotactic bacteria powered biohybrids target E. coli biofilms, ACS Nano 11 (10) (2017) 9968–9978.
[344] L. Gao, J. Zhuang, L. Nie, J. Zhang, Y. Zhang, N. Gu, T. Wang, J. Feng, D. Yang, S. Perrett, X. Yan, Intrinsic peroxidase-like activity of ferromagnetic nanoparticles, Nat. Nanotechnol. 2 (9) (2007) 577–583.
[345] G. Hwang, A.J. Paula, E.E. Hunter, Y. Liu, A. Babeer, B. Karabucak, K. Stebe, V. Kumar, E. Steager, H. Koo, Catalytic antimicrobial robots for biofilm eradication, Sci. Robot. 4 (29) (2019) eaaw2388.
[346] T. Cui, S. Wu, Y. Sun, J. Ren, X. Qu, Self-propelled active photothermal nanoswimmer for deep-layered elimination of biofilm in vivo, Nano Lett. 20 (10) (2020) 7350–7358.
[347] K. Yuan, B. Jurado-Sánchez, A. Escarpa, Dual-propelled lanbiotic based janus micromotors for selective inactivation of bacterial biofilms, Angew. Chem. Int. Ed. 60 (9) (2021) 4915–4924.
[348] Q. Wang, L. Zhang, External power-driven microrobotic swarm: from fundamental understanding to imaging-guided delivery, ACS Nano 15 (1) (2021) 149–174.
[349] J. Yu, D. Jin, K.-F. Chan, Q. Wang, K. Yuan, L. Zhang, Active generation and magnetic actuation of microrobotic swarms in bio-fluids, Nat. Commun. 10 (1) (2019) 5631.
[350] Z. Wu, J. Troll, H.-H. Jeong, Q. Wei, M. Stang, F. Ziemssen, Z. Wang, M. Dong, S. Schnichels, T. Qiu, P. Fischer, A swarm of slippery micropropellers penetrates the vitreous body of the eye, Sci. Adv. 4 (11) (2018) eaat4388.
[351] Y. Dong, L. Wang, K. Yuan, F. Ji, J. Gao, Z. Zhang, X. Du, Y. Tian, Q. Wang, L. Zhang, Magnetic microswarm composed of porous nanocatalysts for targeted elimination of biofilm occlusion, ACS Nano 15 (3) (2021) 5056–5067.
[352] M. Ussia, M. Urso, K. Dolezelikova, H. Michalkova, V. Adam, M. Pumera, Active light-powered antibiofilm ZnO micromotors with chemically programmable properties, Adv. Funct. Mater. 31 (27) (2021) 2101178.
[353] K. Villa, H. Sopha, J. Zelenka, M. Motola, L. Dekanovsky, D.C. Beketova, J. M. Macak, T. Ruml, M. Pumera, Enzyme-photocatalyst tandem microrobot powered by urea for escherichia coli biofilm eradication, Small 18 (36) (2022) 2106612.
[354] Y. Zhang, L. Zhang, L. Yang, C.I. Vong, K.F. Chan, W.K.K. Wu, T.N.Y. Kwong, N. W.S. Lo, M. Ip, S.H. Wong, J.J.Y. Sung, P.W.Y. Chiu, L. Zhang, Real-time tracking of fluorescent magnetic spore–based microrobots for remote detection of C. diff toxins, Sci. Adv. 5 (1) (2019) eaau9650.
[355] V.A.K. Rathinam, K.A. Fitzgerald, Lipopolysaccharide sensing on the inside, Nature 501 (7466) (2013) 173–175.
[356] B. Beutler, E.T. Rietschel, Innate immune sensing and its roots: the story of endotoxin, Nat. Rev. Immunol. 3 (2) (2003) 169–176.
[357] B. Jurado-Sánchez, M. Pacheco, J. Rojo, A. Escarpa, Magnetocatalytic graphene quantum dots janus micromotors for bacterial endotoxin detection, Angew. Chem. Int. Ed. 56 (24) (2017) 6957–6961.
[358] R.P. Feynman, There's plenty of room at the bottom, Eng. Sci. 23 (5) (1960) 22–36.
[359] Y. Mei, A.A. Solovev, S. Sanchez, O.G. Schmidt, Rolled-up nanotech on polymers: from basic perception to self-propelled catalytic microengines, Chem. Soc. Rev. 40 (5) (2011) 2109–2119.
[360] Y. Alapan, U. Bozuyuk, P. Erkoc, A.C. Karacakol, M. Sitti, Multifunctional surface microrollers for targeted cargo delivery in physiological blood flow, Sci. Robot. 5 (42) (2020) eaba5726.
[361] B.J. Williams, S.V. Anand, J. Rajagopalan, M.T.A. Saif, A self-propelled biohybrid swimmer at low Reynolds number, Nat. Commun. 5 (1) (2014) 3081.
[362] S. Schuerle, S. Pané, E. Pellicer, J. Sort, M.D. Baró, B.J. Nelson, Helical and tubular lipid microstructures that are electroless-coated with CoNiReP for wireless magnetic manipulation, Small 8 (10) (2012) 1498–1502.
[363] W. Gao, S. Sattayasamitsathit, J. Orozco, J. Wang, Highly efficient catalytic microengines: template electrosynthesis of polyaniline/platinum microtubes, J. Am. Chem. Soc. 133 (31) (2011) 11862–11864.
[364] M.A. Zeeshan, R. Grisch, E. Pellicer, K.M. Sivaraman, K.E. Peyer, J. Sort, B. Özkale, M.S. Sakar, B.J. Nelson, S. Pané, Hybrid helical magnetic microrobots obtained by 3D template-assisted electrodeposition, Small 10 (7) (2014) 1284–1288.
[365] H. Zhou, B. Wu, L. Dekanovsky, S. Wei, B. Khezri, T. Hartman, J. Li, Z. Sofer, Integration of BiOI nanosheets into bubble-propelled micromotors for efficient water purification, FlatChem 30 (2021), 100294.
[366] Y. Wu, Z. Wu, X. Lin, Q. He, J. Li, Autonomous movement of controllable assembled janus capsule motors, ACS Nano 6 (12) (2012) 10910–10916.
[367] F. Rajabasadi, L. Schwarz, M. Medina-Sánchez, O.G. Schmidt, 3D and 4D lithography of untethered microrobots, Prog. Mater. Sci. 120 (2021), 100808.
[368] D. Li, C. Liu, Y. Yang, L. Wang, Y. Shen, Micro-rocket robot with all-optic actuating and tracking in blood, Light.: Sci. Appl. 9 (1) (2020) 84.
[369] Z. Wu, L. Li, Y. Yang, P. Hu, Y. Li, S.-Y. Yang, L.V. Wang, W. Gao, A microrobotic system guided by photoacoustic computed tomography for targeted navigation in intestines in vivo, Sci. Robot. 4 (32) (2019) eaax0613.
[370] O. Erin, M. Boyvat, M.E. Tiryaki, M. Phelan, M. Sitti, Magnetic resonance imaging system–driven medical robotics, Adv. Intell. Syst. 2 (2) (2020) 1900110.
[371] S. Martel, Beyond imaging: macro- and microscale medical robots actuated by clinical MRI scanners, Sci. Robot. 2 (3) (2017) eaam8119.
[372] J. Rahmer, C. Stehning, B. Gleich, Spatially selective remote magnetic actuation of identical helical micromachines, Sci. Robot. 2 (3) (2017) eaal2845.
[373] H. Ceylan, I.C. Yasa, U. Kilic, W. Hu, M. Sitti, Translational prospects of untethered medical microrobots, Prog. Biomed. Eng. 1 (1) (2019), 012002.
[374] L. Wang, Z. Meng, Y. Chen, Y. Zheng, Engineering magnetic micro/nanorobots for versatile biomedical applications, Adv. Intell. Syst. 3 (7) (2021) 2000267.
[375] A. Aziz, S. Pane, V. Iacovacci, N. Koukourakis, J. Czarske, A. Menciassi, M. Medina-Sánchez, O.G. Schmidt, Medical imaging of microrobots: towards in vivo applications, ACS Nano 14 (9) (2020) 10865–10893.
[376] J. Mei, N.L.C. Leung, R.T.K. Kwok, J.W.Y. Lam, B.Z. Tang, Aggregation-induced emission: together we shine, united we soar!, Chem. Rev. 115 (21) (2015) 11718–11940.
[377] S.-A. Li, Y. Xiang, Y.-J. Wang, J. Liu, W.-H. Lee, Y. Zhang, Naturally occurring antimicrobial peptide OH-CATH30 selectively regulates the innate immune response to protect against sepsis, J. Med. Chem. 56 (22) (2013) 9136–9145.

[378] J. Sun, A. Siroy, R.K. Lokareddy, A. Speer, K.S. Doornbos, G. Cingolani, M. Niederweis, The tuberculosis necrotizing toxin kills macrophages by hydrolyzing NAD, Nat. Struct. Mol. Biol. 22 (9) (2015) 672–678.
[379] D. Pajuelo, N. Gonzalez-Juarbe, U. Tak, J. Sun, C.J. Orihuela, M. Niederweis, NAD + depletion triggers macrophage necroptosis, a cell death pathway exploited by mycobacterium tuberculosis, Cell Rep. 24 (2) (2018) 429–440.
[380] H. Zhou, G. Dong, G. Gao, R. Du, X. Tang, Y. Ma, J. Li, Hydrogel-based stimuli-responsive micromotors for biomedicine, Cyborg Bionic Syst. 2022 (2022) 9852853.

Dr. Jinhua Li is Professor at Beijing Institute of Technology (BIT), Fellow of Alexander von Humboldt Stiftung, Beijing Institute of Technology Teli Young Fellow, and Vebleo Fellow. He is the Responsible Professor in Materials and Regenerative Medicine Engineering of BIT. He obtained his PhD in Materials Science from University of Chinese Academy of Sciences and was Awardee of Marie Skłodowska-Curie Individual Fellowship. His research interests include micro/nanorobots, biomaterials, 3D printing, tissue engineering, regenerative medicine, and intelligent drug delivery.

Dr. Huaijuan Zhou is currently Associate Professor at Beijing Institute of Technology. She is Marie Skłodowska-Curie Fellow. She received her Ph.D. in Materials Physics and Chemistry from University of Chinese Academy of Sciences. Subsequently, she worked at Shanghai Institute of Ceramics Chinese Academy of Sciences, Technische Universität Dresden, and University of Chemistry and Technology Prague. She has hosted Shanghai Sailing Program supported by Science and Technology Commission of Shanghai Municipality and Marie Skłodowska-Curie Actions (MSCA) Individual Fellowship financially sponsored by European Commission. Her research interests include functional micro/nanorobots, photoelectrocatalytic materials & devices, and intelligent energy-saving materials & devices.

Dr. Chengtie Wu is Full Professor at Shanghai Institute of Ceramics, Chinese Academy of Sciences. He completed his Ph. D. in 2006, and then worked at University of Sydney, Dresden University of Technology, and Queensland University of Technology where he was awarded Vice-Chancellor Research Fellow and Alexander von Humboldt Fellow. He was awarded One-Hundred Talent Program of Chinese Academy of Sciences and Recruitment Program of Global Young Experts of China , Young Scientists of Chinese Biomaterials Society in 2016, First Prize of Science and Technology of Chinese Biomaterials Society in 2019, and International Union of Materials Research Society (IUMRS) Young Scientist in 2022. His research focuses on bioactive inorganic materials for tissue engineering.

Professor Paul K. Chu received his PhD in Chemistry from Cornell University. He is Chair Professor of Materials Engineering in the Department of Physics, Department of Materials Science & Engineering, and Department of Biomedical Engineering at City University of Hong Kong. He is Fellow of the Hong Kong Academy of Engineering Sciences. He is also Fellow of the American Physical Society (APS), American Vacuum Society (AVS), Institute of Electrical and Electronics Engineers (IEEE), Materials Research Society (MRS), and Hong Kong Institution of Engineers (HKIE). His research interests are quite diverse encompassing plasma surface engineering, materials science and engineering, surface science, and functional materials. He is a highly-cited researcher in materials science according to Clarivate Analytics.